Doctoral Dissertation

# Observation and Evaluation of Surface Deformation in Complex Landslide Slope of Bobonaro in Timor-Leste by using Remote Sensing

**(リモートセンシングによる東ティモール・ボボナロにおける複雑な地すべり斜面の地表面変状の観測および評価)**

A dissertation submitted in partial fulfilment of the requirements for the degree of

Doctor of Engineering

**September, 2020**

**Benjamim de Oliveira Hopffer Rêgo Silveira Martins**

Graduate School of Sciences and Technology for Innovation
Yamaguchi University

Doctoral dissertation

Graduate School of Sciences and Technology for Innovation,

Division of Civil and Environmental Engineering,

Yamaguchi University, 2-16-1, Tokiwadai, Ube,

Yamaguchi 755-8611, Japan

Reference as: Martins, B.H. (2020) Observation and Evaluation of Surface Deformation in Complex Landslide Slope of Bobonaro in Timor-Leste by using Remote Sensing. Doctoral Dissertation

## DEDICATION

*To my wife, Lurdes Bessa, for all the support, she gave me, all the love, patience, and for closely following my work, at all moments. Thank you for believing in me and for holding on the house during my absence.*

*To my children, Benjamim, Mafalda, and Tânia, (BEMATA), for being who you are and for giving me your love, care, and support. Thank you for being present at all times and simply for being there.*

*A special thank you to Avó Mina, for being there providing care and love to your daughter and your grandchildren.*

# FOREWORD

*Aerial view of Bobonaro Post Administrative, 1963. Photo courtesy: Antonio Milho*

Bobonaro: rotten road shoulders.
The post changes the floor as the land gives them.
From the top you can see roads that slope into abyss or stop suddenly against fallen mountains.

*Original in Portuguese*
*Bobonaro: bermas podres.*
*O posto muda de piso conforme à terra lhes dá.*
*Do alto vêem-se estradas que declivam em abismo ou param subitamente contra monte abatidos.*

*Ruy Cinatti (1974) Paisagens Timorenses Com Vultos. Braga, Editora Paz,p31*

## ACKNOWLEDGEMENTS

First of all, I would like to thank my Academic Supervisor Professor Motoyuki SUZUKI, for having accepted the theme of my research since the first conversation, providing me with all his teaching and knowledge, guidance, encouragement, support and listening ear.

Second, I would like to thank Professor Norikazu SHIMIZU, for having accepted to join the theme of my research as a co-author for the Journal Article, provide the SARSCAPE software for SAR data processing, providing me with all his teaching and knowledge, guidance, encouragement, support and listening ear. I also thank Dr. Putu Edi Yastika, for having accepted to join the theme of my research as a co-author of the Journal Article, processing the SAR data, providing me with all his experiences and knowledge, guidance, encouragement, support and listening ear.

Third, I would like to thank Professor Masahiko NAGAI, Dr. Eguchi TSUYOSHI and Dr. Nopphawan Tamkuan for having accepted to join the theme of my research as co-authors for two Proceedings papers, providing me with all their experiences and knowledge, guidance, encouragement, support and listening ear.

Fourth, I would like to thank the examination committee - Chair: Professor Motoyuki SUZUKI, Professor Norikazu SHIMIZU, Professor Masahiko SEKINE, Professor Masahiko NAGAI, Associate Professor Ariyo KANNO and Associate Professor Shinichiro NAKASHIMA for their valuable comments, suggestions, and questions during the Preliminary Examination of this dissertation.

My special thanks to JICA CADEFEST Project Phase II for the opportunity and trusty to do the Doctoral Program at Yamaguchi University.

My special thanks also to JICA Chugoku Center for the support and monitoring during my stay in Japan.

My special gratitude to Professor Hidehiko KAZAMA for his motivation, support and friendship since the beginning of the cooperation relations between the universities of Japan and the Universidade Nacional Timor Lorosa'e, in 2001. The same gratitude goes to all the other Japanese professors who were part of this group along the way.

To HE Ambassador Filomeno Aleixo da Cruz and HE Ambassador Ilidio Ximenes da Costa for their friendship, motivation, support and monitoring during my stay in Japan.

To Bobonaro Post Administrative authority and Suco's authorities for their support and contributions during the field work in Bobonaro.

To Dr. I Nyoman Sudi Parwata for his motivation, friendship, sharing experiences and knowledge, and his teachings in GMTSAR.

To Dr. Atsushi KOUYAMA as my tutor, for his motivation, friendship and support.

To Mr. Taichi ISHIMARU for his friendship, support and special contribution by translating the summary of this dissertation to Japanese.

To Eng. Alex, Eng. Elfrido, Mr. Domingos Martins, Mr. Lamberto Elezon, Mr. Alcino Santos, and others for their support during the field work in Timor-Leste.

To all colleagues in Professor Motoyuki SUZUKI Laboratory for their friendship, support and sharing experiences and knowledge.

To colleagues and friends Dr. Duong Nguyen, Dr. Kien Nguyen, Dr. I GD Yudha Partama, Dr. I Made Pertiwi, Mr. Nam, and others for their motivation, friendship and support.

My especial thanks to Father Hisashi Hayashi, Father Jun Nakai, dr. Kenji Ohki, Mr. Nagadomi and Mrs. Keishi, Mrs. Kawahara, Mrs. Etsuko Ishikawa and many other friends from Japan Timor-Leste Solidarity Group for their kind support, motivation and strong friendship, especially during my stay in Yamaguchi Prefecture to do my doctoral course.

Finally, to all those who, directly or indirectly, contributed, in the most diverse ways for the accomplishment of this study in japan and Timor-Leste.

## PREFACE

This dissertation is hereby submitted to the Graduate School of Sciences and Technology for Innovation of Yamaguchi University, Japan, in partial fulfilment of the requirement for the degree of Doctor of Engineering. The publications written by the author during his doctoral studies are listed below:

1. Peer-reviewed Journal Paper

   **Ground Surface Deformation Detection in Complex Landslide Area – Bobonaro, Timor-Leste – Using SBAS DInSAR, UAV Photogrammetry and Field Observations**

   Benjamim Hopffer Martins, Motoyuki Suzuki, Putu Edi Yastika, Norikazu Shimizu

   Journal: Geosciences

   Volume, Issue and Pages : **2020,10(6),245**. Special Issue "Scientific Assessment of Recent Natural Hazard Events"

   DOI: https://doi.org/10.3390/geosciences10060245

   **Author Contributions:** BHM carried out this study to fulfil the Doctoral Program at Yamaguchi University under MS orientation. BHM designed and carried out the field observations, UAV campaign, photogrammetry analysis and processing; BHM, PEY and NS designed the DInSAR analysis and image processing; BHM wrote the paper with valuable contributions from MS, PEY and NS; MS and NS conducted the final review of the manuscript. All authors have read and agreed to the published version of the manuscript.

   **Conflicts of Interest:** The authors declare no conflict of interest.

2. Peer-reviewed conference papers
   a. BH Martins, M Suzuki, E Tsuyoshi, N Tamkuan, M Nagai (2018) **FACTORS TRIGGERING LANDSLIDES IN TIMOR-LESTE**. Proceedings of the 4th International Conference VIETGEO 2018 - Geological and Geotechnical Engineering In Response To Climate Change And Sustainable Development of Infrastructure, Quang Binh, Vietnam, 21-22 September 2018, pp 421 – 430

**Author Contributions:** BHM Writing - original draft, data curation, investigation, methodology and software under MS orientation; ET Data curation; MS, ET, NT and MN Review and contribute; MS conduct the final review. All authors have read and agreed to the published version of the proceedings paper.

**Conflicts of Interest:** The authors declare no conflict of interest.

**Publication:** Proceedings Book, 2018,pp421-430

b. BH Martins, M Suzuki, E Tsuyoshi, N Tamkuan, M Nagai (2019) **Ground subsidence induced by shallow earthquake in Timor-Leste**. Proceedings of the ISRM Specialized conference and 8th Conference of Croatian Geotechnical Society Geotechnical challenges in karst, Omiš – Split, Croatia, 11- 13 April 2019, pp 205-210. ISBN 978-953-48525-0-7

Author Contributions: BHM Writing - original draft, data curation, investigation, methodology and software under MS orientation; ET Data curation; MS, ET, NT and MN Review and contribute; MS contributions and final review. All authors have read and agreed to the published version of the proceedings paper.

Conflicts of Interest: The authors declare no conflict of interest.

**Publication:** Proceedings Book, 2019,pp205-210

c. BH Martins, M Suzuki (2019) **Geo-disasters consciousness and preparedness of the people in Timor-Leste**. Proceedings of Technical Forum on Mitigation of Geo-disasters in Asia, 13th – 15th November 2019, Kumamoto, Japan. 2019, pp19-22.

**Author Contributions:** BHM Writing - original draft, data curation, investigation, methodology and software under MS orientation; MS contributions and final review and contributions. All authors have read and agreed to the published version of the proceedings paper.

**Conflicts of Interest:** The authors declare no conflict of interest.

**Publication:** Proceedings Book, 2019, pp19-22

## SUMMARY

### Research Background and Objectives

After gaining independence on 20 May 2002, Timor-Leste's policies have focused on alleviating poverty and addressing the immediate needs of the people, consolidating security and stability, and providing a foundation for the nationhood through the building of state institutions. Following the approval of the Timor-Leste Strategic Development Plan, in 2011, many projects related to the infrastructure started, including the construction of large sections of roads and bridges. However, it has not achieved enough due to unexpected ground deformation in mountain areas that is seriously affecting road constructions, etc. The geomorphology and geoenvironment of the country have led to continuous ground deformation, frequent landslides, flash floods and flooding events during the rainy season, thus disrupting the land transport system by destroying bridges and washing out roads. This situation has led to direct and indirect negative impacts on the activities and safety of the people, and consequently, has delayed the ongoing development, wasting the resources and time. In order to design roads and other infrastructures under such difficult conditions, it is important to know the present and future ground conditions. Continuous monitoring is a significant method for detecting the ground deformation and providing essential information to realize the effective design. The problem arises of "How can ground deformation be monitored in extensive areas, which are generally located in mountain areas that are difficult to access? Satellite-based remote sensing has recently been applied to monitor displacement in extensive areas. In addition, Unmanned Aerial Vehicle (UAV) photogrammetry has been applied to detect and characterize the ground surface deformation in detail alongside field observations.

The purpose of this dissertation is to develop e method for detecting ground deformation by making full use of these remote sensing technologies. To achieve that, the following four objectives are listed:

1. To apply the Differential Interferometry Synthetic Aperture Radar (DInSAR) to detect the recent ground surface deformation since 2007 in complex Landslide Slope in Bobonaro.
2. To employ Unmanned Aerial Vehicle (UAV) Photogrammetry for detecting the detailed deformation.
3. To discuss about the relation of the ground deformation with the earthquake and hard rainfall event's
4. To find the people's consciousness and preparedness about geo-disasters.

**Analysis Data**

ALOS1 PALSAR1 and ALOS2 PALSAR2 datasets were provided by the Japan Aerospace Exploration Agency (JAXA). The first dataset, composed of 22 SAR images collected from PALSAR1, covered the period from 2007/01/22 – 2011/02/02. The second dataset, composed of 13 SAR images collected from PALSAR2, covered the period from 2015/02/10 – 2019/04/02.

A high-resolution orthomosaic and DEM were collected on 19 August 2017 by employing Small UAV Photogrammetry DJI Mavic Pro.

The earthquake data downloaded from the United States Geological Survey (USGS) Earthquake Catalogue covered the two periods of study.

Timor-Leste rainfall data has not been well recorded since 1974. To overcome this unavailability of rainfall data, it was necessary to use the data published by the Climate Forecast System Reanalysis (CFSR) of the National Centers for Environmental Prediction (NCEP), covering the period from January 2007 to February 2011. For the second period, a HOBO ground station rainfall data logger, with a resolution of 0.2 mm per tip, was installed 2 km from the study area. The data collection was conducted from 07/03/2017 until 02/04/2019 partially covering the second period.

**Dissertation structure**

This dissertation is divided in six chapters:

**Chapter 1:**

Presents a) the background and motivation of the study, b) exposition of an essential literature review related to the ground deformation and landslide monitoring techniques, starting from the conventional methods to the recent and common uses portable and automated devices c) aims of the dissertation, d) references.

**Chapter 2:**

Presents essential information of the study location such as a) Overview of the country related to geology, geomorphology, topography, soil, hydrography, rainfall pattern, soil erosion and tectonic, b) information about Bobonaro region related to geographical location, lithology and topography, c) historical of the ground deformation since 1918, d) type and mechanism of the ground deformation and landslide e) description about the study area and the recent evidences of the ground deformation impact, f) references.

**Chapter 3:**

In this chapter is presented the results of questionnaire survey to identify the consciousness and preparedness regarding geo-disasters in Timor-Leste. The theme of this chapter is connected with chapter 1, 2, 5 and matches with the fourth objective of this dissertation. The result presents that, the majority of people have experienced geo-disasters. Consequently, their consciousness about geo-disasters considered high. However, their preparedness is very low. To overcome this situation is very important to introduce the soft countermeasure method through education by introducing the knowledge about the prevention and reduction of nature and man-made disasters in the school curriculum.

**Chapter 4:**

In this chapter is presented the study about factor triggering landslides in Timor-Leste. This chapter is relates to chapter 2 and 5. The theme of this matched with the third objective of this dissertation. The recent landslides triggered by rainfall occurred on 17 January 2018 clearly show that high precipitation events do not trigger landslides. On the other hand, the landslide occurred after it rained for four consecutive days with a gradual increase from 4.2

mm/hour, to 10.2 mm/hour, to 13.6 mm/hour and to 17.8 mm/hour on the day of the landslide occurrence. The earthquake triggering factor, although it is of low magnitude, which is responsible for the topographical change of the ground level. However, these two landslide triggering factors might possibly act together or simultaneously.

**Chapter 5:**

In this chapter the main results of this study are presented. This chapter discussed about: a) the application of Differential Interferometry Synthetic Aperture Radar (DInSAR) for screening usual and usual ground deformation behavior in extensive areas, b) the application of Unmanned Aerial Vehicle (UAV) Photogrammetry for mapping and for detecting ground surface deformation in detail. Both methods have an advantage that they do not require any sensors. This chapter relates to chapter 1, 2, 3 and 4. The theme of this chapter matched with the first, the second and the third objective of this dissertation. The LOS displacement results, clearly showed the trend in the ground surface deformation during the two periods of study. UAV photogrammetry data is useful to perform a detailed interpretation of the ground deformation morphology, the direction of the ground movement, and measurements of the ground surface features with centimeters order of accuracy. The combination of DInSAR and UAV present good coherence. The LOS displacement time-series showed that the time occurrence of the ground deformation, earthquake sequences, and periodic rainfalls are notably related.

**Chapter 6:**

Provide the conclusions of this research and recommendations for future work.

**Final remarks**

It states that the four goals raised at the beginning of this paper have been achieved. Furthermore, it was proved that the combination of the proposed methods would be an effective method for detecting ground deformation in areas where the surveying cannot be performed.

2002 年 5 月 20 日の独立後，東ティモールの政策は，貧困の緩和，国民の当面のニーズへの対応，安全と安定の強化，国家機関の構築を通した国民への生活基盤の提供に焦点を当てている。2011 年，東ティモール戦略開発計画の承認を受けて，大規模な道路や橋梁の建設を含む，インフラに関連する多くのプロジェクトが開始された。しかし，山岳地帯では道路建設等に深刻な影響を及ぼす予期せぬ地盤変形により進捗していない。東ティモールの地形・地質・環境は，雨季の間の継続的な地盤変形，度重なる地すべり，土石流や洪水イベントを引き起こし，橋梁の破壊と道路の流失によって陸上輸送システムを混乱させてきた。このような状況は，人々の活動と安全性に直接的および間接的な悪影響を及ぼし，その結果，進行中の開発を遅らせ，資源と時間を浪費している。このような困難な状況下で道路などのインフラを設計するためには，現在および将来の地盤状況を知ることが重要であり，連続的なモニタリング方法は、地盤変形を検出し，効果的な設計を実現するために不可欠な情報を提供するものとして重要な方法である。ここで，一般的にアクセスが困難な山岳地帯に位置する広範な領域において，どのようにして地面の変形をモニタリングするのかが課題である。近年，人工衛星によるリモートセンシングが，広範囲の変位を監視するために適用されている。また，無人航空機（UAV）の写真測量は，地表観測とともに地表変形を詳細に検出し，特徴付けるために適用されている。本学位論文は、以下の目的を設定して、最終的に、これらのリモートセンシング技術を駆使して地盤変形を検出する方法を開発することを目標とするものである。

1. 差分干渉 SAR 解析 （DInSAR）によって，Bobonaro の複雑な地すべり斜面における 2007 年以降の地表面変形を検出する。
2. 無人航空機（UAV）を用いた写真測量によって，詳細な地表変形を検出する。
3. 地震・豪雨と地盤変形の関係について考察する。
4. 地盤災害に対する人々の意識と備えについて調査する。

ALOS1 PALSAR1 および ALOS2 PALSAR2 のデータセットは，宇宙航空研究開発機構（JAXA）より提供されものである。前者は，2007 年 1 月 22 日から 2011 年 2 月 2 日までの期間に PALSAR1 から収集された 22 枚の SAR 画像で構成されている。後者は，2015 年 2 月 10 日から 2019 年 4 月 2 日までの期間に PALSAR2 から収集された 13 枚の SAR 画像で構成されている。また、2017 年 8 月 19 日，小型 UAV（DJI Mavic Pro）を用いた写真測量によって，高解像度オルソモザイクと DEM を収集した。研究における 2 期間の地震データは，アメリカ地質調査所（USGS）が提供しているデータを使用した。東ティモールの降雨データは，1974 年以降十分に記録されていない。したがって，降雨データの不足を補填するために，2007 年 1 月から 2011 年 2 月までの期間においては，国立環境予測センター（NCEP）の気象予報システムの再分析データ（CFSR）を使用する必要があった。第 2 期においては，解像度 0.2mm の HOBO 地上局降雨データロガーを対象範囲から 2km 離れた場所に設置し，2017 年 3 月 7 日から 2019 年 4 月 2 日までの期間の降雨データを部分的に収集した。

以上の方法により得られた成果をもとに本論文は 6 つの章で構成されている。

第 1 章では，a）研究の背景と動機，b）地盤変形および地すべり監視技術（従来の技術から近年の携帯可能で自動化された装置を使用した技術まで）に関連する主要な文献のレビュー，c）論文の目的，d）参考文献を示す。

第 2 章では，a） 地質学，地形学，土質，水文学，降雨パターン，土壌侵食および地殻変動に関する東ティモールの概要，b）地理的位置，岩石学および地形学に関連する Bobonaro 地域の概要，c）1918 年以降の地盤変形の歴史，d）地盤変形および地すべりの種類とメカニズム，e）調査地域における地盤変形の影響に関する近年の事例，f） 参考文献を示す。

第 3 章では，東ティモールの地盤災害に対する意識と備えに関するアンケート調査の結果を示す。この章のテーマは第 1， 2 及び 5 章に関連し，本研究の 4 つ目の目的と一致する。結果として，ほとんどの人が地盤災害を経験しており，地盤災害

に対する関心はとても高いことが分かったー方で，備えに関する意識はとても低かった。学校カリキュラムとして自然および人的な災害の防災・減災に関する教育を行うことで，上記の問題を解決することが重要である。

第4章では，東ティモールの地すべりを引き起こす要因についての研究を示す。この章のテーマは第2章と第5章に関連し，論文の3つ目の目的とー致する。2018年1月 17 日は豪雨によって発生した地すべりは降雨水量が高いことが原因でないことが明らかであった。4.2mm/時，10.2 mm/時，13.6 mm/時，17.8 mm/時と降水量を増加させながら4日間連続で降り続いた雨がその地すべりの原因であった。また，マグニチュードが小さい地震でも地形変動の原因となりうる。この2つの地すべり要因は同時に作用する可能性がある。

第 5 章では，本研究の主要な結果を示す。本章では，以下の 4 点について考察した。a）広範囲の領域で通常の地盤変形挙動を検出するための差分干渉 SAR 解析（DInSAR）の適用について，b）マッピングおよび詳細な地表変形を検出するための無人航空機（UAV）を用いた写真測量の適用について，c）良好なコヒーレンスを示す DInSAR と UAV の組み合わせについて。なお，どちらの方法も，センサーを必要としない利点がある，d）対象地域の観測または検証に基づく地盤変形の結果について。この章のテーマは第 1, 2, 3 及び 4 章に関連し，本論文の 1〜3 番目の目的とー致する。LOS 変位結果より，2 つの研究期間中の地表面変形の傾向を明らかにした。UAV 写真測量データは、地盤変形の形態，地盤運動の方向および地表面の特徴の測定をセンチメートルオーダーの精度で詳細に解釈するのに役立つ。DInSAR と UAV の組み合わせは良好なコヒーレンスを示す。LOS 変位の時系列は，地盤変形，地震シーケンスおよび周期的な降雨量の時間発生が顕著に関連していることを示した。

第6章では，本研究の結論および今後の研究に対する提案を示す。

本論文の冒頭で掲げた目標が達成されたことを述べた。さらに，提案された方法の組み合わせは測量ができない領域で地盤変形を検出する有効な方法であることが証明された。

## TABLE OF CONTENT

## LIST OF FIGURES

## LIST OF TABLES

## LIST OF APPENDIX

## LIST OF ACRONYMS

| | |
|---|---|
| ALOS | : Advanced Land Observation Satellite |
| AOI | : Area of Interest |
| APS | : Atmospheric Phase Screen |
| BDDTL | : Baze Dadus Dezastre Timor-Leste |
| BM | : Benchmark |
| CFSR | : Climate Forecast System Reanalysis |
| CMOS | : Complementary metal–oxide–semiconductor |
| DEM | : Digital Elevation Model |
| DGNSS | : Differential Global Navigation Satellite System |
| DInSAR | : Differential Interferometry SAR |
| FEMA | : Federal Emergency Management Agency |
| GCP | : Ground Control Point |
| GIS | : Geographic Information System |
| GLONASS | : Global Navigation Satellite System |
| GNSS | : Global Navigation Satellite System |
| GPS | : Global Positioning System |
| IMU | : Inertial Measurements Unit |
| InSAR | : Interferometry SAR |
| LIDAR | : Light Detection and Ranging |
| LOS | : Line of Sight |
| MCF | : Minimum Cost Flow |
| NASA | : National Aeronautics and Space Administration |
| NCEP | : National Centers for Environmental Prediction |

| | |
|---|---|
| NGOs | : Non-Governmental Organizations |
| PALSAR | : Phased Array type L-band Synthetic Aperture Radar |
| POI | : Point of Interest |
| PPK | : Post-Processed Kinematic |
| PSI | : Permanent Scatterer Interferometry |
| QGIS | : Quantum Geographical Information System |
| RMES | : Root Mean Square Error |
| RGS | : Rain Gauge Station |
| RTK | : Real-Time Kinematic |
| SAR | : Synthetic Aperture Radar |
| SBAS | : Small Baseline Subset |
| SfM | : Structure from Motion |
| SRTM1 | : Shuttle Radar Topography Mission 1 |
| TL-PED | : Timor-Leste – Plano Estratégico de Desenvolvimento |
| UAV | : Unmanned Aerial Vehicle |
| USGS | : United State Geological Survey |
| UTM | : Universal Transverse Mercator |
| WGS | : World Geodetic System |

# Chapter 1

# INTRODUCTION

## 1.1 Background and motivation

On 20 May 2002, Timor-Leste became the first new sovereign state of the 21st century, and was declared independent from Indonesia based on a referendum on 30 August 1999 under the auspices of the UN. After gaining its independence, Timor-Leste's policies have focused on alleviating poverty in order to address the immediate needs of the people, consolidating security and stability, and providing a foundation for nationhood through building state institutions. Following the approval of the Timor-Leste Strategic Plan (TL-EDP, 2011), many infrastructure projects were started, including the construction of large parts of roads and bridges. Unfortunately, the results are not meeting the expectations. The geomorphology and geoenvironment of the country have led to continuous ground deformation, frequent landslides, flash flood and flood occurrences during the rainy season, thus disrupting the land transport system by destroying bridges and washing out roads. This situation has caused direct and indirect negative impacts on the activities and safety of the people and, consequently, delayed the ongoing development, wasting resources and time. According to the Baze Dadus Dezatres Timor-Leste (BDDTL, 2019), database for the period of 1992-2019, 60 deaths were recorded. Data on the victims of various types of geo-disasters show that 32 deaths were caused by flash flood and floods, 11 were caused by windstorms, 10 were caused by wildfires, and 7 were caused by landslides. Despite the efforts of the local government and international agencies to introduce disaster management education among the population, the country is facing an extreme lack of capacity to adapt to natural and man-made disasters (Barnett et al, 2007). The country's vulnerability to both natural disasters and their impacts has presented considerable challenges for the authorities. Problems related to the lack of institutional capacity are making it increasingly difficult to solve these problems (Cook et al, 2019). Nevertheless, there are neither no formal records nor assessment techniques for the amplitude, frequency, and spatial distribution of natural and man-made disasters, including the technical data bases, such as hydrometeorology and detailed geology information.

## 1.2 Literature review – ground deformation monitoring techniques

### *1.2.1 General*

Ground deformation is a dynamic process of the Earth's surface that results from a variety of natural and human causes. This dynamic process can lead to natural and/or man-made hazards that may negatively affect human activities and lives. Various efforts have been made to prevent and mitigate landslides and their negative impacts. The results are still far below the expectations due to the complexity of this phenomenon (Corominas et al, 2014; Palenzuela et al, 2016). At this stage, efforts to prevent and/or mitigate landslides and their negative impacts would require a vast knowledge of the distribution of landslides and the state of their activity, particularly in situations where property, infrastructure, and human lives are at risk (Kjekstad and Highland, 2009).

During the last century, several detection and monitoring methods for slope instability have been developed. Conventional ground-based monitoring methods using geotechnical machinery and instruments, e.g., borehole drillers, extensometers, piezometers, and inclinometers, have been combined with surveying instruments—e.g., Global Positioning System (GPS) and Total Station (Ding, 2000; Demoulin and Glade, 2004; Duc, 2013; Shimizu et al, 2014; Uhlemann, 2016). Nowadays, the conventional instruments can be connected to a wireless sensor network system for real-time slope stability monitoring (Ramesh and Vasudevan, 2012; Chang et al, 2013).

The three well-known airborne-based methods for monitoring landslides are Photogrammetry, Light Detection and Ranging (LIDAR), and Synthetic Aperture Radar (SAR) techniques. These methods can cover wide areas, substantially reducing the acquisition time of the images and the costs associated with them. The images can be captured periodically, enabling historical data to be collected and updated. The images are acquired and processed digitally, leading to accurate geometric measurements, qualitative object interpretations, and the generation of a Digital Elevation Model (DEM) assisted by a computer (Walstra et al, 2007; Jaboyedoff et al, 2012; González-Díez et al, 2014; Palenzuela et al, 2016; Ciampalini et al, 2016; Gorsevski et al, 2016; Cigna et al, 2017). Moreover, Airborne-based LIDAR and SAR are considered innovative methods for landslide

identification, classification, and geomorphology interpretation. Most importantly, they can perform the measurements over densely vegetated areas (Singhroy, 1995; Comer et al, 2017).

On a global scale, satellite-based methods for landslide monitoring are more effective than conventional methods based on landform analyses that are only useful over small areas. These satellite-based provide a large amount of information, such as precipitation, land-use, land-cover, and topography data, enabling a quasi-global landslide analysis model (Farahmand and AghaKouchak, 2013). The combination of this variety of data can be used as a base for developing a global landslide detection and forecasting system (Hong et al, 2007; Sassa et al, 2010). During the last two decades, the satellite-based system has provided earth observation using Synthetic Aperture Radar (SAR) data, e.g., Advanced Land Observation Satellite Phased Array type L-band Synthetic Aperture Radar (ALOS PALSAR). The Interferometry Synthetic Aperture Radar (InSAR) technique was developed and has been recognized as an accurate and low-cost method for measuring changes in the Earth´s surface with millimeter or even sub-millimeter accuracy, detecting and monitoring ground deformation and natural hazards (Massonnet and Feigel, 1998; Berardino et al, 2002; Nescoiu and Hooper, 2009). Furthermore, in terms of its application sequence, the InSAR technique was improved by removing the topography contribution in the production of interferograms. The "Differential" term was added to the acronym, which has become the well-known DInSAR. To improve the accuracy of DInSAR, two new algorithms as well as advanced processing were proposed. The first algorithm was proposed by Ferretti et al, (2001) and is widely known as Permanent Scatterer Interferometry (PSI); it has presented good results for deformation measurements in urban areas and on rocky terrain. The second algorithm was proposed by Berardino et al, (2002) and is widely known as the Small Baseline Subset (SBAS); it is very useful for detecting deformation in rural areas on regional and local spatial scales. DInSAR does not require the installation of any devices on the ground and has been widely used for measuring and monitoring the deformation of the Earth's surface. Furthermore, SBAS DInSAR performs better over vegetated areas and presents a better deformation distribution compared to PSI (Raucoules et al, 2007; Guzzetti et al, 2009; Samsonov et al, 2011; Ng et al, 2012; García-Davalillo et al, 2014; Necsoiu et al, 2014; Jebur

et al, 2015; Calvello et al, 2016; Morishita et al, 2016; Lu and Sun, 2017; Cigna et al, 2017; Yastika et al, 2019).

Nowadays, high-resolution aerial photogrammetry can be obtained by employing a generic and light remote sensing platform known as an Unmanned Aerial Vehicle (UAV) or a drone. The UAV is equipped with dual-band satellite positioning—namely, the Global Positioning System (GPS) and the Global Navigation Satellite System (GLONASS)—along with the latest Inertial Measurement Unit (IMU) technology and a 4K digital camera. UAV photogrammetry has been successfully used for mapping and producing valuable ground surface data in vast fields of application. In landslide investigations and monitoring processes, UAV photogrammetry has been considered a low-cost and timeless technique for acquiring high-resolution orthomosaic images and DEM data over a reasonable area of extension with centimeter-order accuracy (Walstra et al, 2007; Gong et al, 2010; Niethammer et al, 2012; Luccier et al, 2014; Turner et al, 2015; Peppa et al, 2016; Peternel et al, 2017; Fan et al, 2017; Cigna et al, 2017; Hu et al, 2018; Ma et al, 2018; O'Driscol, 2018; Rossi et al, 2018; Zhu et al, 2019; Pellicani et al, 2019; Li et al, 2020).

### *1.2.2 Approach of the present study*

DInSAR and UAV Photogrammetry techniques are widely applied for landslide and other geo-disaster monitoring. There is much literature in which the combination of InSAR, UAV Photogrammetry, field observations, and other conventional measurement instruments are presented. However, landslide or geo-disaster characteristics vary from place to place, even those in relative proximity to each other. Some literature also considers the local geoenvironmental characteristics that contribute to geo-disaster occurrences. An example of a literature review table on UAV Photogrammetry Landslide Monitoring is presented in Appendix 1.

Generally, the approach applied in this dissertation is almost the same. However, some specificity can be identified in this dissertation.

a) The application of InSAR and UAV photogrammetry techniques for landslide monitoring in this location, namely, Timor-Leste, is new. This work is considered as a preliminary study. No previous work can be found for this location.
b) The combination of DInSAR and UAV Photogrammetry along with field observations reveals a continuing slow movement of the ground following the average slope of about 12 degrees. This movement is well characterized by the recent contour line acquired from UAV. Even in small areas, DInSAR is also capable of detecting the distribution of and differences in ground displacement measurements and time series displacements.
c) The DInSAR LOS displacement time series reveals that the occurrence of multiple earthquake events, of a certain magnitude or greater, triggers the reactivation of landslides. However, the influence does not always appear immediately after the earthquake. On the other hand, heavy or long rainfall events induce landslides and/or changes in the ground, and their influence can appear a relatively short time after the event under specific ground conditions. Thus, the timing of the occurrence can often be disregarded. Accordingly, it can be confirmed, that ground deformation, earthquake events, and periodic rainfall events are clearly related.
d) Important pieces of evidence recorded during field observations accordingly prove the results of DInSAR.

### *1.2.3 Landslide study in Timor-Leste*

In Timor-Leste, no studies related to ground deformation, including landslides and land subsidence, have ever been carried out or published. However, a few studies have been done on landslides with some details in the master's theses by Soares (2007), Soares (2010), Martins (2011), Jones (2011), Alves (2012), Ximenes (2016), and Jesus (2018). While the study by Soares (2007) was a statistical analysis of landslides in an area in the west of the country, Soares (2010) analyzed an extremely large quaternary landslide in the Ainaro watershed, Martins (2011) analyzed the geomorphological risk in the Bobonaro region, Jones (2011) and Alves (2012) characterized the mass movement in Baucau, Ximenes (2016)

analyzed the geotechnical problems associated with road constructions and Jesus (2018) analyzed the slope stability and rockfall hazards along the Karimbala road. The spatial distribution and characteristics of landslides and land subsidence in Timor-Leste remain unclarified. Many reports have been produced by various entities, such as the government, UN, World Bank, Non-Governmental Organizations (NGOs), and local media, and are mainly related to the types of natural hazards experienced, material damage and loss, the number of victims and deceased, climate change, and humanitarian aid. However, there are no formal records or assessment techniques for the amplitude, frequency, and spatial distribution of the occurrences of natural and man-made disasters, including technical databases, such as hydrometeorology and detailed geology information. Thus, it is difficult to establish a system to monitor and mitigate landslides, including the associated damage they cause. The development of further research on ground deformation involves considerable challenges due to the lack of technical and scientific information.

### 1.3 Objective

The aim of this study is to apply the Remote Sensing technique to detect the recent ground surface deformation since 2007 in complex Landslide Slope in Bobonaro. In addition, Unmanned Aerial Vehicle (UAV) photogrammetry is employed to detect the ground deformation in detail along with the field observations. The relation of this ground deformation to earthquake and hard rainfall events is also discussed. Another aim of this paper is to increase people's consciousness of geo-disasters and their knowledge of how to best prepare for these disasters.

## References


Alves AE (2012) Caracterização dos movimentos de massa no distrito de Baucau (zona este) Master's thesis, Universidade de Évora, Portugal. http://hdl.handle.net/10174/15177

Barnett J, Dessai S, Jones RN (2007) Vulnerability to climate variability and change in East Timor. AMBIO: A Journal of the Human Environment 36(5):372-379. https://doi.org/10.1579/0044-7447(2007)36[372:VTCVAC]2.0.CO;2

BDDTL (2019) Baze Dadus Dezastres Timor-Leste. http://www.tldd.mss.gov.tl/

Berardino P, Fornaro G, Lanari R, Sansosti E (2002) A new algorithm for surface deformation monitoring based on small baseline differential SAR interferograms. IEEE Transactions on geoscience and remote sensing 40(11):2375-2383. https://doi.org/10.1109/TGRS.2002.803792

Calvello M, Peduto D, Arena L (2017) Combined use of statistical and DInSAR data analyses to define the state of activity of slow-moving landslides. Landslides 14(2):473-489. https://doi.org/10.1007/s10346-016-0722-6

Chang DTT, Tsai YS, Yang KC (2013) Study of Real-Time Slope Stability Monitoring System Using Wireless Sensor Network. Telkomnika 11(3):1478-1488. e-ISSN: 2087-278X

Ciampalini A, Raspini F, Frodella W, Bardi F, Bianchini S, Moretti S (2016) The effectiveness of high-resolution LiDAR data combined with PSInSAR data in landslide study. Landslides 13(2):399-410. https://doi.org/10.1007/s10346-015-0663-5

Cigna F, Banks VJ, Donald AW, Donohue S, Graham C, Hughes D, McKinley JM, Parker K (2017) Mapping ground instability in areas of geotechnical infrastructure using satellite InSAR and Small UAV surveying: A case study in Northern Ireland. Geosciences 7(3),51. https://doi.org/10.3390/geosciences7030051

Comer DC, Chapman BD, Comer JA (2017) Detecting landscape disturbance at the Nasca lines using SAR data collected from airborne and satellite platforms. Geosciences, 7(4),106. [https://doi.org/10.3390/geosciences7040106]

Cook AD, Suresh V, Nair T, Foo YN (2019) Integrating disaster governance in Timor-Leste: Opportunities and challenges. International Journal of Disaster Risk Reduction 35:12p. https://doi.org/10.1016/j.ijdrr.2018.12.013

Corominas J, van Westen C, Frattini P, Cascini L, Malet JP, Fotopoulou S, Catani Van Den Eeckhaut M, Mavrouli O, Agliardi F, Pitilakis K, Winter MG, Pastor M, Ferlisi S, Tofani V, Herva´s J, Smith JT (2014) Recommendations for the quantitative analysis of landslide risk. Bulletin of Engineering Geology and the Environment, 73(2),209-263. [https://doi.org/10.1007/s10064-013-0538-8]

Demoulin A, Glade T (2004) Recent landslide activity in Manaihan, East Belgium. Landslides 1(4):305-310. https://doi.org/10.1007/s10346-004-0035-z

Ding X, Ren D, Montgomery B, Swindells C (2000) Automatic monitoring of slope deformations using geotechnical instruments. Journal of Surveying Engineering 126(2):57-68. https://doi.org/10.1061/(ASCE)0733-9453(2000)126:2(57)

Duc DM (2013) Rainfall-triggered large landslides on 15 December 2005 in Van Canh district, Binh Dinh province, Vietnam. Landslides 10:219-230. https://doi.org/10.1007/s10346-012-0362-4

Fan X, Xu Q, Scaringi G, Dai L, Li W, Dong X, Zhu X, Pei X, Dai k, Havenith, HB (2017) Failure mechanism and kinematics of the deadly June 24th 2017 Xinmo landslide, Maoxian, Sichuan, China. Landslides 14(6):2129-2146. https://doi.org/10.1007/s10346-017-0907-7

Farahmand A, AghaKouchak A (2013) A satellite-based global landslide model. Nat. Hazards Earth Syst. Sci. 13:1259–1267. https://doi.org/10.5194/nhess-13-1259-2013

Ferretti A, Prati C, Rocca F (2001) Permanent scatterers in SAR interferometry. IEEE Trans. Geosci. Remote Sens. 39:8–20. https://doi.org/10.1109/36.898661

García-Davalillo JC, Herrera G, Notti D, Strozzi T, Álvarez-Fernández I (2014) DInSAR analysis of ALOS PALSAR images for the assessment of very slow landslides: the Tena Valley case study. Landslides 11(2):225-246. https://doi.org/10.1007/s10346-012-0379-8

Gong J, Wang D, Li Y, Zhang L, Yue Y, Zhou J, Song Y (2010) Earthquake-induced geological hazards detection under hierarchical stripping classification framework in the Beichuan area. Landslides 7(2):181-189. https://doi.org/10.1007/s10346-010-0201-4

González-Díez A, Fernández-Maroto G, Doughty MW, De Terán JD, Bruschi V, Cardenal J, Pérez JL,Mata E, Delgado J (2014) Development of a methodological approach for the accurate measurement of slope changes due to landslides, using digital photogrammetry. Landslides 11(4):615-628. https://doi.org/10.1007/s10346-013-0413-5

Gorsevski PV, Brown MK, Panter K, Onasch CM, Simic A, Snyder J (2016) Landslide detection and susceptibility mapping using LiDAR and an artificial neural network approach: a case study in the Cuyahoga Valley National Park, Ohio. Landslides 13(3):467-484. https://doi.org/10.1007/s10346-015-0587-0

Guzzetti F, Manunta M, Ardizzone F, Pepe A, Cardinal M, Zeni G, Paola R, Lanari R (2009) Analysis of ground deformation detected using the SBAS DInSAR technique in Umbria, Central Italy. Pure and Applied Geophysics 166(8-9):1425-1459. https://doi.org/10.1007/s00024-009-0491-4

Hong Y, Adler RE, Huffman GJ (2007) Satellite remote sensing for global landslide monitoring. Eos, Transactions American Geophysical Union 88(37):357-358. https://doi.org/10.1029/2007EO370001

Hu S, Qiu H, Pei Y, Cui Y, Xie W, Wang X, Yang D, Tu X, Zou Q, Cao P, Cao M (2018) Digital terrain analysis of a landslide on the loess tableland using high-resolution topography data. Landslides 16(3):617-632. https://doi.org/10.1007/s10346-018-1103-0

Jaboyedoff M, Oppikofer T, Abellán A, Derron MH, Loye A, Metzger R, Pedrazzini A (2012) Use of LIDAR in landslide investigations: a review. Natural hazards 61(1):5-28. https://doi.org/10.1007/s11069-010-9634-2

Jebur MN, Pradhan B, Tehrany MS (2015) Using ALOS PALSAR derived high-resolution DInSAR to detect slow-moving landslides in tropical forest: Cameron Highlands, Malaysia. Geomatics, Natural Hazards and Risk 6(8):741-759. https://doi.org/10.1080/19475705.2013.860407

Jesus, OVTD (2018) Slope Stability and Rockfall Hazard Analysis along Karimbala Road, Liquiça Municipality, Timor-Leste. Master's Thesis, Universidade de Coimbra, Coimbra, Portugal. http://hdl.handle.net/10316/86456

Jones FJG (2011) Caracterização dos movimentos de massa no distrito de Baucau:(Zona Oeste) (Master's thesis, Universidade de Évora, Portugal. http://hdl.handle.net/10174/14181

Kjekstad O, Highland L (2009) Economic and social impacts of landslides. In Landslides–disaster risk reduction (pp. 573-587). Springer, Berlin, Heidelberg. https://doi.org/10.1007/978-3-540-69970-5_30

Li HB, Xu YR, Zhou JW, Wang XK, Yamagishi H, Dou J (2020) Preliminary analyses of a catastrophic landslide occurred on July 23, 2019, in Guizhou Province, China. Landslides 17:719–724. https://doi.org/10.1007/s10346-019-01334-0

Lu X, Sun X (2017) Ground Subsidence Monitoring in Cheng Du Plain Using DInSAR SBAS Algorithm. In International Conference on Geo-Informatics in Resource Management and Sustainable Ecosystem (pp. 535-545). Springer, Singapore. https://doi.org/10.1007/978-981-10-3966-9_59

Lucieer A, Jong SMD, Turner D (2014) Mapping landslide displacements using Structure from Motion (SfM) and image correlation of multi-temporal UAV photography. Progress in Physical Geography 38(1):97-116. https://doi.org/10.1177/0309133313515293

Ma S, Xu C, Shao X, Ahang P, Liang X, Tian Y (2018) Geometric and kinematic features of a landslide in Mabian Sichuan, China, derived from UAV photography. Landslides 16(2):373-381. https://doi.org/10.1007/s10346-018-1104-z

Martins, BDOHRS (2011). Análise de riscos geomorfológicos na região de Bobonaro, Timor-Leste Master's Thesis, Universidade do Algarve, Portugal. http://hdl.handle.net/10400.1/1669

Massonnet D, Feigl KL (1998) Radar interferometry and its application to changes in the Earth's surface. Reviews of geophysics 36(4):441-500. https://doi.org/10.1029/97RG03139

Morishita Y, Kobayashi T, Yarai H (2016) Three-dimensional deformation mapping of a dike intrusion event in Sakurajima in 2015 by exploiting the right-and left-looking ALOS-2 InSAR. Geophysical Research Letters 43(9):4197-4204. https://doi.org/10.1002/2016GL068293

Necsoiu M, Hooper DM (2009) Use of emerging InSAR and LiDAR remote sensing technologies to anticipate and monitor critical natural hazards. Building safer communities — risk governance, spatial planning and responses to natural hazards. 58: NATO Science for Peace and Security, Series E: Human and Societal Dynamics. U. Fra Paleo ed. 246 – 267. https://doi.org/10.3233/978-1-60750-046-9-246

Necsoiu M, McGinnis RN, Hooper DM (2014) New insights on the Salmon Falls Creek Canyon landslide complex based on geomorphological analysis and multitemporal satellite InSAR techniques. Landslides 11(6):1141-1153. https://doi.org/10.1007/s10346-014-0523-8

Ng AHM, Ge L, Li X, Abidin HZ, Andreas H, Zhang K (2012) Mapping land subsidence in Jakarta, Indonesia using persistent scatterer interferometry (PSI) technique with ALOS PALSAR. International Journal of Applied Earth Observation and Geoinformation 18:232-242. https://doi.org/10.1016/j.jag.2012.01.018

Niethammer U, James MR, Rothmund S, Travelletti J, Joswig M (2012) UAV-based remote sensing of the Super-Sauze landslide: Evaluation and results. Engineering Geology 128:2-11. https://doi.org/10.1016/j.enggeo.2011.03.012

O'Driscoll J (2018) Landscape applications of photogrammetry using unmanned aerial vehicles. Journal of Archaeological Science Reports 22:32-44. https://doi.org/10.1016/j.jasrep.2018.09.010

Palenzuela JA, Jiménez-Perálvarez JD, El Hamdouni R, Alameda-Hernández P, Chacón J, Irigaray C (2016) Integration of LiDAR data for the assessment of activity in diachronic landslides: a case study in the Betic Cordillera (Spain). Landslides 13(4):629-642. https://doi.org/10.1007/s10346-015-0598-x

Palenzuela JA, Jiménez-Perálvarez JD, El Hamdouni R, Alameda-Hernández P, Chacón J, Irigaray C (2016) Integration of LiDAR data for the assessment of activity in diachronic landslides: a case study in the Betic Cordillera (Spain). Landslides, 13(4),629-642. [https://doi.org/10.1007/s10346-015-0598-x]

Pellicani R, Argentiero I, Manzari P, Spilotro G, Marzo C, Ermini R, Apollonio C. (2019) UAV and airborne LiDAR data for interpreting kinematic evolution of landslide movements: the case study of the Montescaglioso landslide (Southern Italy). Geosciences,9(6),248. [https://doi.org/10.3390/geosciences9060248]

Pellicani, R.; Argentiero, I.; Manzari, P.; Spilotro, G.; Marzo, C.; Ermini, R.; Apollonio, C. UAV and airborne LiDAR data for interpreting kinematic evolution of landslide movements: the case study of the Montescaglioso landslide (Southern Italy). Geosciences. 2019,9(6),248. https://doi.org/10.3390/geosciences9060248

Peppa MV, Mills JP, Moore P, Miller PE, Chambers JE (2016) Accuracy assessment of a UAV-based landslide monitoring system. ISPRS-International Archives of the Photogrammetry, Remote Sensing and Spatial Information Sciences 41:895-902. https://doi.org/10.5194/isprsarchives-XLI-B5-895-2016

Peternel T, Kumelj Š, Oštir K, Komac M (2017) Monitoring the Potoška planina landslide (NW Slovenia) using UAV photogrammetry and tachymetric measurements. Landslides 14(1):395-406. https://doi.org/10.1007/s10346-016-0759-6

Ramesh MV, Vasudevan N (2012) The deployment of deep-earth sensor probes for landslide detection. Landslides 9(4):457-474. https://doi.org/10.1007/s10346-011-0300-x

Raucoules D, Colesanti C, Carnec C (2007) Use of SAR interferometry for detecting and assessing ground subsidence. Comptes Rendus Geoscience 339(5):289-302. https://doi.org/10.1016/j.crte.2007.02.002

Rossi G, Tanteri L, Tofani V, Vannocci P, Moretti S, Casagli N (2018) Multitemporal UAV surveys for landslide mapping and characterization. Landslides 15(5):1045-1052. https://doi.org/10.1007/s10346-018-0978-0

Samsonov S, Beavan J, González PJ, Tiampo K, Fernández J (2011) Ground deformation in the Taupo Volcanic Zone, New Zealand, observed by ALOS PALSAR interferometry. Geophysical Journal International 187(1):147-160. https://doi.org/10.1111/j.1365-246X.2011.05129.x

Sassa K, Nagai O, Solidum R, Yamazaki Y, Ohta H. (2010) An integrated model simulating the initiation and motion of earthquake and rain induced rapid landslides and its application to the 2006 Leyte landslide. Landslides 7(3):219-236. https://doi.org/10.1007/s10346-010-0230-z

Shimizu, N.; Nakashima, S.; Masunari, T. ISRM Suggested Method for Monitoring Rock Displacements Using the Global Positioning System (GPS), Rock Mech. Rock Eng. 2014,47,313-328. https://doi.org/10.1007/978-3-319-07713-0_16

Singhroy V (1995) SAR integrated techniques for geohazard assessment. Advances in Space Research, 15(11),67-78. [https://doi.org/10.1016/0273-1177(95)00076-Q]

Soares L (2007) Actual condition and characteristics of slope failure in East Timor by multivariate statistical analysis. Master's Thesis, Saitama University, Japan.

Soares, S.F.V. (2010) The role of landslides in active mountain belts: A geomorphological study of East Timor. Master's Thesis, University of Melbourne, Australia.

TL-EDP (2011) Timor-Leste Strategic Development Plan. 279p. http://timor-leste.gov.tl/wp-content/uploads/2011/07/Timor-Leste-Strategic-Plan-2011-20301.pdf

Turner D, Lucieer A, de Jong S (2015) Time series analysis of landslide dynamics using an unmanned aerial vehicle (UAV). Remote Sensing, 7(2), 1736-1757. https://doi.org/10.3390/rs70201736

Uhlemann S, Smith A, Chambers J, Dixon N, Dijkstra T, Haslam E, Meldrum P, Merritt A, Gunn D, Mackay J (2016) Assessment of ground-based monitoring techniques applied to landslide investigations. Geomorphology 253:438-451. https://doi.org/10.1016/j.geomorph.2015.10.027

Walstra J, Chandler JH, Dixon N, Dijkstra TA (2007) Aerial photography and digital photogrammetry for landslide monitoring. Geological Society, London, Special Publications, 283(1), 53-63. https://doi.org/10.1144/SP283.5

Ximenes FGO (2016) Levantamento de Problemas Geotécnicos Associados à Construção de Vias de Comunicação. O Caso de Timor-Leste. Master's Thesis, Universidade do Porto, Portugal. https://repositorio-aberto.up.pt/bitstream/10216/85060/2/139263.pdf

Yastika PE, Shimizu N, Abidin HZ (2019) Monitoring of long-term land subsidence from 2003 to 2017 in coastal area of Semarang, Indonesia by SBAS DInSAR analyses using Envisat-ASAR, ALOS-PALSAR, and Sentinel-1A SAR data. Advances in Space Research, 63(5), 1719-1736. https://doi.org/10.1016/j.asr.2018.11.008

Zhu L, Deng Y, He S (2019) Characteristics and failure mechanism of the 2018 Yanyuan landslide in Sichuan, China. Landslides 16(12):2433-2444. https://doi.org/10.1007/s10346-019-01262-z

## Chapter 2

## LOCATION AND GEOENVIRONMENTAL SETTINGS

### 2.1 Overview of the country

Timor is a non-volcanic island located between the south-eastern part of the Indonesian archipelago and the northern part of the Australian continent (Audley-Charles, 1968). It is approximately 500 km long and 100 km at its greatest width, elongated in the SW-NE orientation. Timor-Leste comprises of the eastern half of Timor Island, including the enclave of Oecusse in West Timor, and two islands, Ataúro and Jaco, which correspond to about 15,000 km2 of territorial extension. Timor-Leste is a topographically mountainous country (Figure 2.1a). The flat area, with slopes in the range of 0% to 3%, occupies approximately 30% of the total country's extension. The rest is mountainous, with slopes between 3% and 25%. The mountain range located in the central region of the island, reaching the highest elevation at Ramelau Peak at 2960 m, belongs to the territory of Timor-Leste. This mountain range extends to the east following Matebean Peak at 2373 m and ending at Paichau Peak at 975 m. To the north side, the mountain slopes decrease, falling moderately and then almost abruptly into the ocean, characterized by a steep slope that extends practically along the entire coast. In contrast, to the south the relief is much smoother, forming a long flat coastal strip. This central region is crossed by a dense hydrographic network dividing the rainfall-runoff to the north and south through deep and narrow valleys with short steep courses to the sea. The dominant vegetation consists of grass and shrubs, and dense forests are spatially distributed in small areas. Bouma and Kobryn (2004) identified a significant level of deforestation and devegetation from 1989 to 1999. The types of soils identified in Timor-Leste are predominantly cambisols, vertisols and fluvisols (Garcia and Cardoso, 1978). Cambisols are spatially distributed in the highlands, vertisols in the lowlands, and fluvisols in coastal zones. Currently, the soil erosion levels are considered catastrophic (Gonçalves, 1966; Garcia and Cardoso, 1978; Bouma and Kobryn, 2004; Barnett et al, 2007). The rain distribution is affected by the mountainous terrain and the position of the island of Timor relative to the Australian mainland and the Indonesian archipelago (Figure 2.1a). The annual seasons are determined by the Australian monsoon (SE) and the Asian monsoon (NW). The

geography generates two distinct rainfall patterns: 1) the Northern Monomodal Rainfall Pattern, where the rainy season starts in December, has a duration of 4 to 6 months, and affects most parts of the north of the country and some eastern regions; 2) the Southern Bimodal Rainfall Pattern, where the rainy season starts in December, has a duration of 7 to 9 months and two rainfall peaks starting in December and May, and affects the southern side of the country (Thornwaite, 1948; Silva, 1956; Soares, 1957; Garcia and Cardoso, 1978; Keefer, 2000). The rainfall is extremely intense, with an annual average of more than 1500 mm in the mountainous areas and less than 1500 mm in the lowland areas (Thornwaite, 1948; Silva, 1956; Soares, 1957; Garcia and Cardoso, 1978). Timor is an island of rapid and relatively recent formation, located at the collisional margin between the oceanic Banda volcanic arc and the Australian continental margin. This location is characterized by deformation, uplift movement, and high seismic activity (Figures 2.1a and 2.1b). Several theories about the tectonic evolution of Timor have been proposed in relation to its structural complexity (Figure 2.1b). Two main tectonic models have been discussed, namely, the overthrust model (Audley Charles, 1968; Barber, 1981; Charlton, 1991) and the imbricate model (Hamilton, 1979; Kaneko et al, 2007; Ota and Kaneko, 2010). This tectonic mechanism is reflected in the mountainous characteristics of the island, followed by the fragmented and chaotic structures of thrust and fold zones illustrated by Norvick (1979) in (Figure 1c). Measurements indicate that the Australian continent is moving ~7 cm/yr NNE relative to the South Banda arc (Nugroho et al, 2009). Geologically, Timor Island presents great diversity and complexity in its lithology, characterized typically by softer sediments, shale, sand and limestone (Audley-Charles, 1968).

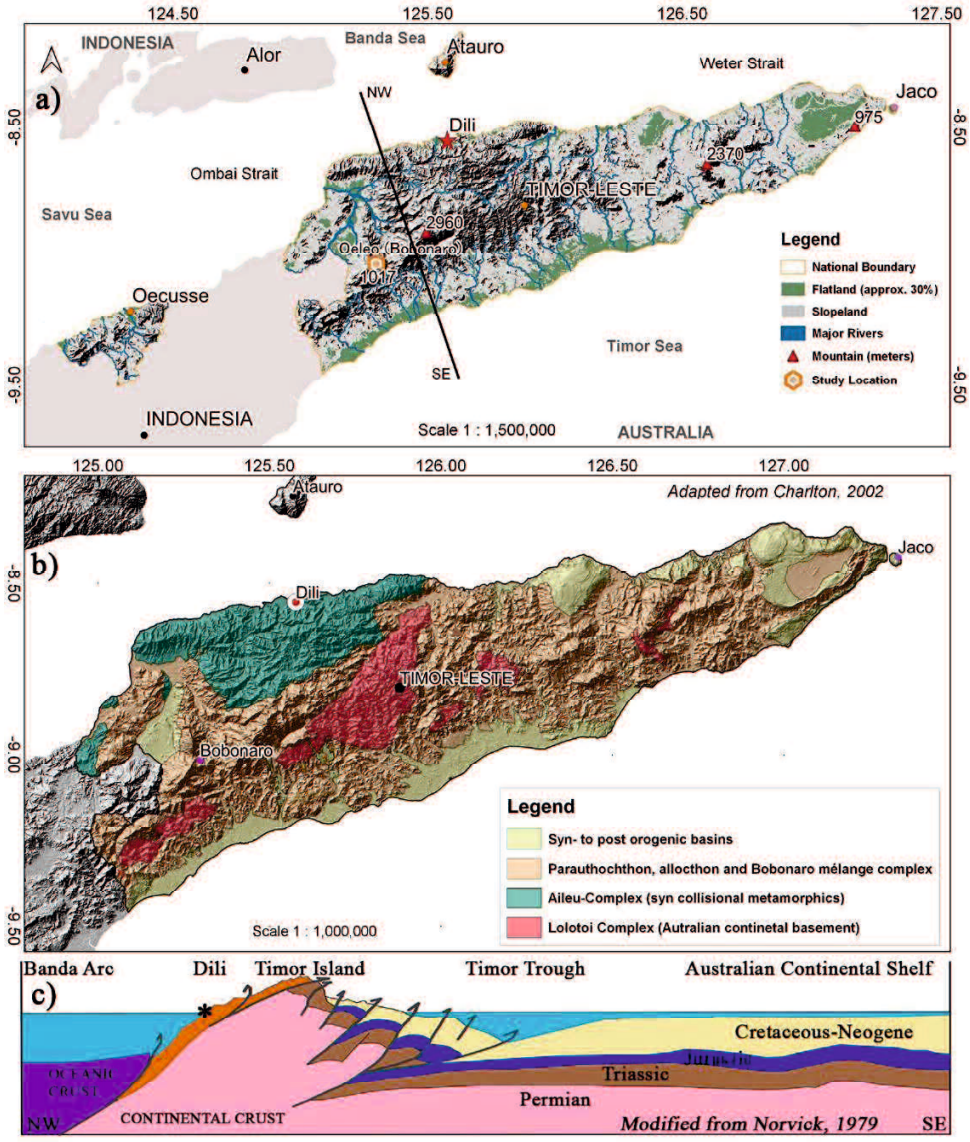


**Figure 2.1. a)** Simplified geomorphology of Timor-Leste, **b)** Simplified structural map of Timor-Leste (Charlton, 2002), and **c)** Mountainous characteristics of the island with fragmented and chaotic structures of thrust and fold zones (Novick, 1979)

## 2.2 Bobonaro region

The Bobonaro region is located in the center of Timor Island; it covers 216 km2 and is located 180 km from the capital, Dili. Its geographic coordinates range between 125.21694183° and −9.13041210°: 125.43438720° and −8.95447254°, and it is approximately 1000 m above the

mean sea level (Figure 2.1a). The Bobonaro Administrative Post is subdivided into 18 villages, with a total population of 24,719 (Census, 2015). This area is part of the Bobonaro Scaly Clay Formation, previously defined by Audley-Charles (1968) with a type-locality beside the Lomea River, east of Bobonaro City. Bobonaro Scaly Clay, also well known as Bobonaro mélange or broken formation, is much more widespread throughout Timor-Leste than any other existing geological formation. Bobonaro Scaly Clay is a lithotectonic unit composed mostly of broken, clay-rich layers that are mixed to varying degrees with structurally and stratigraphically overlying units. The layers range in thickness from thin to over 2000 m and contain blocks of all of the stratigraphic units in Timor, as well as serpentinites and metaigneous rocks, surrounded by a clay matrix (Harris et al, 1998). The matrix clay of the Bobonaro mélange is mostly composed of bentonitic clay with 35% average smectite (Audley-Charles, 1965). This type of clay commonly produces discontinuities and shear planes that lead to unstable hill slopes (Vannucchi and Betteli, 2010). The erosion of the Bobonaro Scaly clay formation due to the tropical conditions gives rugged topography to the region that is characterized by deep gullies, landslides, and knobbly hillsides (Audley-Charles, 1968).

### 2.3 Historical ground deformation

A large number of ground deformations, exposed by a variety of mechanisms and magnitudes, are spatially well distributed in the Bobonaro region. It has been possible to collect valuable information related to this phenomenon from the local people, extending from the past years to the present (Figure 2.2). The biggest landslide was registered in Fatuk Monu (literally Rock Fall) at the end of the 18th century. The phenomenon took place at the end of the wet season. There was no rain at the time; however, all the springs in the area were over-watered, which was not usual. At the time, Fatuk Monu was very populated with the Lamak Hitu ethnic people. This landslide occurrence was clearly remembered and passed down by people in the local culture by means of legends, prayers, dances, etc., and was reflected in the toponymy and in the names given to the new settlements or villages established in the Bobonaro region. The landslide completely destroyed the populated area, causing material damage as well as the loss of many human lives. After the catastrophe, new

settlement sites were established in the south, now Malilait, the current capital of the Bobonaro Administrative Post, and in the northern villages of Taimea and Grotu. In 1918, at the same place the Portuguese administration built a road passing through the old landslide area, linking Malilait and Taimea. However, the road has been impassable since 1969. At present, there are no traces of the road. The slope movement in that area has remained active on a small scale. In January 1983, a large ground movement occurred in the center of Bobonaro City, affecting the public buildings constructed in early 1956 as well as people, houses, and the main road, causing material damage but without the loss of human lives. Cracks on the walls and floors of buildings and on public roads have increased over time, caused by the phenomena of the slow movement of slopes. In February 2003, a landslide occurred in the village of Aiassa after rain continuously fell for more than four hours. The landslide started at midnight and continued until early morning, destroying one house and 40 parcels of garden land but without the loss of any human live.

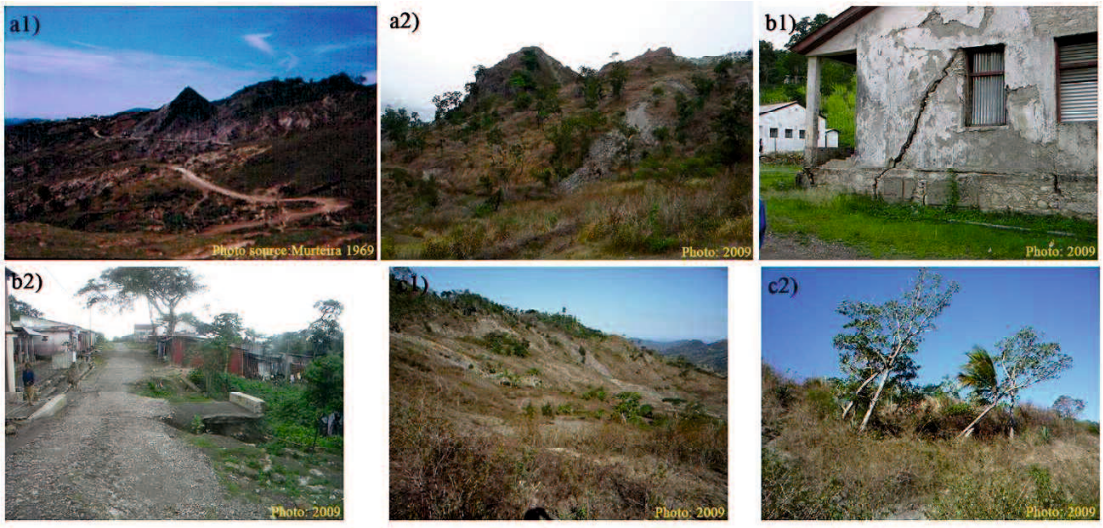


**Figure 2.2. a1)**, **a2**) Locations of old landslides at end of the 18th century, **a1**) road built in 1918 which has been impassable since 1969 and **a2)** present condition with no traces of the road, slope movement remained active on a small scale; **b1, b2**) Examples of damage due to ground movement in 1983; **c1), c2**) Locations of landslides occurring in 2003 and the condition of a tilted tree after adaptation over a period of six years as a natural witness

## 2.4 Types of mechanisms

The processes of ground deformation and landslides observed in the Bobonaro region are herein described following the Varnes (1978) classifications. The types of mechanisms vary from simple and isolated occurrences to more complex ones in a chain sequence from the peak of the mountain to the base. Figure 2.3 illustrates the types of mechanisms and their locations classified into three groups: (i) slopes closest to the top of the mountain, (ii) steep slopes or ravines, and (iii) more at the base of the slopes, that is, specifically in the areas near watercourses.

The slope became unstable along the riverbank; and consequently, it collapsed and was followed by other types of slope movements such as fall, topple, spread, sliding, and flow. It also resulted in the appearance of the deposition of detritus material close to the watercourses as a result of the flow-type movement. Sliding movements (translational or rotational) and debris flows normally contain large amounts of materials that can intercept the main streamline, consequently, generating a natural dam with the capacity to temporarily flood a wide area until the sediment is removed and transported naturally by the water stream.


**Figure 2.3.** Types of ground deformation mechanisms in the Bobonaro Region: **Group (i)** located closest to crest of a mountain, **Group (ii)** on a steep slope, and **Group (iii)** at the base of slopes and close to water courses

## 2.5 Study area

The study area is located in a highland, about 1000 m in altitude, within an area of 0.35 km2 of extension. Its surface is covered by grassland vegetation, with a moderate natural slope of around 12°. The natural condition of the study area is presented in a 3D model image along with the locations of the Points of Interest (POI) and Areas of Interest (AOI) (Figure 2.4). The material outcrops essentially consist of serpentinites and metaigneous rocks and are surrounded by a clay matrix (Figure 2.5). In 2007, a few months after the construction of the road, a section near the village of Oeleo began deforming. This phenomenon has continued to the present, causing damage to residential housing, agricultural fields, roads, and other infrastructures. Every year, this section of the road is affected by ground deformation, often making it impassable to vehicles during the rainy season. The area around this road section has widely shown ground surface deformation features. Recent evidence of the ground surface deformation includes degraded road conditions, a high density of ground fissures and cracks, slope movements, new water ponds, tilted electrical poles, and the ruins of a masonry

house, (Figures 2.4 and 2.6). Additional relevant information was collected from the local people and Google Earth historical imagery in order to confirm the evidence. The present authors clarified and recorded the four most notable pieces of evidence. The first three occurred at AOI2 and AOI3 and the fourth at AOI4. First, a masonry house was destroyed by a landslide in January 2017 during heavy rain, with material losses but no victims. Second, the electrical transmission line established in 2012 was deviated from the original alignment and tilted. Third, very frequent road restoration work has been performed during the rainy season with minimum conditions to allow the passage of transport vehicles. Fourth, a small slope failure induced by an earthquake event on 24 June 2019, with a magnitude of 7.3, occurred 518 km from the epicenter with a focal depth of 212 km.

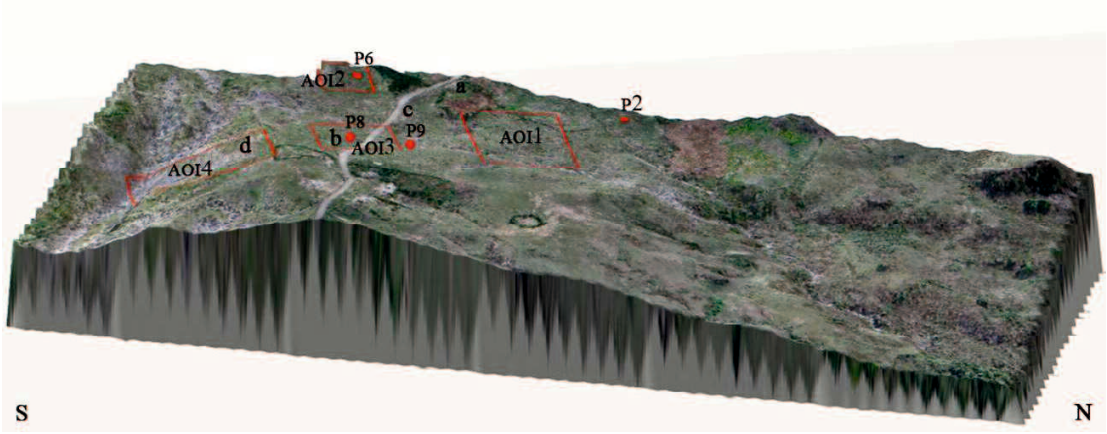


**Figure 2.4.** Study area in a 3D model and the positions of Points of Interest (POIs), Areas of Interest (AOIs), and photos of evidence

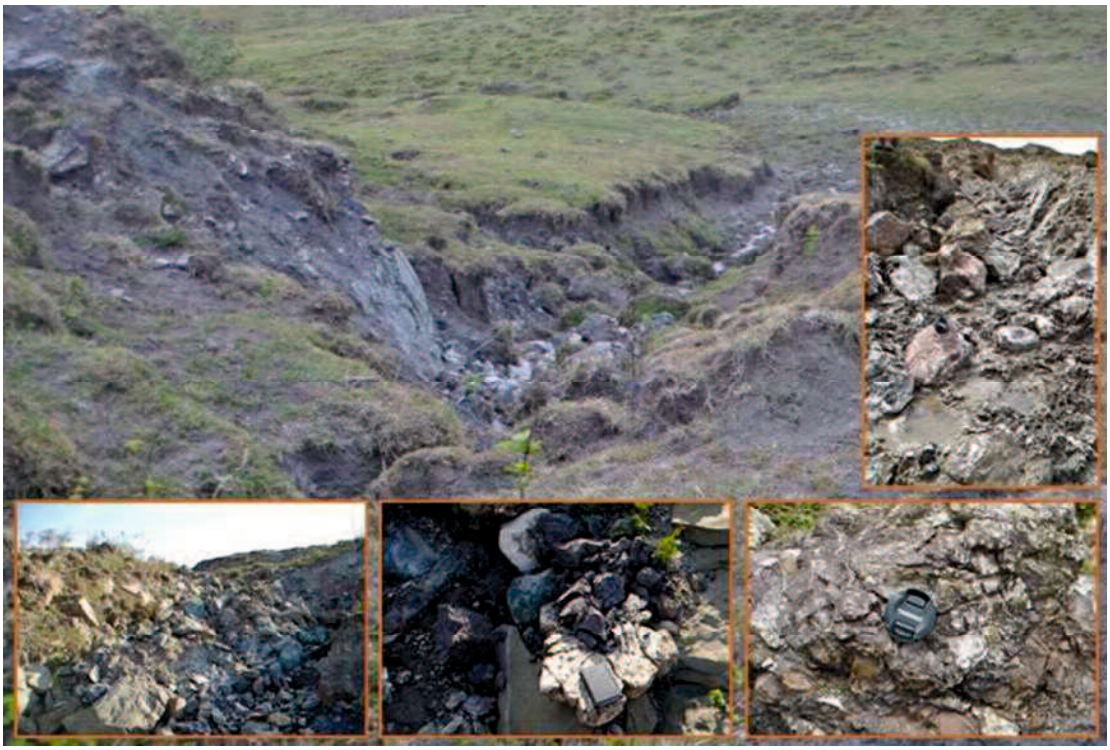

**Figure 2.5.** Types of material outcrops essentially composed of serpentinites and metaigneous rocks and surrounded by a clay matrix.

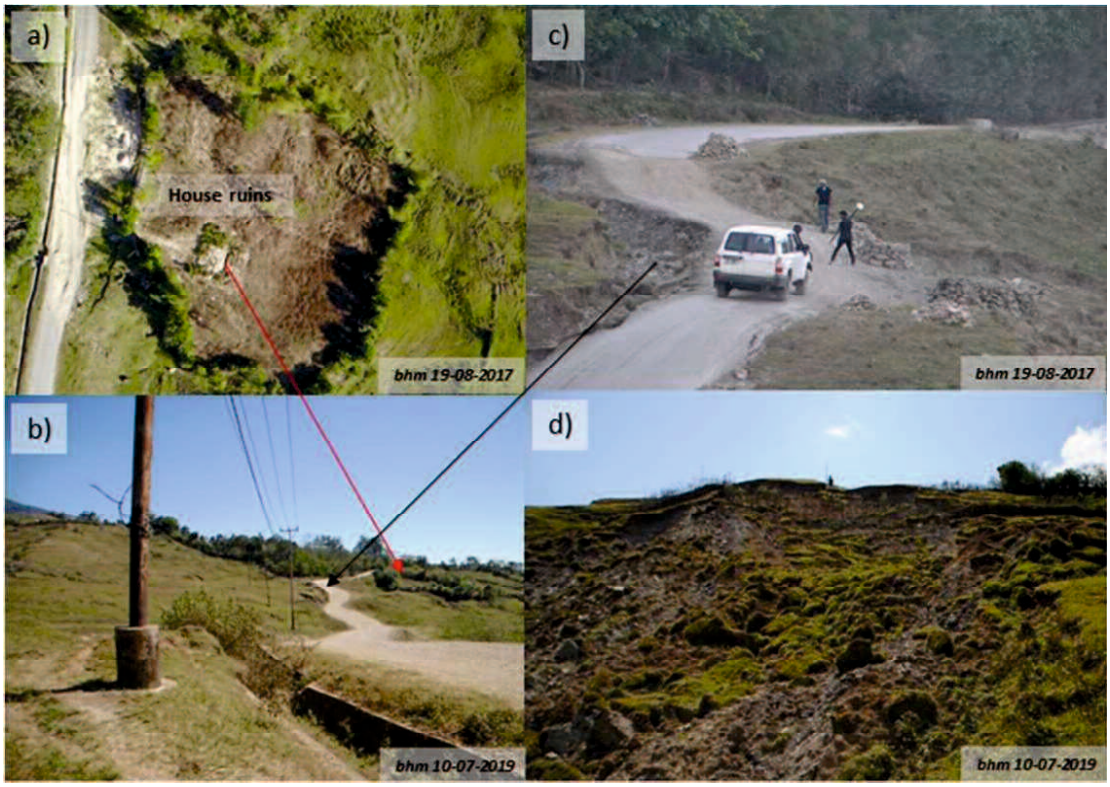


**Figure 2.6.** Evidence of ground deformation and its impact: **a**) house ruins, **b**) electrical pole that moved and tilted, **c**) degraded road conditions, and **d**) small landslide induced by an earthquake

## References


Audley-Charles MG, (1968) The geology of Portuguese Timor. Geological Society of London. Memoirs, 4, 4-84, 1968, https://doi.org/10.1144/GSL.MEM.1968.004.01.02

Bouma GA, Kobryn HT (2004) Change in vegetation cover in East Timor, 1989–1999. In Natural resources forum (Vol. 28, No. 1, pp. 1-12). Oxford, UK: Blackwell Publishing Ltd.. https://doi.org/10.1111/j.0165-0203.2004.00067.x

Garcia J, Cardoso J (1978) Os solos de Timor. Memórias da Junta de Investigações Científicas do Ultramar. Memoria's. N. º 64, II série,743p.

Gonçalves MM (1966) O Problema da Erosão em Timor. Missão de Estudos Agronómicos do Ultramar, Lisboa, N. º 236, 18p.

Thornthwaite, C.W. (1948) An Approach toward a Rational Classification of Climate. Geographical Review, 38(1), 55-94. http://dx.doi.org/10.2307/210739

Silva HJL (1956) Timor e a cultura do café, Lisboa. Junta de Investigações do Ultramar, Memória – Série de Agronomia Tropical I, 196p.

Soares FA (1957) O Clima e o Solo de Timor – Suas Relações com a Agricultura, Lisboa. Junta de Investigações do Ultramar (Estudos, Ensaios e Documentos. no. 34). pp. 118.

Keefer GD (2000) Report on Restoration of Meteorological Network-Timor Lorosa'e. United Nation Translation Administration in East Timor. 114p.

Barber AJ (1981) Structural interpretations of the island of Timor eastern Indonesia. Geological Research and Development Centre, Spec. Publ. 2: 183-197. http://searg.rhul.ac.uk/pubs/barber_1981%20Timor%20structure.pdf

Charlton TR, Barber AJ, Barkham ST (1991) The structural evolution of the Timor collision complex, eastern Indonesia. Journal of Structural Geology 13(5):489-500. https://doi.org/10.1016/0191-8141(91)90039-L

Hamilton WB (1979) Tectonics of the Indonesian region. Vol. 1078, US Government Printing Office. https://doi.org/10.3133/pp1078

Kaneko Y, Maruyama S, Kadarusman A, Ota T, Ishikawa M, Tsujimori, T., Ishikawa A, Okamoto K (2007) On-going orogeny in the outer-arc of the Timor–Tanimbar region, eastern Indonesia. Gondwana Research 11(1-2):218-233. https://doi.org/10.1016/j.gr.2006.04.013

Ota T, Kaneko Y (2010) Blueschists, eclogites, and subduction zone tectonics: Insights from a review of Late Miocene blueschists and eclogites, and related young high-pressure metamorphic rocks. Gondwana Research 18(1):167-188. https://doi.org/10.1016/j.gr.2010.02.013

Norvick MS (1979) The tectonic history of the Banda Arcs, eastern Indonesia; a review. Journal of the Geological Society. 136,5,519-526. https://doi.org/10.1144/gsjgs.136.5.0519

Nugroho H, Harris R, Lestariya AW, Maruf B (2009) Plate boundary reorganization in the active Banda Arc–continent collision: Insights from new GPS measurements. Tectonophysics 479(1-2):52-65. https://doi.org/10.1016/j.tecto.2009.01.026

Census (2015) Estatística de Timor-Leste. http://www.statistics.gov.tl

Harris RA, Sawyer RK, Audley-Charles MG (1998) Collisional melange development: Geologic associations of active melange-forming processes with exhumed melange facies in the western Banda orogen, Indonesia. Tectonics 17(3):458-479. https://doi.org/10.1029/97TC03083

Audley-Charles MG (1965) A Miocene gravity slide deposit from eastern Timor. Geological Magazine, 102(3):267-276. https://doi.org/10.1017/S0016756800053309

Vannucchi P, Bettelli G (2010) Myths and recent progress regarding the Argille scagliose, Northern Apennines, Italy. International Geology Review 52(10-12):1106-1137. https://doi.org/10.1080/00206810903529620

Varnes DJ (1978) Slope Movement Types and Processes. In: Schuster RL, Krizek RJ, Eds., Landslides, Analysis and Control, Transportation Research Board, Special Report No. 176, National Academy of Sciences pp11-33. http://onlinepubs.trb.org/Onlinepubs/sr/sr176/176.pdf

Charlton TR (2002) The structural setting and tectonic significance of the Lolotoi, Laclubar and Aileu metamorphic massifs, East Timor. Journal of Asian Earth Sciences, 20(7), 851-865. https://doi.org/10.1016/S1367-9120(01)00075-X

## Chapter 3

## GEO-DISASTERS CONSCIOUSNESS AND PREPAREDNESS OF THE PEOPLE

### 3.1 Introduction

Considerable improvements have recently been achieved in our understanding of the instability mechanisms and the availability of a wide range of monitoring and mitigation techniques have been achieved. However, geo-disasters still cause noteworthy losses of life and important economic losses all over the world (Corominas et al, 2013). Thus, knowledge and experience of the geomorphological processes and mechanisms are of fundamental importance to ensure the success of several human activities, such as the research of natural resources and urban planning (Conacher, 2002; Gregory and Goudie, 2011). The human occupation of the Earth's surface, through urban area expansion, and infrastructure development have led to the concept of geo-disasters, involving all surface phenomena capable of disturbing, in a more or less dramatic way, human lives and activities (Godschalk, 2003; Zêzere, 2007; Gaspar et al, 2008). It is clear that the concept of geo-disasters is directly linked with human lives and activities. Therefore, the geo-disaster consciousness and preparedness of the people are key factors to alert and to ensure the authorities to take important measures for the integration of the environmental component in the territorial development plans to guarantee and to build a safe and sound society (Castellanos Abella, 2008).

Timor-Leste is located in the southern-most part of Southeast Asia on the eastern half of the island of Timor and to the north of the Timor Sea, between Indonesia and Australia. The country has a population of approximately 1.2 million people, of which the population aged 0–14 represents 39%, that aged 15–59 represents 53%, and that aged above 60 represent 8% of the total population. Among them, 74% live in rural areas, whereas the rest live in urban areas (Census, 2015).

Timor Island is located near the intersection of three continental plates, thereby making it vulnerable to severe earthquakes (Audley-Charles, 2004). The annual seasons are determined by the Australian monsoon (SE) and the Asian monsoon (NW). The Rainfall distribution is

affected by mountainous terrains and generates two distinct rainfall patterns: (1) the Northern Monomodal Rainfall Pattern and (2) the Southern Bimodal Rainfall Pattern. According to the Northern Monomodal Rainfall Pattern, the monsoon season starts in December, continues for a duration of 4–6 months, and affects most northern and some eastern regions of the country. According to the Southern Bimodal Rainfall Pattern, the monsoon season starts in December, continues for a duration of 7–9 months, and has two rainfall peaks starting in December and May, thereby affecting the southern region of the country. This rainfall is intense, with an annual average of more than 1,500 mm in mountainous areas and less than 1,500 mm in low-lying areas. From a geomorphological perspective, Timor has been classified as an island of rapid and relatively recent formation, where erosion agents have not yet had time to shape and grade the relief. Therefore, the island presents an extremely rugged relief and is cut by deep valleys (Garcia and Cardoso, 1978).

The country is prone to severe and recurrent droughts, flooding and landslides, tropical cyclones, earthquakes and tsunamis. Landslides, flash floods, and debris flows are the most common geo-disasters in Timor-Leste, disrupting the land transport system by destroying bridges and washing out roads. According to the Baze Dadus Dezatres Timor-Leste (BDDTL) database for the period of 1992-2019, 60 deaths were recorded (Table 3.1).

**Table 3.1.** Data on deaths caused by geo-disasters from BDDTL-Database

| Event | Affected | House Destroyed | Death |
|---|---|---|---|
| Drought | 8502 | 0 | 0 |
| Wildfire | 1374 | 887 | 10 |
| Wind storm | 7954 | 1011 | 11 |
| Rain storm | 28 | 128 | 0 |
| Flash flood | 34 | 9 | 6 |
| Flood | 13667 | 771 | 26 |
| Landslide | 376 | 96 | 7 |

Data on the victims of various types of geo-disasters shows that 32 deaths were caused by flash flood and floods, 11 were caused by windstorms, 10 were caused by wildfires and 7 were caused by landslides. Despite the efforts of international agencies and the local government to introduce disaster management education among the population, the country

is facing an extreme lack of capacity to adapt to natural and man-made disasters. The country's vulnerability to both natural disasters and their impacts has presented considerable challenges for the country, and problems related to the lack of institutional capacity are making it increasingly difficult to overcome these challenges (Cook et al, 2019).

### 3.2 Objective

The objective is to gather information regarding the consciousness and preparedness among the people in Timor-Leste for geo-disasters.

### 3.3 Methodology

This study has applied a descriptive questionnaire method, focusing on the local population by interviewing them spontaneously, without the presence or influence of the local authorities or NGOs. The questionnaire survey was conducted in 2018, distributed in areas with variations in local geomorphology conditions and types of geo-disaster occurrences. The questionnaire targeted people living in rural places located in coastal and mountainous areas (Figure 3.1). The targeted respondents were adults, who were preferably homeowners or heads of their households. The confidentiality of the respondents of the questionnaire has been maintained and the data has been used for research purposes only. The total number of respondents was 166 householders, from a total of 3,191 households. The average members per households is 5.5.The respondents come from 27 villages (Table 3.2), spatially distributed around the Bobonaro region (Figure 3.1).

**Table 3.2** Location and number of respondents from each *Aldeia* (Village)

| Index | Municipality | Administrative Post | Suco | Aldeia | Respondents |
|---|---|---|---|---|---|
| 1 | Ainaro | Maubisse | Maubisse | Vila | 32 |
| 2 | Ainaro | Maubisse | Aituto | Aihou | 10 |
| 3 | Bobonaro | Bobonaro | Aiassa | Ai-Assa | 11 |
| 4 | Bobonaro | Bobonaro | Bobonaro | Lactil | 4 |
| 5 | Bobonaro | Bobonaro | Bobonaro | Lesigatal | 3 |
| 6 | Bobonaro | Bobonaro | Malilait | Taimea | 4 |
| 7 | Bobonaro | Bobonaro | Lourba | Zo-Belis | 2 |
| 8 | Bobonaro | Bobonaro | Oeleo | Oeleo Tas | 7 |
| 9 | Bobonaro | Bobonaro | Tapo | Tapo Tas | 3 |
| 10 | Bobonaro | Maliana | Tapo/Memo | Lepguen | 6 |
| 11 | Bobonaro | Maliana | Lahomea | Galasapulu | 1 |
| 12 | Bobonaro | Lolotoe | Lebos | Mapelai | 1 |
| 13 | Bobonaro | Atabae | Aidabaleten | Biacou | 4 |
| 14 | Bobonaro | Atabae | Aidabaleten | Sulilaran | 4 |
| 15 | Bobonaro | Atabae | Aidabaleten | Tasi Mean | 5 |
| 16 | Bobonaro | Atabae | Aidabaleten | Tutubaba | 4 |
| 17 | Liquiça | Maubara | Guguleur | Raenaba | 2 |
| 18 | Liquiça | Maubara | Vaviquinia | Delesuvati | 2 |
| 19 | Liquiça | Maubara | Vaviquinia | Morae | 2 |
| 20 | Liquiça | Maubara | Vatuboro | Vaupu | 2 |
| 21 | Liquiça | Maubara | Vatuboro | Cai-Bair | 2 |
| 22 | Liquiça | Maubara | Guguleur | Dair | 2 |
| 23 | Liquiça | Maubara | Guguleur | Palistla | 5 |
| 24 | Manufahi | Same | Betano | Bemetan | 19 |
| 25 | Manufahi | Same | Betano | Loro | 1 |
| 26 | Manufahi | Same | Betano | Sessurai | 24 |
| 27 | Covalima | Suai | Suai Loro | Lo'o | 4 |
| | | **Total respondents** | | | **166** |

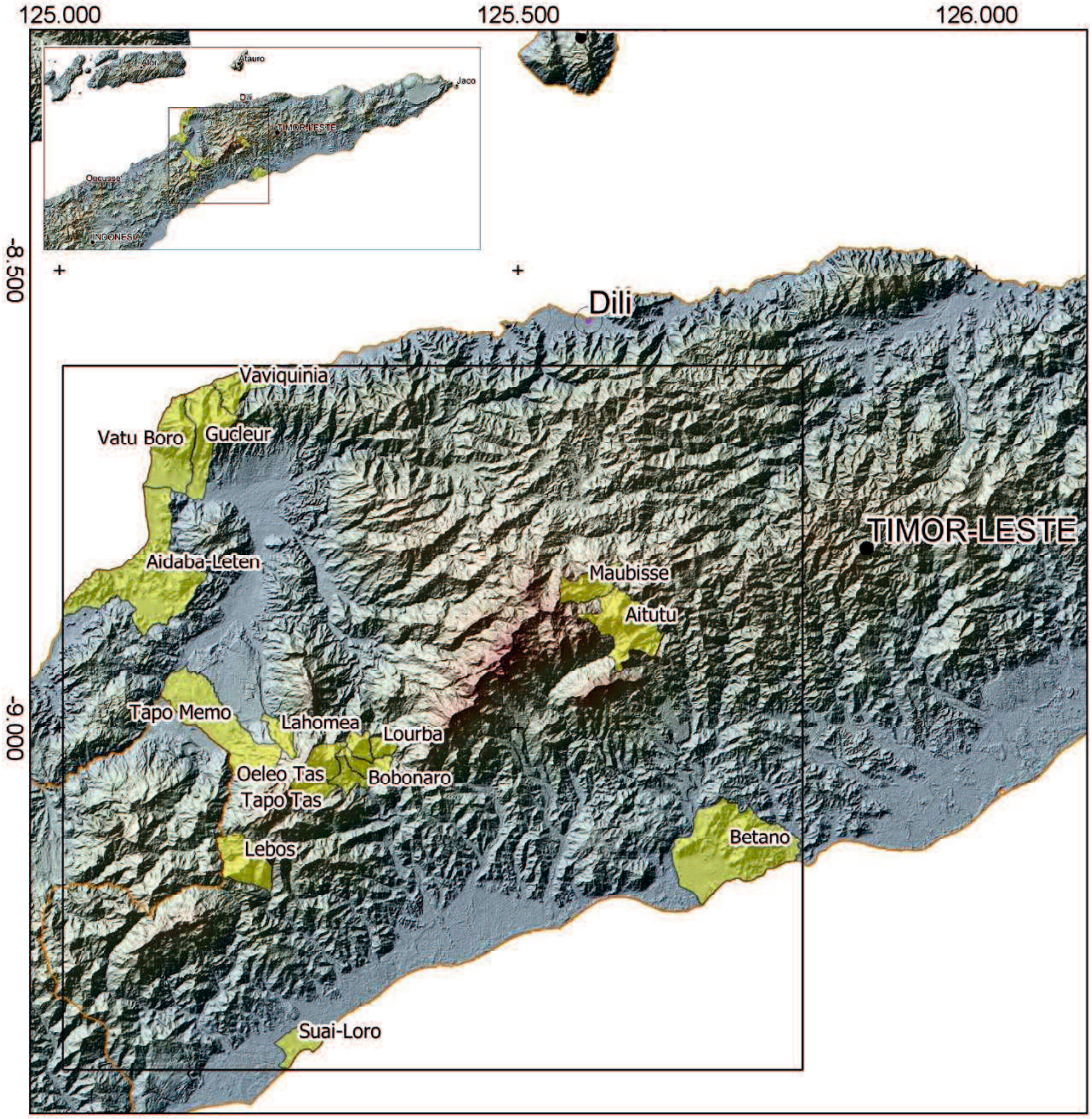


**Figure 3.1** Distribution map of respondents

## 3.4 Results and discussion

### *3.4.1 Respondents information*

The general householders were 69% male and 31% female, 61% young and 3% elderly. Illiterate householders comprised 20% and those with a tertiary education comprised 19%. Among the total respondents, 45% of them reported agriculture as their occupation, whereas

19% of the respondents selected 'Public Servant' as their occupation. Moreover, 51% of the respondents were living in mountainous areas (Figure 3.2).

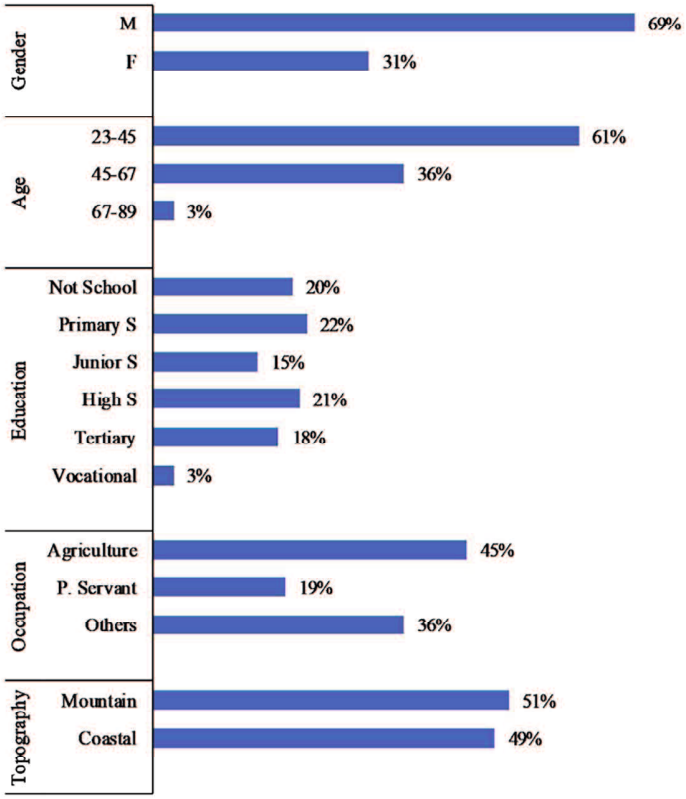


**Figure 3.2.** General information about householders

### *3.4.2 Results of the questionnaire*

The respondents expressed concern over the type of geo-disasters affecting their communities (Figure 3.3). Their choices were based on the type of geo-disasters and the level of concern varied from one location to the other. Based on the results of the questionnaire, it was evident that the respondents were familiar with each type of geo-disaster presented in the questionnaire. Rainstorms and windstorms scored the highest percentages, followed by landslides and ground deformation. On the other hand, 56% of the respondents were unconcerned about tsunamis and only 26% of the respondents expressed concerns over this type of geo-disaster. The majority of the respondents, 85%, had lived at their current location for a maximum of more than 10 years, and a minimum of 1–5 years.

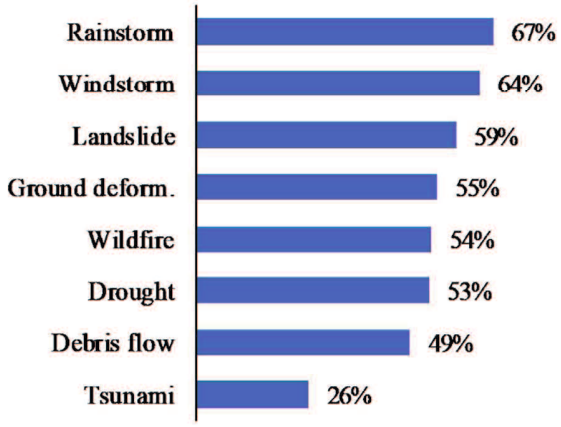


**Figure 3.3.** Consciousness of the types of geo-disasters

Among the respondents, 61% had received information about their houses being located in a natural risk zone. Among the total respondents, 34% reported elderly residents as their source of information, whereas 20% selected the local authorities, and 7% selected NGOs. During the past 10 years, 67% of the respondents noted that they, or someone in their household had experienced a geo-disaster. Rainstorms represented the highest percentage, followed by landslides, ground deformation, and windstorms (Figure 3.4).

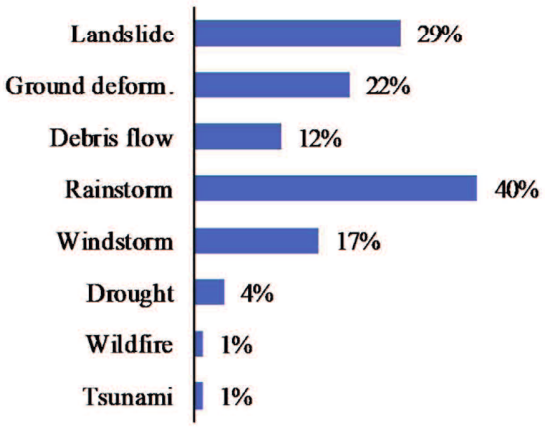


**Figure 3.4.** Geo-disasters experienced over 10 years

Most respondents had not received information about ensuring the safety of their families and homes against geo-disasters. Among the respondents, 75% had not received logistic or financial support. However, the remaining 25% of the respondents reported having received support from their neighbors, the local government, and/or NGOs (Figure 3.5).

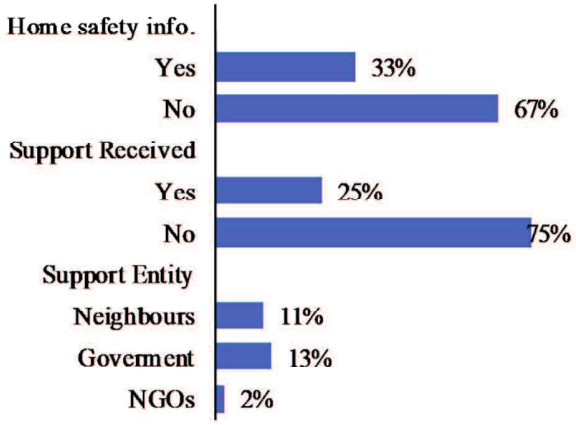


**Figure 3.5.** Family/home safety information and logistic/financial support

Considering the number of respondents that were illiterate, the most effective way through which respondents received information about ensuring the safety of their homes against geo-disasters was found to be through television broadcasts, representing 46%, followed by the local authorities at 36%, and radio broadcasts at 34%. Moreover, it was noted that 6% of the respondents were unconcerned about geo-disasters information (Figure 3.6).

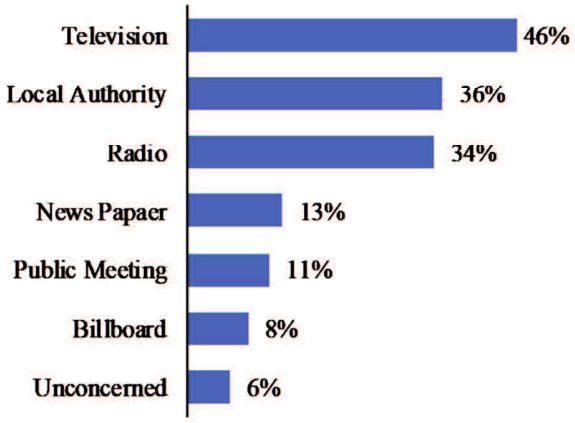


**Figure 3.6.** Effective methods for receiving information about geo-disasters

The responses to the typical questions prepared by FEMA (2002), related to emergency preparedness in the case of geo-disasters (Table 3.3), showed that most respondents were unconcerned about this topic. Figure 3.7 illustrates that more than 50% of the respondents have not completed any of these activities. Among the total respondents, of 28% had attended a meeting or received information regarding geo-disaster preparedness and had received training in First Aid or CPR.

**Table 3.3.** Typical questions related to emergency preparedness in the case of geo-disasters, prepared by FEMA (2002)

| **Have you or someone in your household:** | |
|---|---|
| **Q11a** | Attended meetings or received written information on natural disasters or emergency preparedness? |
| **Q11b** | Talked with family members about what to do in case of a disaster or emergency? |
| **Q11c** | Developed a "Household/Family Emergency Plan" in order to decide what everyone would do in the event of a disaster? |
| **Q11d** | Prepared a "Disaster Supply Kit" (extra food, water, medications, batteries, first aid items and other emergency supplies)? |
| **Q11d** | Has anyone been trained in First Aid or Cardio-Pulmonary Resuscitation (CPR)? |

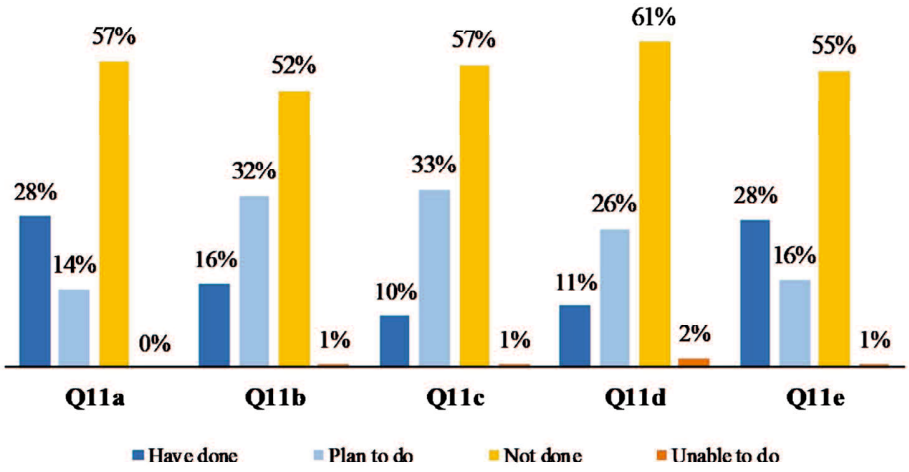


**Figure 3.7.** Emergency preparedness in the case of geo-disasters

Natural and man-made disasters can significantly impact a community. However, planning for these events can help to reduce the impact. The following question was also presented in the questionnaire survey: "Is it very important for the authorities and the community to develop, in the future, a plan to face those hazards?". The remarkable and spontaneous response from the respondents, with a majority of 91%, was answering "very important". They requested that the authorities, as soon as possible, draw up and present a national plan to reduce the risks caused by nature and humankind. In general, the respondents stated that they had selected the locations where their houses had been built. Moreover, while selecting their house locations, 51% of the respondents said that they had considered the potential occurrence of geo-disasters. Among the total respondents, 48% said that they were willing to spend more money to repair their houses with fissures or damages to make them more resistant to geo-disasters, whereas 52% of the respondents said that they would prefer not to reinforce their existing houses, but to move to another location. The preferred material for building houses was masonry, noted by 62% of the respondents, instead of local materials which would be used to build traditional houses. To select a safer location for building their houses, 60% of the respondents preferred to make the decision together with a public agency, whereas 40% of the respondents preferred to continue living at their current locations, despite being aware of the risk of remaining there. The complete charts of the questionnaire survey

results are presented in Appendix 2. Figure 3.8 presented an example of the conditions in the study area, for example, how the people are living and dealing with geo-disasters and how they make decisions in terms of survival in times of geo-disasters.


**Figure 3.8. a)** Location of house destroyed by a landslide in January 2017, **b)** New place chosen to build new house after January 2017 landslide, **c)** Expensive house built on unstable ground, **d)** House roof destroyed by a windstorm in February 2018, **e)** Landslide induced by an earthquake on 24$^{th}$ June 2019, and **f)** Location of the study area related to the ground deformation

### 3.5 Countermeasures

There are two well-known types of natural risk prevention and mitigation measures, namely, hard and soft countermeasures. Hard countermeasures consist of the construction of heavy infrastructures, such as retaining walls and dams. This measures require a high state budget. Soft countermeasures consist of enhancing the capacity and promoting the collaboration of stakeholders (Okubo, 2015). Since attaining its independence, Timor-Leste has faced

considerable challenges in managing natural and man-made disasters over the years. These challenges reflect the limitations of institutional and financial knowledge as well as the technical training of agents (Cook, 2019). Hard countermeasures would be difficult to implement in Timor-Leste and are expensive. Soft countermeasures are implemented by strengthening the institutional capacity, promoting stakeholder coordination, and improving the disaster response plan, thus providing the an ideal solution. This approach will be very important for increasing the people's consciousness and preparedness. It will also increase the values presented in Figure 3.6 to reach at least 50% in the short term. One advantage for Timor-Leste is that a higher percentage of the population, more than 50%, is in the age range of students attending school (Census, 2015). Therefore, it is important to incorporate knowledge about the prevention and reduction of natural and man-made disasters into the school curriculum. UNICEF and UNESCO have recognized the effectiveness and importance of the role of education in reducing vulnerability and in increasing the resilience of children and young people because of examples of the successful implementation of these plans in 30 countries (Selby and Kagawa, 2012). The knowledge, experiences, and perspectives that children acquire at school can easily spread throughout society to help ensure the safety and well-being of the students and of the entire society.

## 3.6 Conclusion

The results show that, among a total of 166 respondents, many people are aware of geo-disasters and their associated risks, such as landslides, ground deformation, debris flows, rainstorms, windstorms, droughts, wildfires, and tsunamis. However, they consider the occurrence of these disasters to be rare. Among the respondents, 34% reported that they had received information regarding previous geo-disasters from elderly people, whereas 20% reported that they had received this information from the local authorities, and 7% reported that they received this information through NGOs. More than 52% of the respondents stated that they were unaware of any plans related to geo-disaster emergency preparedness. Most respondents (91%) considered it important for the government to develop future plans through community participation regarding geo-disaster mitigation. Most respondents (51%)

were aware of the possibility of geo-disasters occurring at their current locations, whereas the remaining respondents were not concerned about this problem. Therefore, 52% of the respondents choose not to spend more money to strengthen the structure of their homes, in order to increase their resistance to geo-disasters. Among the respondents, 62% said they would prefer to build masonry houses, instead of opting for traditional architecture, despite the unstable ground conditions. Moreover, 60% of the respondents would prefer, on their own initiative or with the guidance of the government, to search for houses in safer locations. One advantage for Timor-Leste is that a higher percentage of the population, more than 50%, is in the age range of students attending school. The introduction of knowledge, experiences, and perspectives on the reduction and prevention of natural and man-made risks into the school curriculum is considered an effective soft countermeasure. This will be important for reducing their vulnerability to geo-disasters and for building resilience among children and young people, thereby benefiting society through information diffusion by students.

**Acknowledgements**

We would like to express our deepest gratitude to Alex Marques, Elfrido Neus and Alcino dos Santos for their partial contributions in completing the questionnaire survey, in the Maubisse and Betano areas, as well as to everyone else who provided valuable information for this chapter.

## References


Audley-Charles M G (2004) Ocean trench blocked and obliterated by Banda forearc collision with Australian proximal continental slope. Tectonophysics, 389 (1-2), 65-79. https://doi.org/10.1016/j.tecto.2004.07.048

BDDTL (2019) http://www.tldd.mss.gov.tl/.

Castellanos Abella EA (2008) Multi-scale landslide risk assessment in Cuba, Utrecht, Utrecht University. ITC Dissertation number 154, 273p. [https://dspace.library.uu.nl/handle/1874/30890]

Census, (2015): http://www.statistics.gov.tl.

Conacher A (2002) A role for geomorphology in integrated catchment management. Australian Geographical Studies, 40(2),179-195. [https://doi.org/10.1111/1467-8470.00173]

Cook AD, Suresh V, Nair T, Foo YN (2019) Integrating disaster governance in Timor-Leste: Opportunities and challenges. International Journal of Disaster Risk Reduction 35:12p. https://doi.org/10.1016/j.ijdrr.2018.12.013

Corominas J, van Westen C, Frattini P, Cascini L, Malet J P, Fotopoulou S, Catani Van Den Eeckhaut M, Mavrouli O, Agliardi F, Pitilakis K, Winter MG, Pastor M, Ferlisi S, Tofani V, Herva´s J, Smith JT (2014) Recommendations for the quantitative analysis of landslide risk. Bulletin of Engineering Geology and the Environment, 73(2),209-263. [https://doi.org/10.1007/s10064-013-0538-8]

FEMA (2002) Federal Emergency Management Agency. https://www.fema.gov/

Garcia J, Cardoso J, (1978) Os solos de Timor. Memórias da Junta de Investigações Científicas do Ultramar. Memoria's. N. º 64, II série,743p.

Gaspar J, Fernandez Rodriguez J, Queirós M, Henriques EB, Palma P, Vaz T (2008). Determinação das Vulnerabilidades Humanas em Situação de Risco Sísmico e Tsunamis. O Caso do Algarve. ANPC e Faculdade de Letras/Centro de Estudos Geográficos da Universidade de Lisboa, Inforgeo, p51-66.

Godschalk DR (2003) Urban hazard mitigation: creating resilient cities. Natural hazards review, 4(3), 136-143. [https://doi.org/10.1061/(ASCE)1527-6988(2003)4:3(136)]

Gregory KJ, Goudie AS (2011). The SAGE handbook of geomorphology. SAGE publications. London, p645

Okubo N (2015) Disaster Management in Japan: Towards Comprehensive and Collaborative Flood Control. Carbon & Climate Law Review, 9(1), 32-39. https://www.jstor.org/stable/43859671

Selby D, Kagawa F (2012) Disaster risk reduction in school curricula: case studies from thirty countries. UNESCO and UNICEF, ISBN 978-92-3-001087-4. http://repositorio.minedu.gob.pe/handle/123456789/4189

## Chapter 4

# FACTORS TRIGGERING LANDSLIDES IN TIMOR-LESTE

## 4.1 Introduction

The geomorphology, geoenvironment, and climate of the country has led to frequent landslides and flood occurrences. These phenomena have caused damage with both direct and indirect negative impacts on the population, housing, gardens, equipment, infrastructure, and safety of the people. The main factor triggering landslides in Timor-Leste is rainfall. Thus, landslides often occur during the rainy season. However, there is no information on earthquake-induced landslides or combined rainfall events, although Timor-Leste is in a zone of high seismic risk. Timor-Leste is facing an extreme lack of capacity to adapt to natural and man-made disasters. Timor-Leste has been experiencing serious problems due to natural disasters, specifically landslides (Barnett et al, 2007; Cook et al, 2019). Nevertheless, there are no formal records or assessment techniques for the amplitude and frequency of landslide occurrences. In addition, scientific studies and research have either not been carried out or have not been published. Thus, it is difficult to establish a system to monitor and mitigate landslides and the associated damage they cause.

## 4.2 Objective

The aim of this chapter is to expose the ground instability and slope failure that are commonly triggered by torrential rainstorms and the influence of earthquakes due to topography changes of the ground level. As there are no formal records or evaluation techniques for the amplitude and frequency of landslide occurrences, current records and observations covering the last ten years are presented. Even without records of landslides caused by earthquakes, the tectonic activity cannot be ignored because Timor-Leste is located in a collisional region with high seismic intensity.

## 4.3 Study area

The study area is in the Bobonaro region, which belongs to the Bobonaro Administrative Post in Universal Transverse Mercator (UTM) Zone 51 South (E746304.000-765517.000, N9009266.000-89899147.000) approximately 950 meters above mean sea level. The area covers 216 km2 and is subdivided into 18 sucos (villages). The capital of the Administrative Post of Bobonaro is located in the Bobonaro Suco. This area was selected after considering the spatial distribution of landslides and ground subsidence, geological and geomorphological features of the terrain, main or national roads, the electrical distribution network, public and social infrastructures, population concentrations, and public services.

## 4.4 Data sources

Earthquake data from the USGS (United State Geological Survey), covering the period from January 2007 to February 2011 was employed to investigate the relationship between earthquakes and ground subsidence in Oeleo suco.

Rainfall data from 1953 to 1974 were used to analyze the intensity and distribution of past rainfall. Recent rainfall data (March 2017 to March 2018) were used to investigate the relationship between rainfall and the landslide occurrence on 17 January 2018.

## 4.5 Results and discussion

The instability of the terrain and mass movements are widespread phenomena that illustrate the landscape of the study area; they vary in their mechanisms and magnitudes. There are two main triggering factors that induce landslides and ground subsidence, namely, earthquakes and rainfall. They will be analyzed in this study.

### *4.5.1 Earthquake*

The earthquake catalogue with more than one century of records, was downloaded for free from the USGS website. Based on the data, the Seismic Map for the period from 1990 to

2018 could be generated in the Quantum Geographical Information System (QGIS) as shown in Figure 4.1. The map shows that the seismic activity in the Timor region is very high. The eastern part of the region is dominated by deep earthquakes and the northern part of Timor is dominated by shallow earthquakes. The epicenters of the shallow and deep earthquakes are located on Timor Island and in the Timor Sea, respectively. Ten earthquakes that occurred within the study period, with epicenters within and around the study area, were analyzed in this study. The magnitude and depth of the earthquakes varied from 4.2 to 5.0 and 10 to 51.4 km, respectively (Figure 4.2).

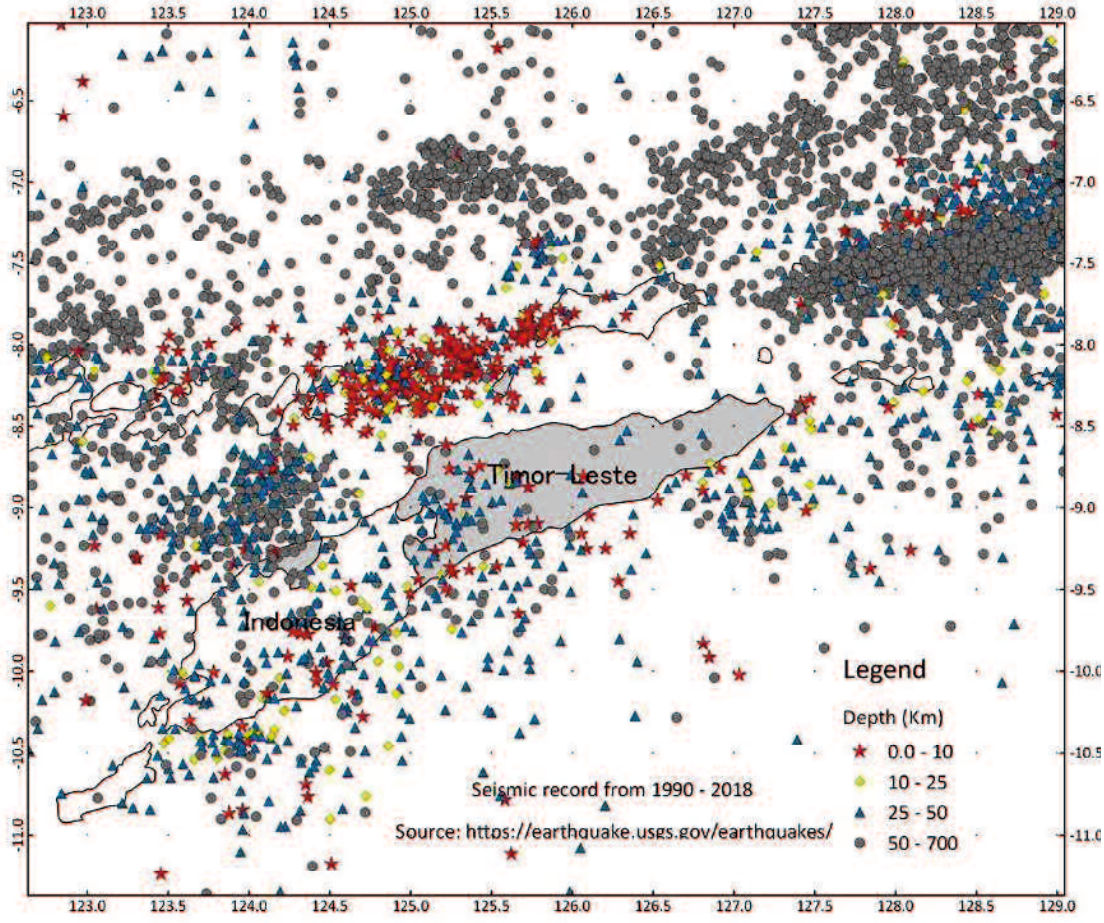


**Figure 4.1.** Seismic distribution map for period 1990 to 2018

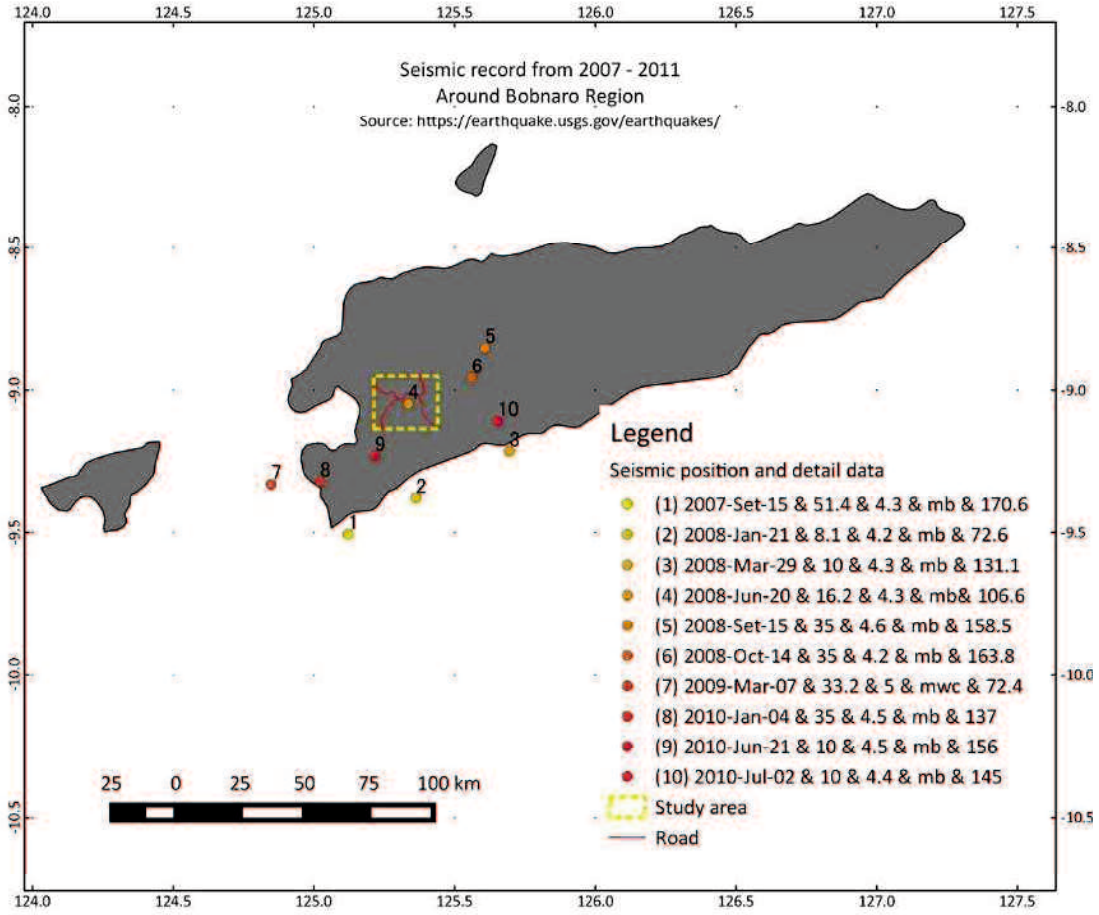


**Figure 4.2**. Ten earthquake events distributed around the study area

The seismic map (Figure 4.2) shows the ten epicenter locations and the sequences of the earthquake events from 1–10. The sequences seem to form three parallel lines, that is, the first line (1, 2, 3), the second line (4, 5, 6), and the third line in the middle (7, 8, 9, 10) - and have the same direction (NEE). The first line shows the earthquake depth movement from deep to shallow. The second line shows the movement from shallow to deep and the third line shows the movement back from deep to shallow. Five of the ten earthquakes occurred in 2008, with a maximum of three-month's time interval. The seismic wave is a body wave, which moves through the interior of the Earth as P and S waves, which shaking the ground in different ways (USGS, 2018). The three other earthquake events occurred in 2010. The

earthquake with the maximum magnitude occurred in 2009 and the deepest earthquake occurred in 2007 (Figure 4.3).

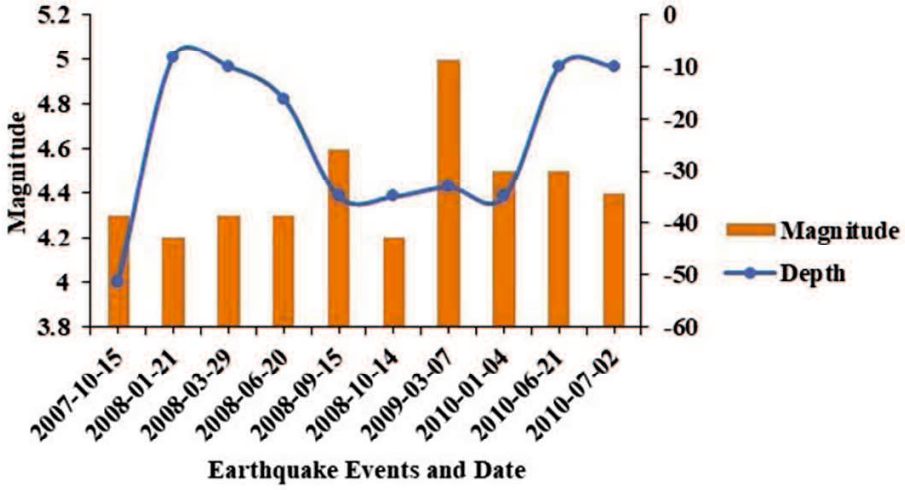


**Figure 4.3.** Earthquake depth and magnitude from 2007 to 2010

Figure 4.4a shows evidence of the ground subsidence. This ground subsidence took place in 2007, a few months after the construction of a road. Land-forming processes, such as topographical changes of the ground, can be observed. An aerial photogrammetry of the affected area was taken in August 2017 (Figure 4.4a) and the longitudinal profile of the road was measured using Total Station (Figure 4.4b). This phenomenon continues even today, causing damage to the population, housing, gardens, roads and other infrastructures.

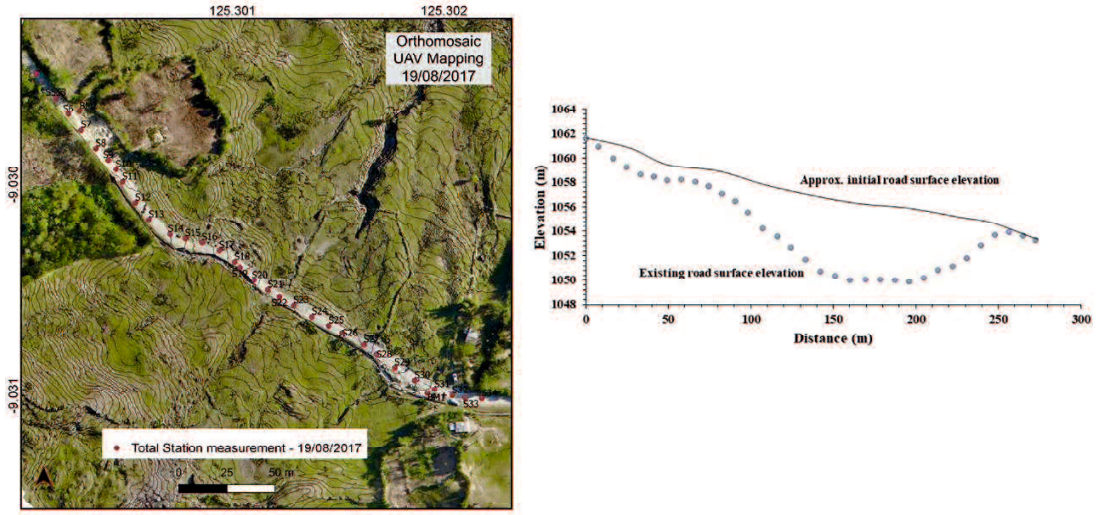


**Figure 4.4. a**) Aerial photogrammetry of Oeleo ground subsidence, August 2017 and **b**) Longitudinal section of road surface elevation measured using Total Station in 19 August 2017

*4.5.2 Rainfall*

It is known that rainfall is the major cause of landslides in Timor-Leste, causing great damage to farmlands, road infrastructures, and houses. As aforementioned, rainfall data have not been recorded well since 1974. However, meteorological data were recorded monthly at 37 stations from 1953 until 1974, covering the whole territory. The study area includes two meteorology stations. One is located in the Bobonaro highlands with an elevation of about 900 m and the other one is located in Maliana in lowlands with an elevation of about 200 m. Figures 4.5a and 4.5b show the variations in monthly rainfall during the rainy months from October to April. Unfortunately, the landslides triggered by rainfall events were not documented properly at that time. Thus, it is difficult to establish the relationship among the intensity of rainfall, the duration of the rainfall, and landslide occurrences. To define the rainfall threshold using an empirical model, it is necessary to analyze past rainfall events that caused landslides. The rainfall conditions that resulted in landslides are plotted in a graph and the threshold is visually determined (Guzzetti et al, 2007). Nevertheless, past rainfall data provided valuable information on the rainfall intensity, duration, and distribution, even at monthly temporal resolutions. A new Rain Gauge Station (RGS) was installed for this

study at the Bobonaro Administrative Post, with rainfall events recorded sub-hourly temporal resolution. Rain event data were collected from 2 October 2017 to 12 March 2018, covering the rainy months of the region. The precipitation during that year was very high compared with the previous five years (Figure 4.7a)

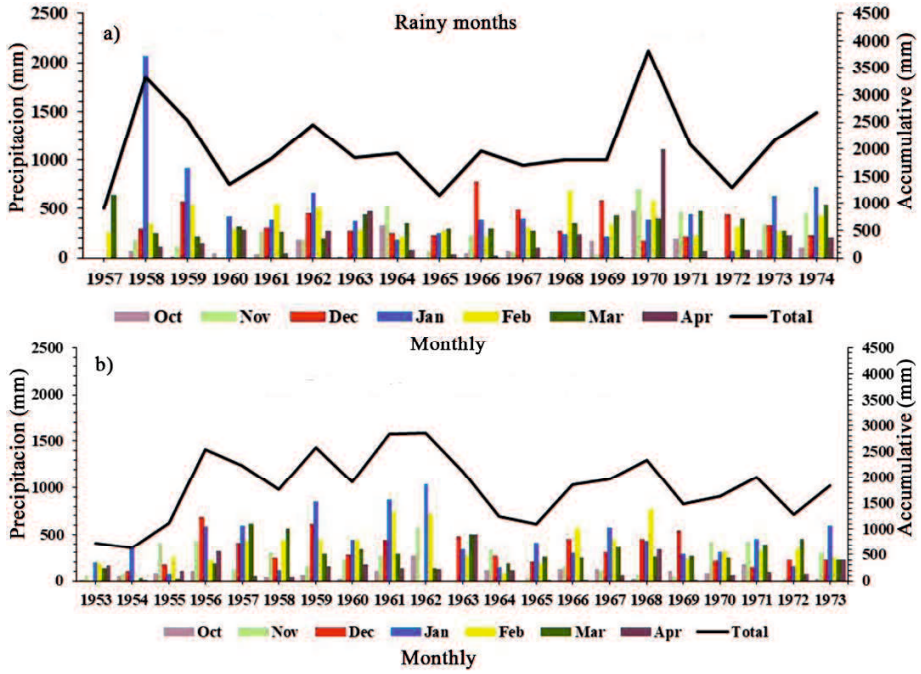


**Figure 4.5. a**) Rainfall data obtained from Bobonaro Meteorology Station, from 1957 until 1974 and **b**) Rainfall data obtained from Maliana Meteorology Station, from 1953 to 1973

Three recent landslides triggered by rainfall were analyzed in this study. These landslides occurred on the same date, that in, in the early morning of 17 January 2018. The first landslide occurred in the village of Lekiatchi, located approximately 8 km from the RGS (Figure 4.6a). The second landslide occurred in the village of Builico, located approximately 20 km from the RGS (Figure 4.6b). The third landslide occurred in the village of Batuboru, located approximately 46 km from the RGS (Figure 4.6c).


**Figure 4.6. a**) Aerial photo of Lekiatchi Landslide area, **b**) Landslide in Builico and affecting the road, photo ***by Biky***, and **c**) Landslide in Batuboro and affected road, photo ***by Babo***

The recent rainfall data were plotted based on cumulative and antecedent rainfall data. The numbers of days chosen for this case are 3, 7, 15, 30, and 107 days (Figures 4.7a-e). The last number includes the first rainy day of the rainy season (Figure 4.7a). Parts of the antecedent rainfall will infiltrate the soil and play an important role in the initiation of landslides by reducing the soil suction and increasing the porewater pressure (Bogaard and Greco, 2016).

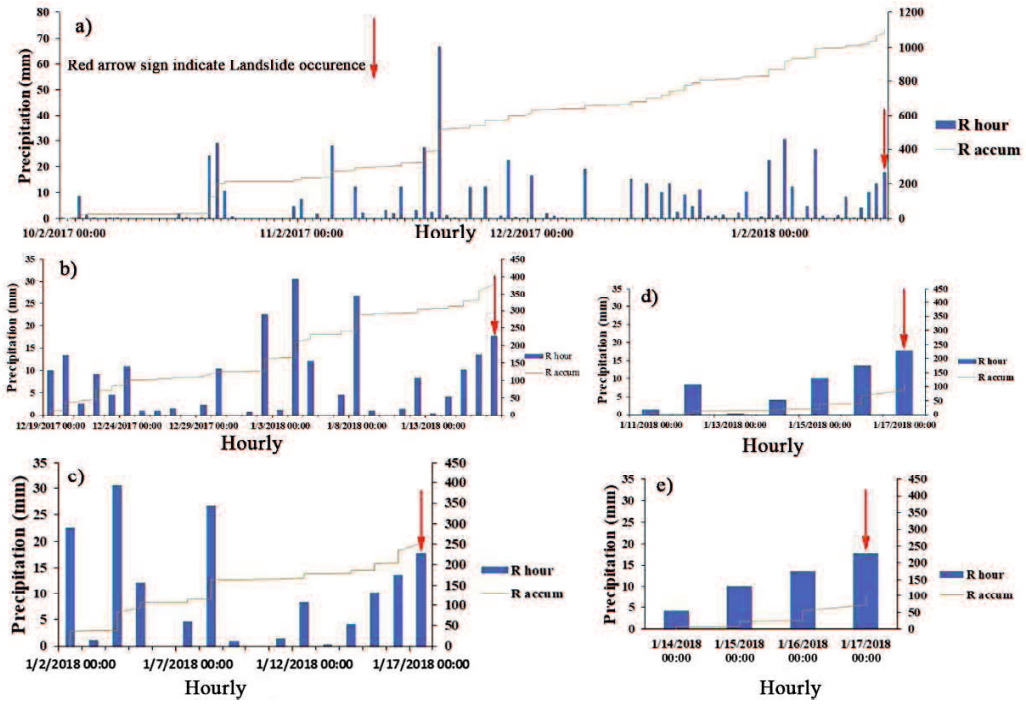


**Figure 4.7. a**) 107 days of antecedent rainfall, starting from 2 October 2017, with total accumulation 1106.3 mm, **b**) 30 days of antecedent rainfall, with total accumulation 403.0 mm **c**) 15 days of antecedent rainfall, with total accumulation 277.0 mm **d**) 7 days of antecedent rainfall, with total accumulation 112.6 mm, and **e**) 3 days of antecedent rainfall, with total accumulation 97.8 mm

The following information can be extracted from the above figures in reference to the maximum antecedent rainfall and days before the initiation of the landslide. After 107 days, the maximum precipitation reached 67 mm/hour, on 20 November 2017, 58 days before the event. After 30 days, on 4 January 2018, the maximum precipitation reached 30.6 mm/hour, 13 days before the event, the same as for the period of 15 days. The periods of 7 and 3 days reached the maximum precipitation on the day of the landslide occurrence. It rained for four consecutive days with a gradual increase, that is, 4.2 mm/hour, 10.2 mm/hour, 13.6 mm/hour, and 17.8 mm/hour, on the day of the landslide.

No landslide occurred on 20 November 2017, with the maximum rainfall of 67 mm/hour. Approximately 50% of the first precipitation amount, that is, 30.6 mm/hour, was recorded on 1 January 2018. A landslide did not occur. In fact, landslides occurred when the precipitation of 17.8 mm/hour was recorded for the three-days antecedent rainfall, as previously

mentioned. This clearly shows that high precipitation events do not trigger landslides. However, extraordinary precipitation events trigger most landslides. It can also be verified that even low precipitation over a period of several consecutive days can trigger landslides.

## 4.6 Conclusion

The recent landslides triggered by rainfall which occurred on 17 January 2018 and clearly show that high precipitation events do not trigger landslides. On the other hand, a landslide occurred after it had rained for four consecutive days with a gradual increase from 4.2 mm/hour, to 10.2 mm/hour, to 13.6 mm/hour and to 17.8 mm/hour on the day of the landslide occurrence.

Thus, it is considered to be extremely important to continue to study the factors triggering landslides in Timor-Leste. Such factors include precipitation, which is very common, and seismic activity (even that of a magnitude), which are responsible for the topographical change on the ground level. However, these two landslide triggering factors might possibly act together or simultaneously. Rainfall Threshold Landslides model for Timor-Leste has not been studied yet. It will be addressed in future works.

## Acknowledgements

We would like to thank all individuals and institutions who contributed direct and indirectly to this chapter.

## References


Audley-Charles M G (2004) Ocean trench blocked and obliterated by Banda forearc collision with Australian proximal continental slope. Tectonophysics, 389 (1-2), 65-79. https://doi.org/10.1016/j.tecto.2004.07.048

Audley-Charles MG (1968) The geology of Portuguese Timor. Geological Society of London.

Barber AJ (1981) Structural interpretations of the island of Timor eastern Indonesia. Geological Research and Development Centre, Spec. Publ. 2: 183-197. http://searg.rhul.ac.uk/pubs/barber_1981%20Timor%20structure.pdfHamilton WB (1979) Tectonics of the Indonesian region. Vol. 1078,p345 US Government Printing Office. https://doi.org/10.3133/pp1078

Benincasa P (2015) On-shell diagrammatics and the perturbative structure of planar gauge theories. arXiv preprint arXiv:1510.03642.

Bogaard TA, Greco R (2016) Landslide hydrology: from hydrology to pore pressure. Wiley Interdisciplinary Reviews: Water, 3(3), 439-459. https://doi.org/10.1002/wat2.1126

Census (2015) http://www.statistics.gov.tl/category/publications/census-publications/

Chamalaun FH, Grady AE (1978) The tectonic development of Timor: a new model and its implications for petroleum exploration. The APPEA Journal, 18(1), 102-108. https://doi.org/10.1071/AJ77012

Charlton TR (2000) Tertiary evolution of the eastern Indonesia collision complex. Journal of Asian Earth Sciences, 18(5), 603-631. https://doi.org/10.1016/S1367-9120(99)00049-8

Garcia J, Cardoso J (1978) Os solos de Timor. Memórias da Junta de Investigações Científicas do Ultramar. Memórias. N. º 64, II série,743p.

Gonçalves MM (1966) O Problema da Erosão em Timor. Missão de Estudos Agronómicos do Ultramar, Lisboa, N. º 236, 18p.

Guzzetti F, Peruccacci S, Rossi M, Stark CP (2007) Rainfall thresholds for the initiation of landslides in central and southern Europe. Meteorology and atmospheric physics, 98(3-4), 239-267. https://doi.org/10.1007/s00703-007-0262-7

Haig DW, McCartain E (2010) Triassic organic-cemented siliceous agglutinated foraminifera from Timor-Leste: conservative development in shallow-marine environments. Journal of Foraminiferal Research, 40(4), 366-392. https://doi.org/10.2113/gsjfr.40.4.366

Haig DW, McCartain EW, Keep M, Barber L (2008) Re-evaluation of the Cablac Limestone at its type area, East Timor: Revision of the Miocene stratigraphy of Timor. Journal of Asian Earth Sciences, 33(5-6), 366-378. https://doi.org/10.1016/j.jseaes.2008.03.002

Hall R, Wilson MEJ (2000) Neogene sutures in eastern Indonesia. Journal of Asian Earth Sciences, 18 (6), 781-808. https://doi.org/10.1016/S1367-9120(00)00040-7

Harris R A (1991) Temporal distribution of strain in the active Banda orogen: a reconciliation of rival hypotheses. Journal of Southeast Asian Earth Sciences, 6(3-4), 373-386. https://doi.org/10.1016/0743-9547(91)90082-9

Harris R, Kaiser J, Hurford A, Carter A (2000) Thermal history of Australian passive margin cover sequences accreted to Timor during Late Neogene arc–continent collision, Indonesia. Journal of Asian Earth Sciences, 18(1), 47-69. https://doi.org/10.1016/S1367-9120(99)00036-X

Keefer GD (2000) Report on Restoration of Meteorological Network-Timor Lorosa'e. United Nation Translation Administration in East Timor.

Leme JCA (1968) Breve ensaio sobre a geologia da província de Timor. Junta de Investigação do Ultramar. Curso de Geologia do Ultramar I, pp. 105-161.

Nugroho H, Harris R, Lestariya AW, Maruf B (2009) Plate boundary reorganization in the active Banda Arc–continent collision: Insights from new GPS measurements. Tectonophysics 479(1-2):52-65. https://doi.org/10.1016/j.tecto.2009.01.026

Seton M, Müller RD, Zahirovic S, Gaina C, Torsvik T, Shephard G, Talsma A, Gurnis M, Turne M, Maus S, Chandler M (2012) Global continental and ocean basin reconstructions since 200 Ma. Earth-Science Reviews, 113(3-4), 212-270. https://doi.org/10.1016/j.earscirev.2012.03.002

Silva HJL (1956) Timor e a cultura do café, Lisboa. Junta de Investigações do Ultramar, Memória – Série de Agronomia Tropical I, 196p.

Soares FA (1957) O Clima e o Solo de Timor – Suas Relações com a Agricultura Lisboa. Junta de Investigações do Ultramar. pp. 118 (Estudos, Ensaios e Documentos. no. 34).

Spakman W, Hall R (2010) Surface deformation and slab-mantle interaction during Banda arc subduction rollback: Nature Geoscience, v. 3, no. 8, p. 562–566. https://doi.org/10.1038/ngeo917

Tate GW, McQuarrie N, van Hinsbergen DJ, Bakker RR, Harris R, Jiang H (2015) Australia going down under: Quantifying continental subduction during arc-continent accretion in Timor-Leste. Geosphere, 11(6), 1860-1883. https://doi.org/10.1130/GES01144.1

Thornthwaite, C.W. (1948) An Approach toward a Rational Classification of Climate. Geographical Review 38(1):55-94. http://dx.doi.org/10.2307/210739

TL-EDP (2011) Timor-Leste Strategic Development Plan. 279p. http://timor-leste.gov.tl/wp-content/uploads/2011/07/Timor-Leste-Strategic-Plan-2011-20301.pdf

United States Geological Survey (2018) https://earthquake.usgs.gov/earthquakes/

## Chapter 5

# GROUND SURFACE DEFORMATION DETECTION USING SBAS DInSAR, UAV PHOTOGRAMMETRY AND FIELD OBSERVATIONS

## 5.1 Introduction

During the past ten years, Timor-Leste has concentrated all its efforts on infrastructure development. However, it has not achieved enough due to unexpected ground deformation in mountain areas, seriously affecting road constructions, etc. In order to design roads and other infrastructures under such difficult conditions, it is important to know the present and future ground conditions. Continuous Monitoring is the most significant methods for detecting the ground deformation and for providing essential information to realize effective design. A problem arises, "How can ground deformation be monitored in extensive areas, which are generally located in mountain areas that are difficult to access"? Differential Interferometry Synthetic Aperture Radar (DInSAR) has recently been applied to monitor the displacement over extensive areas. In addition, Unmanned Aerial Vehicle (UAV) Photogrammetry is useful for detecting the deformation in detail. Both methods are advantageous in that they do not require any sensors. Therefore, the combination of DInSAR and UAV Photogrammetry is one of the solutions for monitoring ground deformation in Timor-Leste. In this dissertation, DInSAR and UAV Photogrammetry are applied to unstable ground in the Bobonaro region, Timor-Leste to find the recent ground deformation, since 2007 due to earthquakes and hard rainfall events. It is found that DInSAR is capable for screening both usual and unusual ground behavior and that UAV Photogrammetry is flexible to use and to detect displacements with cm accuracy after DInSAR screening.

## 5.2 Study area

This method will be applied to a road section, including the area around it, which has been affected by ground deformation since 2007. No technical observations or precise measurements were made on this ground deformation. Information related to this study area has been presented in chapter 2 of this dissertation.

## 5.3 Data

In this research, deformation measurements from Advanced Land Observation Satellite (ALOS) Phased Array type L-band Synthetic Aperture Radar (PALSAR) are presented (Appendix 3). The first ALOS1 PALSAR1 was in operation from 2006 to 2011, and the second ALOS2 PALSAR2 has been in operation from 2015 to the present day. These SAR datasets were provided by the Japan Aerospace Exploration Agency (JAXA). The first dataset, composed of 22 SAR images collected from PALSAR1, covered the period from 22 January 2007 to 2 February 2011. The second dataset, composed of 13 SAR images collected from PALSAR2, covered the period from 10 February 2015 to 2 April 2019. High-resolution orthomosaic and DEM images were collected on 19 August 2017 by employing Small UAV Photogrammetry DJI Mavic Pro. The earthquake data, downloaded from the United States Geological Survey (USGS) Earthquake Catalogue, covered the two periods of study. Timor-Leste rainfall have not been recorded well since 1974. To overcome this unavailability of rainfall data, it was necessary to use the data published by the Climate Forecast System Reanalysis (CFSR) of the National Centers for Environmental Prediction (NCEP). Fortunately, the first study period, January 2007 to February 2011, covered daily rainfall data, with a spatial resolution of 38 km. Two imaginary stations, namely, p-891253 and p-921250, located above the mountainous area were selected. For the second period, a HOBO ground station rainfall data logger with a resolution of 0.2 mm per tip was installed 2 km from the study area. The data collection was conducted from 7 March 2007 to 2 April 2019, partially covering the second period.

## 5.4 Methodology and processes

*5.4.1.1 SBAS DInSAR*

Synthetic Aperture Radar (SAR) is a specific imaging radar system mounted on an aircraft or artificial satellite (Hanssen, 2001). SAR provides high-resolution remote sensing images, independent of daytime (day/night) and weather. The images acquired from SAR are used for vast applications and research in fields such as geoscience, environmental, climate change, and Earth system observation (Moreira et al, 2013). Interferometric SAR (InSAR) is a technique for deriving the topographic surface or digital elevation model (DEM) by

extracting the signal phase changes (interference) from two SAR images acquired from the same position in repeated orbits of the satellite.

Differential interferometry SAR (DInSAR) is a technique for measuring the deformation of the Earth's surface induced by natural and or artificial processes. In DInSAR, the topographic contribution is removed by using out-source elevation information from a DEM. However, during the interferogram processing by the DInSAR technique, besides the deformation component some residual terms appear due to the topographic pattern as well as defects in the orbital parameters (Pepe and Caló, 2017). To enhance the accuracy of DInSAR, some methods have been proposed based on persistent scatters (PS) and distributed scatters (DS). The two most widely used methods are called Permanent Scatters InSAR (PSI) (Feretti et al, 2001) and Small Baseline Subsets (SBAS) DInSAR (Berardino et al, 2002).

*5.4.1.2 SBAS DInSAR Processing*

For the time-series analysis, this study employs the SBAS method that was proposed by Berardino et al, (2002). The SBAS method was applied for both datasets, PALSAR1 and PALSAR2, separately for the first period and second periods (Appendix 4). The HH polarization data were selected to generate the interferograms. The topography phase component was removed using the SRTM1 DEM data with a 30 m resolution which was acquired in 2000. The perpendicular and temporal threshold criteria for SBAS processing depend on the conditions of the study area (Liu and Mason, 2016). A perpendicular baseline of up to 5 km can be used for ALOS PALSAR data, since longer wavelengths are less sensitive to geometric distortion (Sandwell et al, 2008).

For the PALSAR1 data, the maximum perpendicular and temporal baselines of the interferogram for the SBAS processing are ±2000 m and 270 days, respectively. Accordingly, 55 pairs of interferograms met the criteria. For the PALSAR2 data, the maximum perpendicular and temporal baselines of the interferogram for the SBAS processing are ±400 m and 365 days, respectively. Thus, 33 pairs of interferograms met the criteria for further processing. Figure 5.1 a and b show the baseline tables of SBAS DInSAR for PALSAR1 and PALSAR2, respectively.

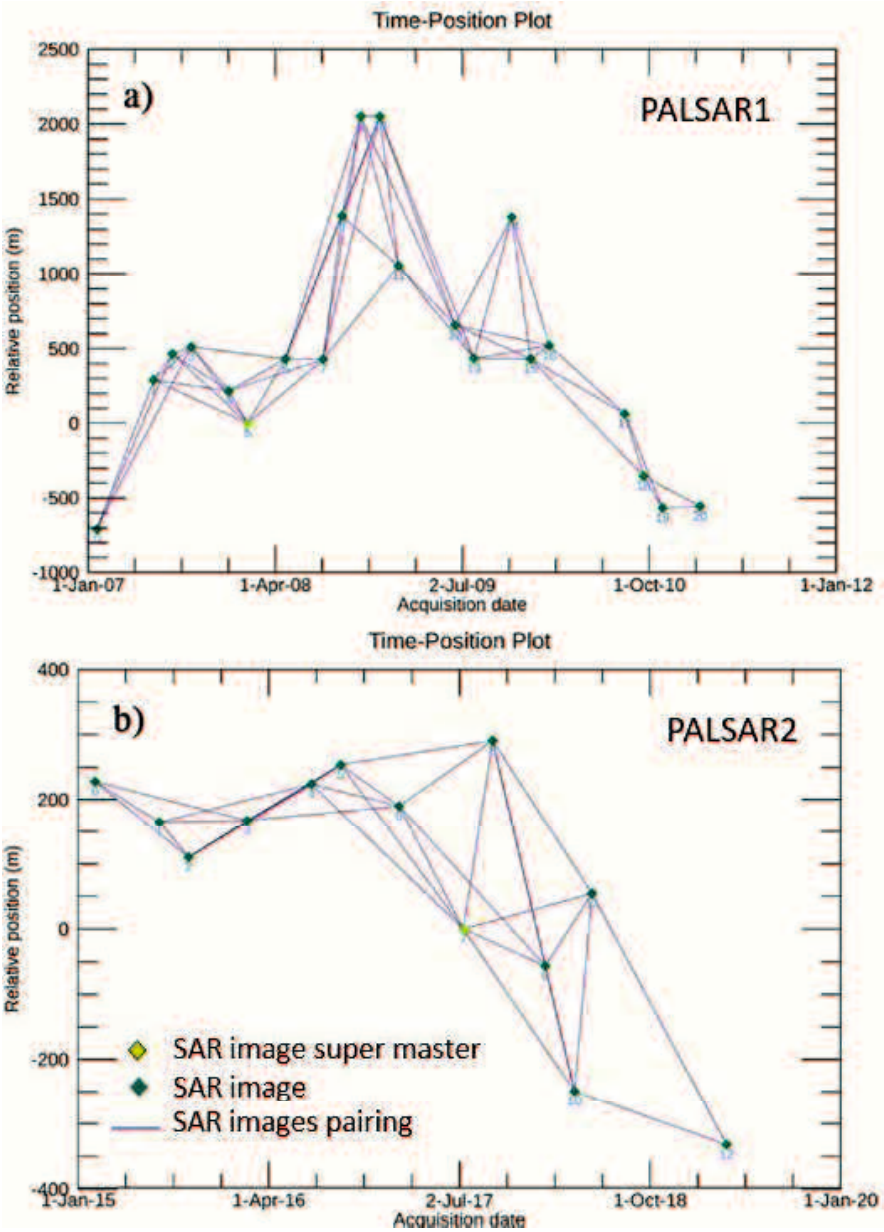


**Figure 5.1.** Small Baseline Subset (SBAS) Differential Interferometry Synthetic Aperture Radar (DInSAR) baseline tables: **a**) Phased Array type L-band Synthetic Aperture Radar (PALSAR) 1 for the first period and **b**) PALSAR2 for the second period

The generation of interferograms is affected by many types of noise, namely, speckle noise, orbital errors, and atmospheric errors. In order to reduce the noise, an interferogram multi-

looks operation was conducted. The number of range looks was two and the number of azimuth looks was four for PALSAR1, while the number of range looks was one and the number of azimuth looks was three for PALSAR2. Interferogram multi-looking is effective for reducing noise, with the trade-off of a worse spatial resolution (Hansen, 2001). In addition, to improve the quality of the interferograms, the Goldstein filter (Goldstein and Werner, 1998) was applied. The unwrapping process was then conducted for each interferogram by using the robust minimum cost flow (MCF) algorithm (Costantini, 1998). In the unwrapping step, the coherence threshold was set at 0.2 for both PALSAR1 and PALSAR2, which means that the pixels with a coherence of less than 0.2 were removed and not involved in the calculation.

The orbital error fringes interfered with some interferograms (Hanssen, 2001). To redefine these orbital fringe errors, a 2nd order polynomial estimation in the azimuth and range directions was applied and calibrated with the number of ground control points (GCPs). A total of 134 GCPs located in Maliana and Zumalae were used for PALSAR1, while 36 GCPs located in Maliana were used for PALASR2 (Figure 8b). The GCPs are located on flat land where the unwrapped phase error is minimum. A repeated unwrapping process will redefine the interferograms. The atmospheric phase screen (APS) is the dominant error source for InSAR [82]. A custom spatio-temporal filter, whose spatial low pass window size is 1.2 km × 1.2 km and whose temporal high pass size is 365 days, was applied to reduce those errors. After minimizing all the associated errors, the next steps were the geocoding process and image resampling. For these processes, the temporal coherence threshold coefficient was defined at 0.4 for PALSAR1 and at 0.2 for PALSAR2. Finally, maps for the time-series LOS displacement were generated by each dataset (Appendix 5,6). The spatial resolution was 15 m × 15 m for PALSAR1 and 10 m × 10 m for PALSAR2. Examples of the interferogram map and the coherence map are presented in Figure 5.2. The results of the ground surface deformation screening for both the first period and the second period are presented in the Figure 5.3. The LOS mean displacement velocities for the first period and second periods are presented in Figure 5.4.

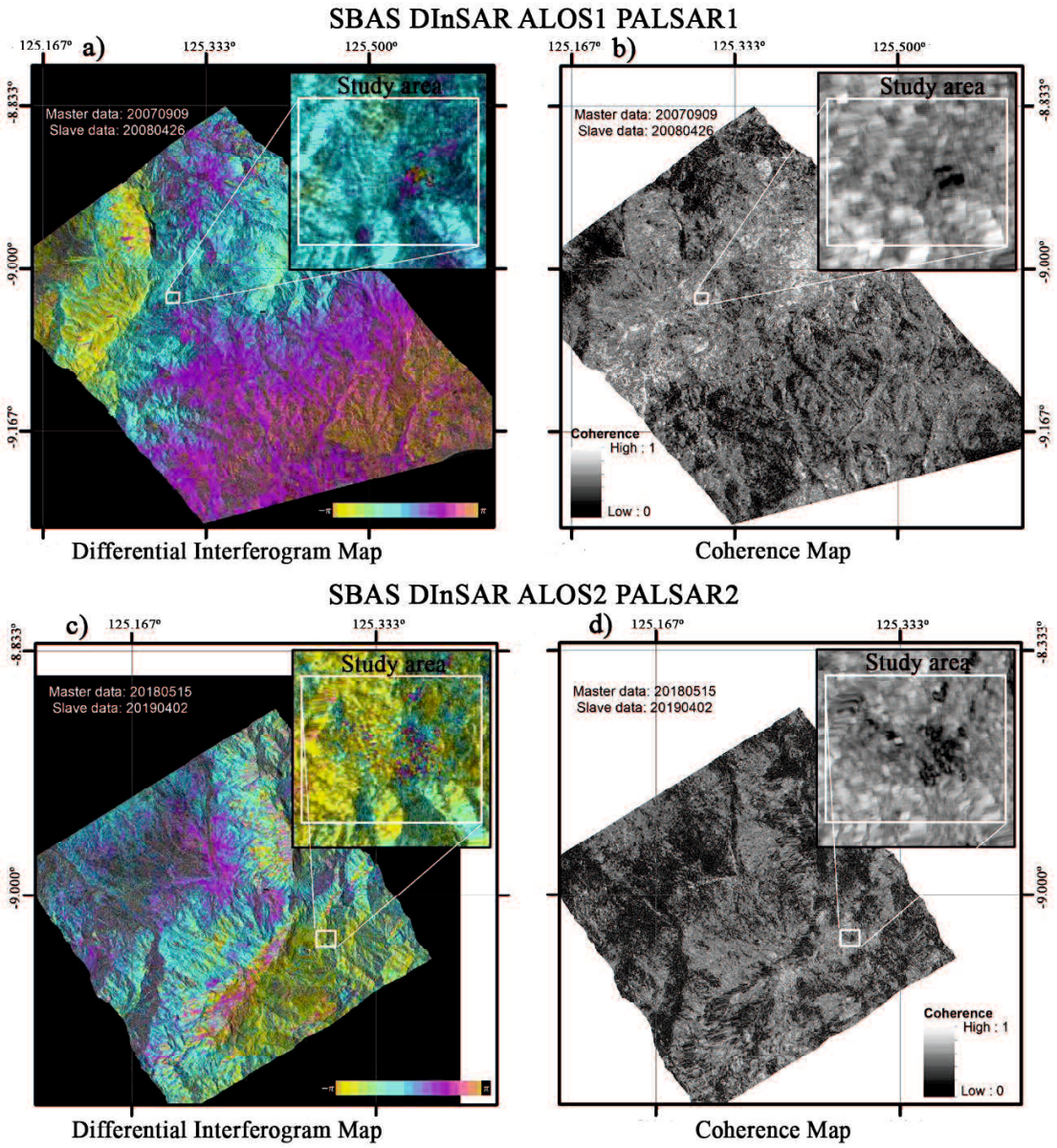


**Figure 5.2.** (**a**) PALSAR1 Interferogram map, (**b**) PALSAR1 Coherence map, (**c**) PALSAR2 Interferogram map and (**d**) PALSAR2 Coherence map

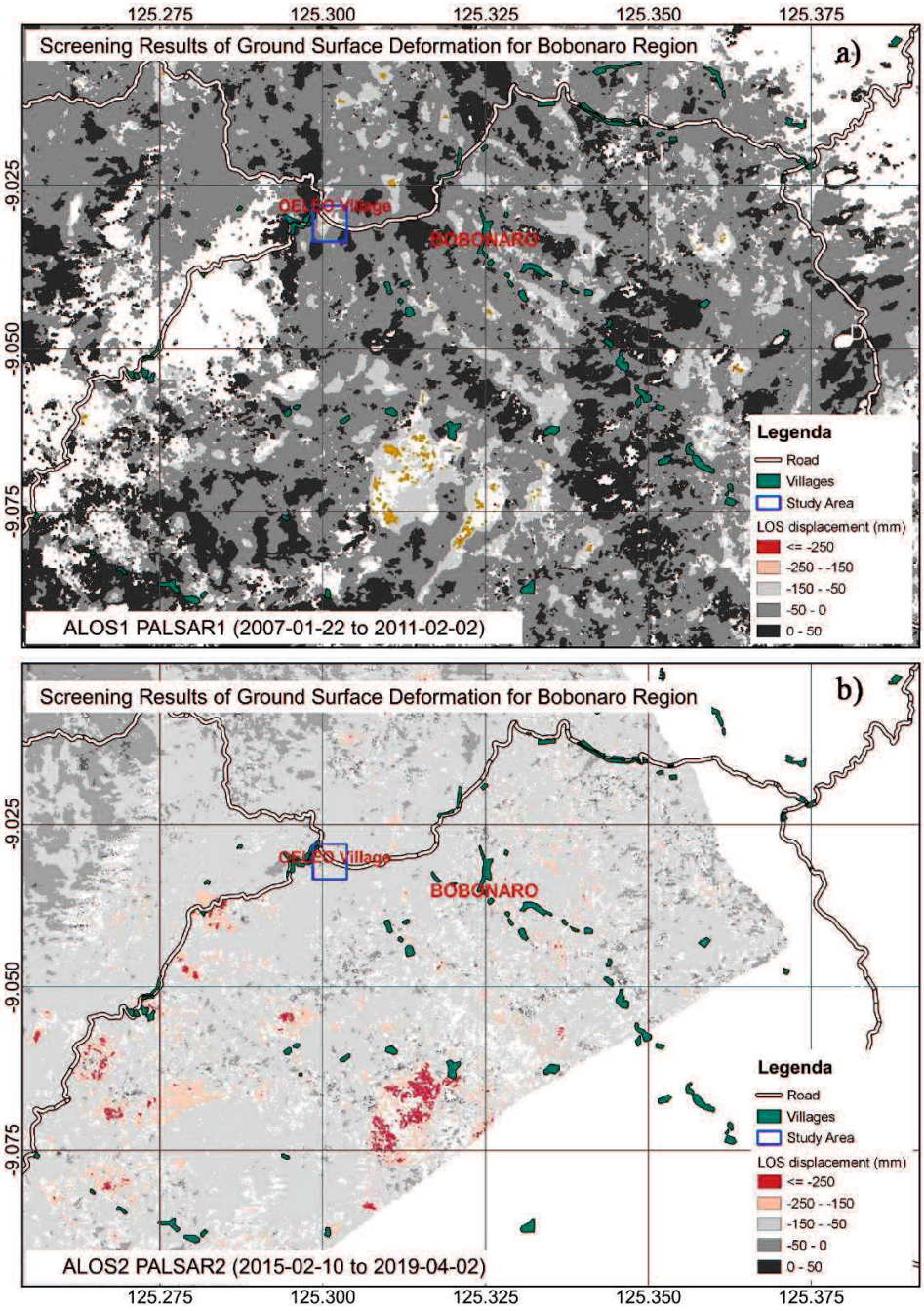


**Figure 5.3.** SBAS DInSAR ground surface deformation screening results over extensive area for **a**) first period and **b**) second period

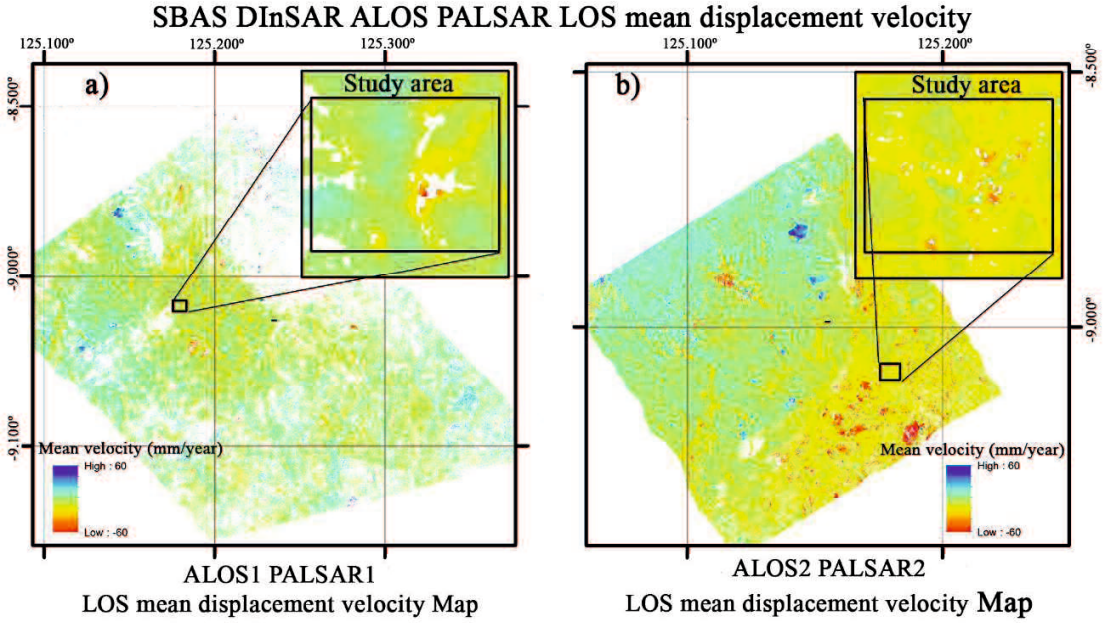


**Figure 5.4.** (**a**) PALSAR1 LOS mean displacement velocity for the first period of study and (**b**) PALSAR2 LOS mean displacement velocity for the second period of study

*5.4.2.1 UAV Photogrammetry*

UAV photogrammetry is a small remote sensing platform for acquiring high-resolution images of the ground surface. High-resolution and georeferenced UAV photogrammetry images allow for a wider range of applications with much greater detail and accuracy than satellite data. The Structure-from-Motion (SfM) technique is capable of generating georeferenced high-resolution orthomosaic and DEM images (Niethammer et al, 2012; Lucieer et al, 2014; Turner et al, 2015; Peppa et al, 2016; Hu et al, 2017; Ma et al, 2018; Rossi et al, 2018; Pellicani et al, 2019). The UAV DEM has high accuracy in the centimeter to millimeter order for estimating and measuring ground surface deformation. Henceforward, in the Geographic Information System (GIS) environment, other information can be generated from the DEM, such as contour lines, the cross section and profile, hillshade, slope, aspect, and water flow.

A small UAV, DJI Mavic Pro, was employed for ground mapping in the study area (Appendix 7). The DJI Mavic Pro has been used in various fields of research (Ardi et al,

2017; Djimatoro and Suharjanto, 2017; Burdziakowaski, 2018; Auer et al, 2018; O'Driscol, 2018; He et al, 2019; Zhang et al, 2019; Patrucco et al, 2019; Windle et al, 2019). This is a foldable drone with a flight weight of 743 g, a maximum flight time of about 27 min, and a maximum flight distance of 13 km under a no-wind condition. The platform is equipped with one GPS/GLONASS module, the latest Inertial Measurements Unit (IMU) module and flight control stabilization technology in order to fly smoothly, and a 4K stabilized integrated gimbal and autopilot module for navigation. The camera specification is a non-metric camera with a sensor size of 1/2.3" (CMOS). It has 12.35 million pixels; a lens with a viewing angle of 78.8°, 26 mm (35 mm equivalent); an f/2.2 distortion of <1.5%; and a focus of 0.5 m to infinity. It can take images with a maximum still image size of 4000 × 3000 and is capable of direct image georeferencing. The main disadvantage of this drone is certainly its high sensitivity to wind turbulence due to its small size and light weight.

*5.4.2.2 UAV Photogrammetry data acquisition and processing*

Drone Deploy provides a user-friendly and free application for flight planning and mapping. This application can be installed both in smart mobile devices (iOS or Android) and provides online access to desktop computers. It is very convenient and makes it easy to prepare all the plans and record them in the office, either hours or days before going to do the fieldwork. The online software automatically generates the flight path and is user configurable. Some adjustments are needed, such as the flight altitude, flight direction, flight mapping speeds, front and side overlap percentages, and manual camera settings, when necessary. During the flight plan configuration, the software automatically calculates the flight duration in minutes, the total area covered in hectares, the number of images, the amount of battery consumption, and the image resolution in cm/px. Once the flight plan is completed, the smart device only needs to be connected to the Internet and the Drone Deploy application opened in order to update the latest information or project. At the desired location, the smart device can be connected via USB to the drone, the proper project chosen, the preflight checklist started, and the flight initiated. The drone will automatically start the rotors, record the home point, and take off, following all the flight plan instructions and recording images in the onboard micro memory card. After completing all the instructions, the drone will fly back to land at

the home point. For this study, the percentage of overlap was set to 75% for the front overlap, 65% for the side overlap, 80 m for the flight altitude, and 2.4 cm for the resolution; the camera was set to automatic mode. The survey mapping was conducted without ground control points (Li et al, 2011; Carrilo et al, 2012; Turner et al, 2012; Hu et al, 2017; Sanz-Ablanedo et al, 2018; He et al, 2019).

The images collected were georeferenced in the WGS84 geographic coordinate system, including the ellipsoid altitude (Appendix 8). The georeferenced images allow the photogrammetry software to detect the three-dimensional positions at which the images were taken. The recent improvement in the georeferenced image processing by a powerful computer and the application of computer vision modelling using the SfM technique allow the building of a three-dimensional terrain model with high quality and low time consumption (Li et al, 2016; Niethammer et al, 2012; Turner et al, 2012; guan Li et al, 2016; O'Driscoll, 2018; Ma et al, 2018; Hu et al, 2017). In this study, the SfM-based software, AgiSoft PhotoScan version 1.4.5, was employed. The output can be immediately manipulated using GIS software such as ArcGIS 10.4 and QGIS 3.4 to correct geometric errors and to extract other spatial information.

## 5.5 Results

### *5.5.1 Time-series SBAS DInSAR*

The ground deformation detected by SBAS DInSAR, from both PALSAR1 and PALSAR2, is presented in line of sight (LOS) displacement values and their spatial distribution (Figures 5.5c and 5.5d). These LOS displacement values were further used for geoprocessing in GIS software environments. Seven points of interest (POIs), namely, P1, P2, P3, P4, P5, P6 and P7, were defined around the study area, near the village of Oeleo (Figures 5.5c and 5.5d). In order to identify the distribution of ground deformation with more detail, four areas of interest (AOIs), AOI1, AOI2, AOI3 and AOI4, were defined (Figures 5.5c and 5.5d). These AOIs were applied for the first period. Six more POIs, namely, P8, P9, P10, P11, P12 and P13, were defined for the second period (Figure 5.5d). The definition for the additional POIs and AOIs were based on the LOS displacement images, the recent field observations and UAV

orthomosaic image interpretation. The LOS displacement values were extracted and converted to points for further analysis. The PALSAR1 and PALSAR2 LOS displacement time-series related to P1, P2, P3, P4, P5, P6, and P7 are presented in Figures 5.5e and 5.5f, respectively.

The PALSAR1 LOS displacement time-series values related to AOI1, AOI2, AOI3 and AOI4 were extracted and applied to calculate the mean, minimum and maximum values. These values were used to show the ground deformation trend in Figures 5.6a, 5.6b, 5.6c, and 5.6d, respectively. AOI2 and AOI3 show high displacement values while AOI4 seems more stable.

The PALSAR2 LOS displacement time-series values related to P8, P9, P10, P11, P12 and P13 were extracted and are presented in Figure 5.6e. Based on the LOS displacement values, both POIs, P3 and P7, seemed more constant than the others during the first period. However, during the second period, P3 and P7 presented displacements as well. POIs P2 and P6 presented very high values of LOS displacement during the two periods (Figures 5.5e and 5.5f). In Figure 5.6e, P8 and P9 showed LOS displacement values of more than 200 mm compared to other POIs.

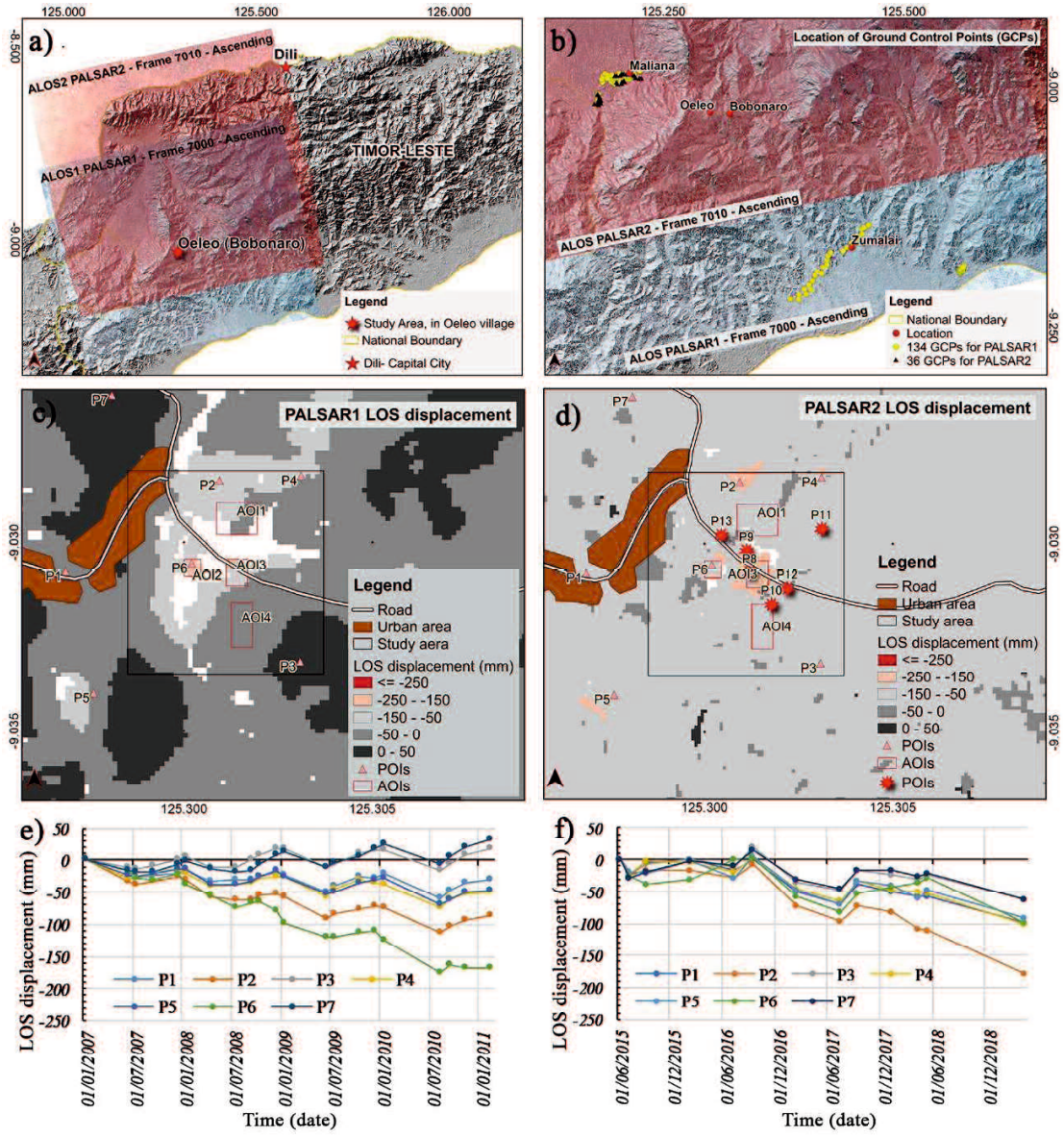


**Figure 5.5.** **a**) PALSAR1 and PALSAR2 data frames covering study the area, **b**) spatial distribution of ground control points (GCPs), **c**) spatial distribution of line of sight (LOS) displacement from PALSAR1, **d**) spatial distribution of LOS displacement from PALSAR2, **e**) LOS displacement time-series from PALSAR1, and **f**) LOS displacement time-series from PALSAR2.

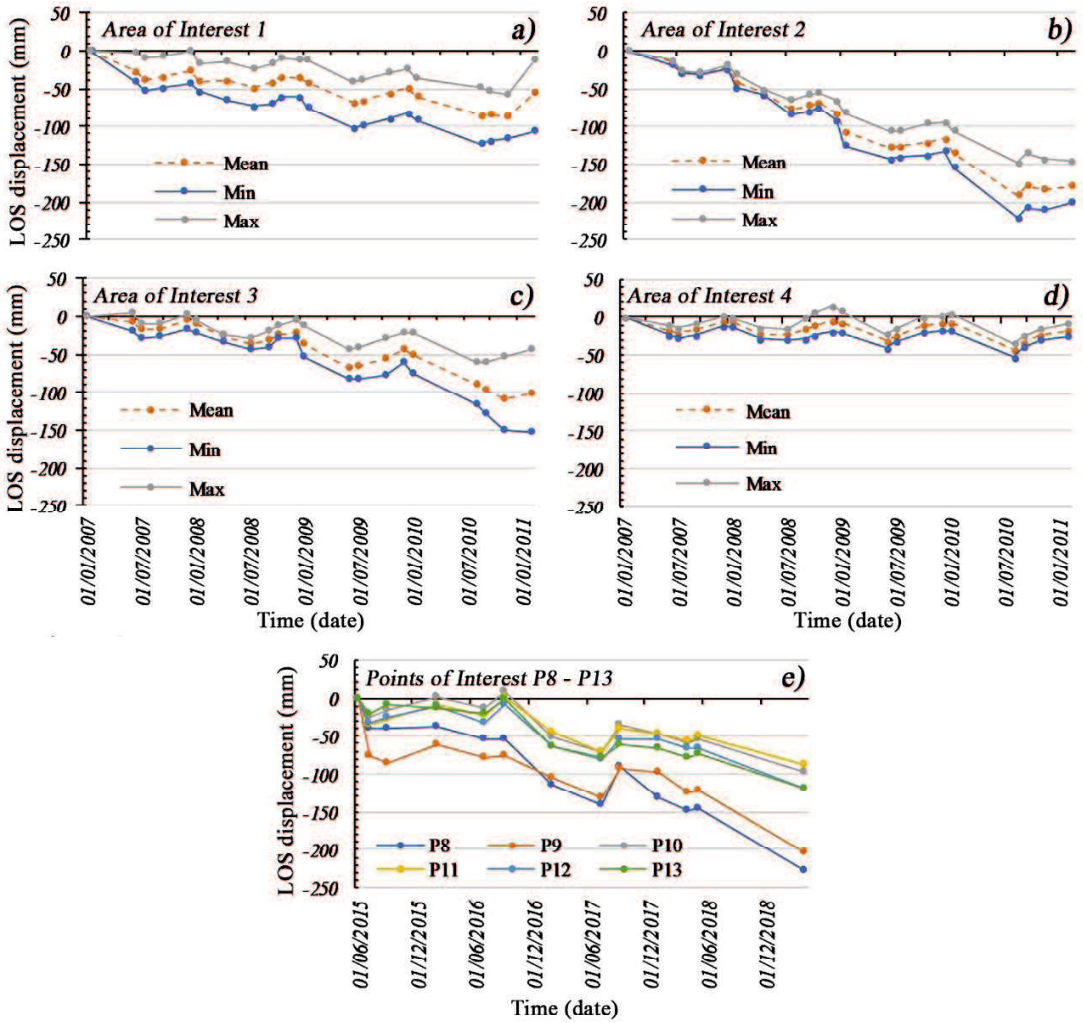


**Figure 5.6.** PALSAR1 LOS displacement time-series: **a**) AOI1, **b**) AOI2, **c)** AOI3, **d**) AOI4 and PALSAR2 LOS displacement time-series, and **e**) POIs P8–P13

### *5.5.2 UAV georeferenced Photogrammetry*

For this study, a UAV aerial mapping mission was conducted on 19 August 2017 without the application of GCPs. The positioning system was based on a single built-in unit GPS/GLONASS module installed inside the drone. Thus, a minimum of 12 numbers had to be obtained from the satellite in order to get a strong signal from the GPS before starting the flight for survey mapping. This requirement is very important for realizing good quality georeferencing images. For most of the acquired images, the quality was good, with values

of quality estimation coefficients greater than 0.8, as analyzed by the Agisoft PhotoScan 1.4.5 software. It was necessary to check the image quality before proceeding to the image processing stage. For the next step, the workflow presented in the Agisoft PhotoScan software was followed. The results presented very high-resolution orthomosaic images and digital elevation models for both (Figures 5.8 and 5.9). Figure 5.7 shows the acceptable georeferencing quality of the orthomosaic image, which matched the Google Maps Hybrid. From the orthomosaic image, it was possible to interpret and measure the ground fissures in the GIS environment with centimeter-order accuracy. The digital elevation model allows for the generation of other spatial information, such as contour lines and surface profiles.

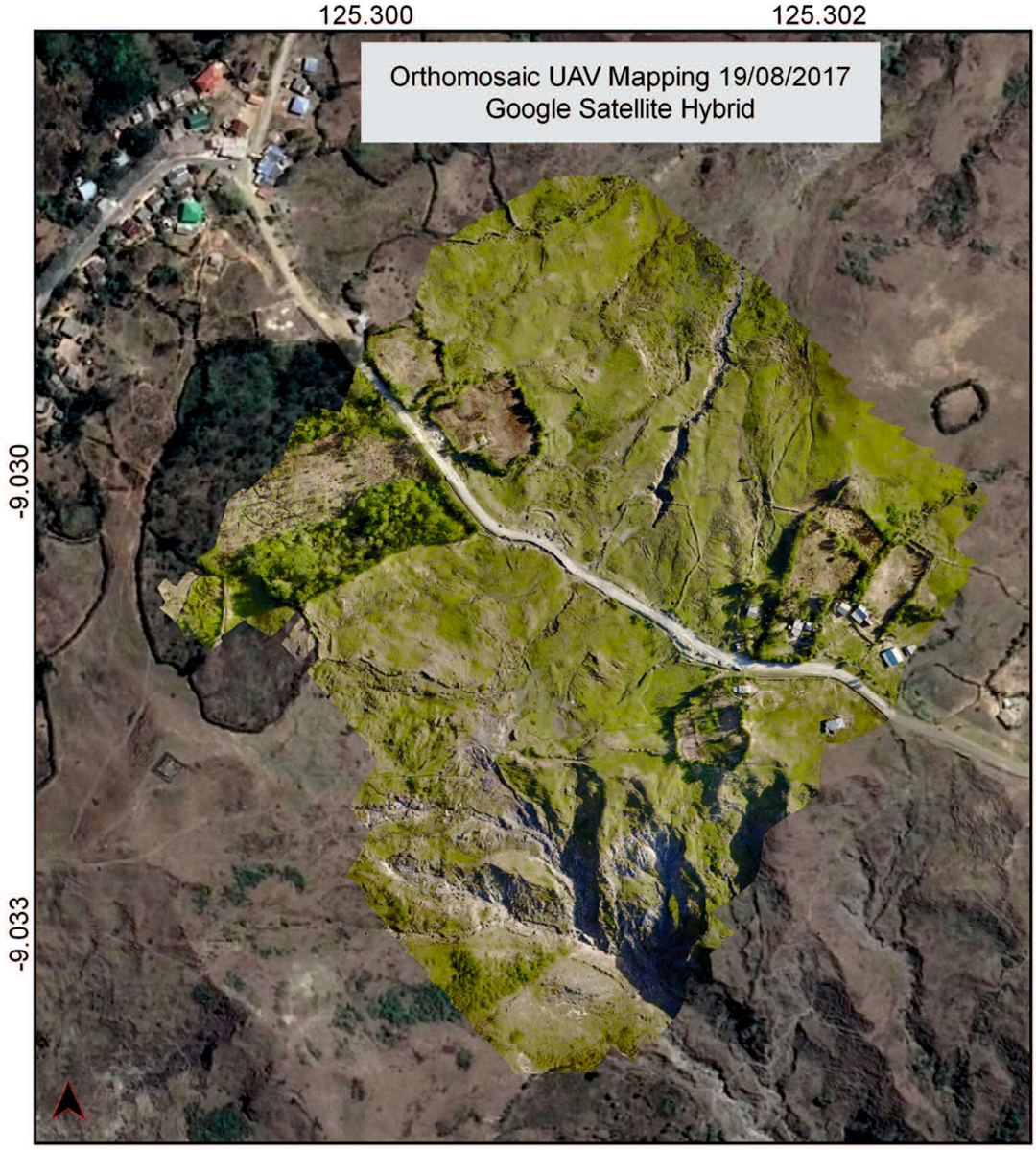


**Figure 5.7.** Unmanned Aerial Vehicle (UAV) orthomosaic image overlaid on Google Maps Hybrid

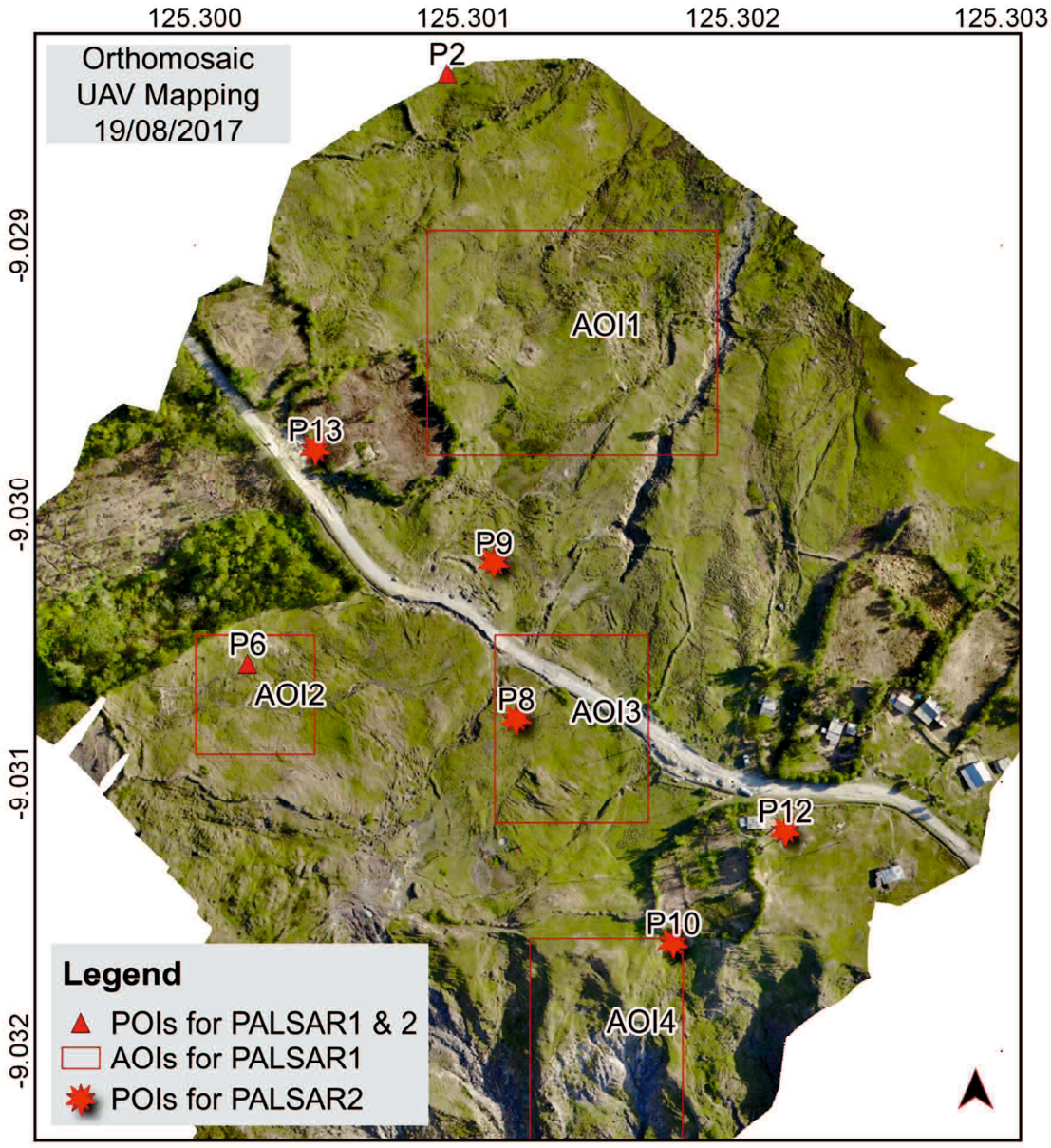


**Figure 5.8.** Unmanned Aerial Vehicle (UAV) orthomosaic image

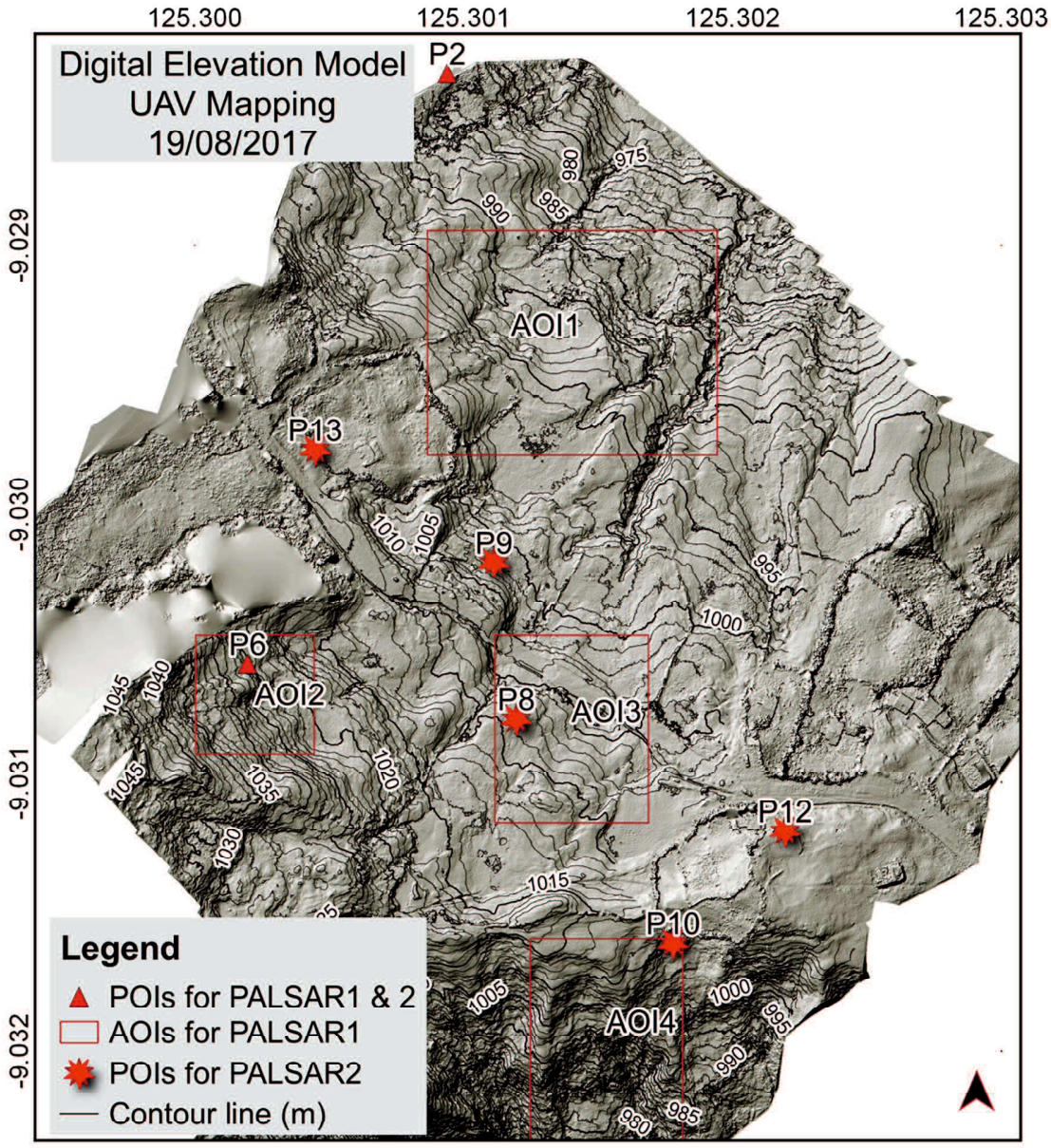


**Figure 5.9.** Unmanned Aerial Vehicle (UAV) Digital Elevation Model

### 5.6 Discussion

The ground surface deformation detected by the SBAS DInSAR derived from PALSAR1 and PALSAR2 will be discussed in this section. Multi-temporal SBAS DInSAR is a very effective technique for detecting the subsidence over a vast area. However, for detecting local

ground displacement this technique still has limitations, namely, it cannot be used in densely vegetated areas and under steep slope conditions (Yastika et, 2019). Thus, although discussions on the precise measurements of local ground displacements are very important, they will be considered as a topic to be addressed in future works. The advantage of this technique was taken to find the relation between the LOS displacement results and the behavior of the ground surface deformation, from the past until the present. UAV georeferenced photogrammetry will be used to interpret the ground surface deformation and to confirm the latest LOS displacements synchronously.

The LOS displacement time-series clearly shows a trend in the ground deformation during these two periods of study (Figures 5.5e and 5.5f). The tendency was to move in the negative direction, and the LOS displacement values varied among the POIs. From Figure 5.5d, it seem that the POIs have been classified into three groups, Group 1 (P3 and P7), Group 2 (P1, P4 and P5), and Group 3 (P2 and P6). Group 1 was more stable during the first period. However, during the second period, the LOS displacements were increasing or moving down, starting from 9 February 2016 until the end of the period. Group 2 presented uniform displacements during the first period and continued until March 2016. After that, the LOS displacements increased drastically. Group 3 presented the highest values of the LOS displacements during the first period. During the second period, the POIs in this group differed from the LOS displacement values. P6 tended to be stabilized, while P2 showed a continuous increase in the LOS displacement values during the second period. The differences in behavior between P2 and P6 reveal important information for understanding and describing the relative movement and direction of the ground deformation in this location. For this purpose, the latest PALSAR2 LOS displacements were overlayered on the UAV DEM. The results showed a good coherence between the LOS displacements and the ground surface conditions (Figure 5.10). As can be observed in Figure 5.6e, that something interesting occurred in relation to the additional POIs. P8 and P9 reached LOS displacement values of above 200 mm. Further investigation will focus on area of interest 3 (AOI3).

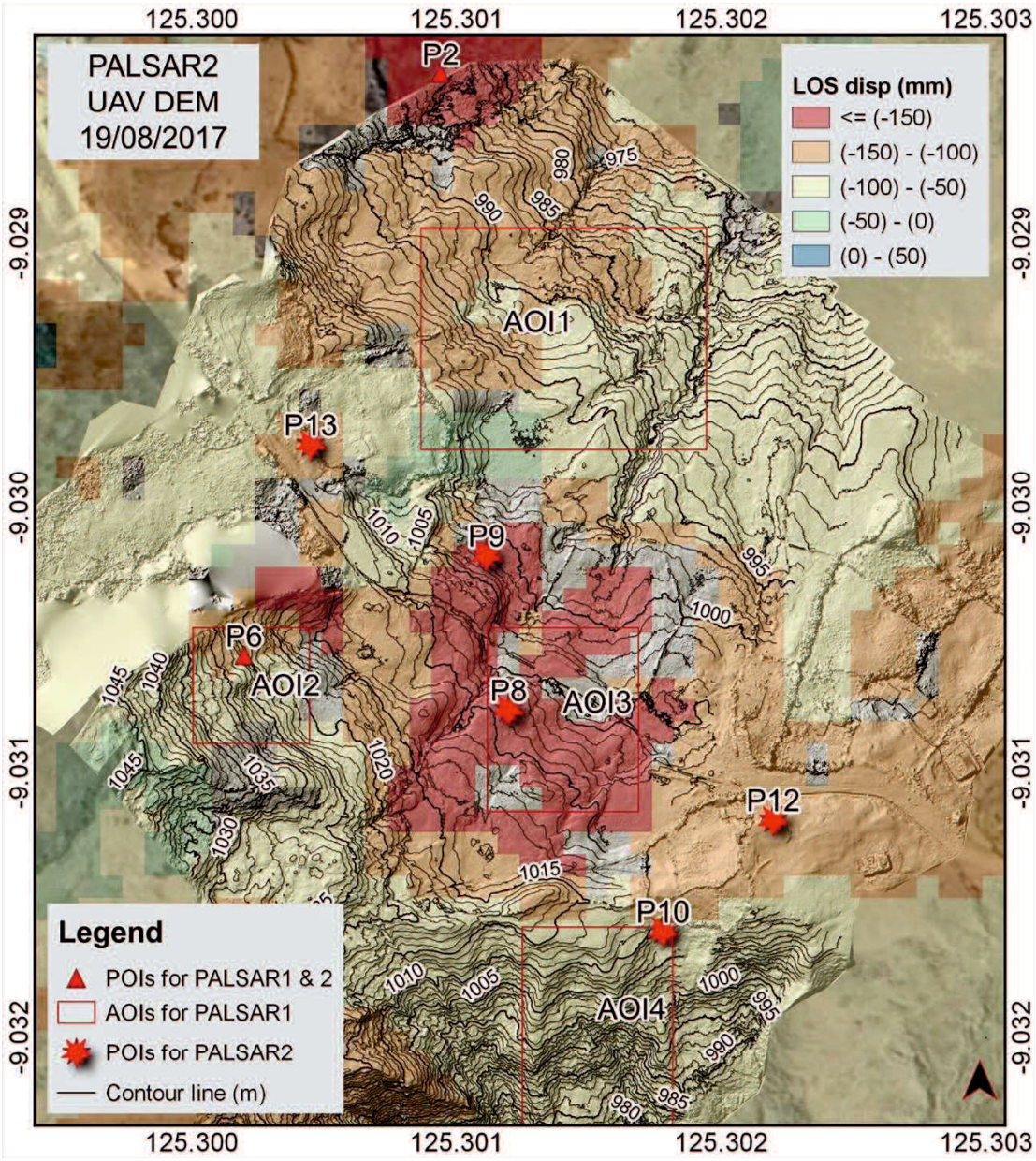


**Figure 5.10.** Latest PALSAR2 LOS displacement image overlaid on UAV Unmanned Aerial Vehicle (DEM) acquired on 19 August 2017

The next step will focus on the ground surface interpretation, based on the very high resolution of the UAV orthomosaic and DEM images (Figures 2.4 and 5.11). P6 is located at the highest location, at an elevation of 1030 meters, and P2 is located at a lower location, at

an elevation of 990 meters. AOI2 and AOI3 are located near P6 and AOI1 is located near P2. Based on the landslide morphology presented by Varnes (1978), it was possible to identify the typical features of the ground movement or landslide. In Figure 5.8, some important ground morphology features, such as the main fracture, transverse fracture, internal fracture, pond water and water courses, can be identified. AOI2 and AOI3 are situated in the depletion zone and are characterized by crowns, main scarps, heads and flanks. Two main scarps, several heads, and discreet flanks were identified. AOI1 lies in the accumulation zone, characterized by radial cracks, transverse cracks, toe ridges and transverse ridges. Based on this ground morphology, it was assumed that the ground surface deformation occurred during the first period and that the process continued until the end of the second period. The ground is seen to be moving down following the natural streamline in the NE direction. The ground at AOI4 is seen to be moving in the opposite direction. The slope is steeper and characterized by translational movement, and no water pond was found.

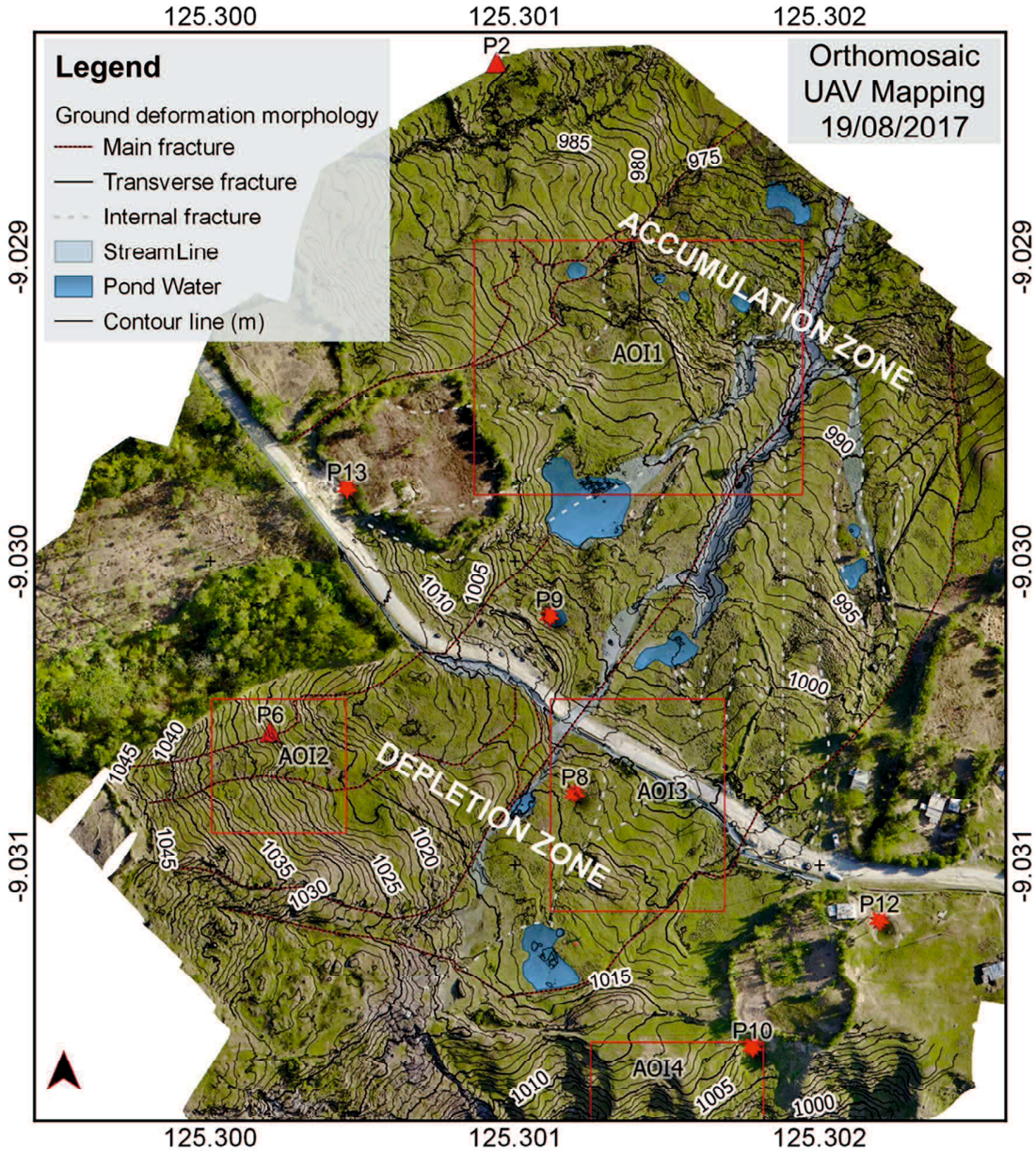


**Figure 5.11.** Ground surface deformation morphology interpretation based on the UAV orthomosaic images acquired on 19 August 2017

The very high-resolution orthomosaic images and DEM allowed for a more detailed interpretation of the morphology of the ground surface deformation (Niethammer et al, 2011). Specific terrain profile sections were extracted from the UAV DEM (Figure 5.12a).

For each profile section, the ground surface as well as the remarkable ground features and objects are presented in the graphs (Figures 5.12 and 5.13). The results show that the ground surface deformation measurements vary from centimeters to meters in both vertical and horizontal directions. From Profile 1, the results of the road surface elevation extracted from UAV DEM are presented and compared with the total station measurements. The graph shows a good coherence between these two measurement methods (Figure 5.12c). The line of Profile 2 follows the electrical pole line. It is noted that the electrical pole moved horizontally more than 4 meters from the initial position (Figures 5.12b and 5.12d). Profile 3 represents the natural ground surface condition and a ground crack, shown in Figure 5.12e. Profiles 4 and 5 represent some parts of the roads that were affected by the ground deformation (Figures 5.13f and 5.13g). Profiles 6 and 7 represent the main scarps that were measured and illustrated in Figures 5.13h and 5.13i, respectively.

Some examples comparing the measurements on UAV direct georeferenced orthomosaic images and field measurements using Total Station are presented in Appendix 12,13 and 14. For georeferencing purposes, the process was simply based on GNSS measurements, for both UAV Mapping and Total Station. Remarkable objects on the ground were chosen to conduct measurements, such as the road surface presented in Profile 1, the electrical pole presented in Profile 2, the ground crack presented in Profile 3, and the scarps presented in Profile 6 and 7.

A single GPS Receiver Trimble R6 was employed to obtain the geographic coordinates for setting the two benchmarks (BM) for the Total Station measurement. Before proceeding with the measurements, the GPS coordinates for both BM were measured and recalculated to reduce the error.

The road surface profile section was roughly defined following the center line of the road that was thought to be in an ideal condition (bare ground) for a measurement comparison, between UAV and Total Station (TS). The profile line for the TS was defined during the measurement following the inclination discontinuity of the ground surface, and the UAV was based on the orthomosaic images, following the road's centerline, for further profile creation with an equidistance of 50 cm. To connect the values of these measurements, it was necessary

to define one starting point. It was defined as a Local Altimetry Datum with an UAV elevation value of 1012.23 meters. TS values were adjusted to the Datum by applying an offset procedure. From the UAV measurements some elevation points that matched the TS measurement points were selected based on the minimum horizontal distance or proximity criteria and presented in the table. The calculation of the gap was made with a maximum value of 0.263 meters and a Root Mean Square Error (RMSE) of 0.153 meters. No adjustments were made for the position measurement of either results and the scale was not modified. The comparison of the measurements for Profile 2, was based on the differences in the calculation. The electrical pole number 5 was set at a certain elevation and distance datum for each measurement. The RMSE consist of a distance measurement of 0.288 meters, a position of 1.576 meters, and an Elevation of 0.494 meters. The comparison of the measurements for the Profile 6 and 7 was based on the differences between UAV and the levelling scale reading through the photo. The maximum difference was a value of about 8 centimeters. A comparison of the measurements, in terms of distance and altimetry, presented agreeable results. For acceptable accuracy in global positioning, it is required that positioning measurement methods be used with satellite signal correction such as Real Time Kinematic (RTK), Post Processing Kinematic (PPK), and Differential Global Navigation Satellite System (DGNSS) for both measurements and additional GCPs for UAV Mapping.

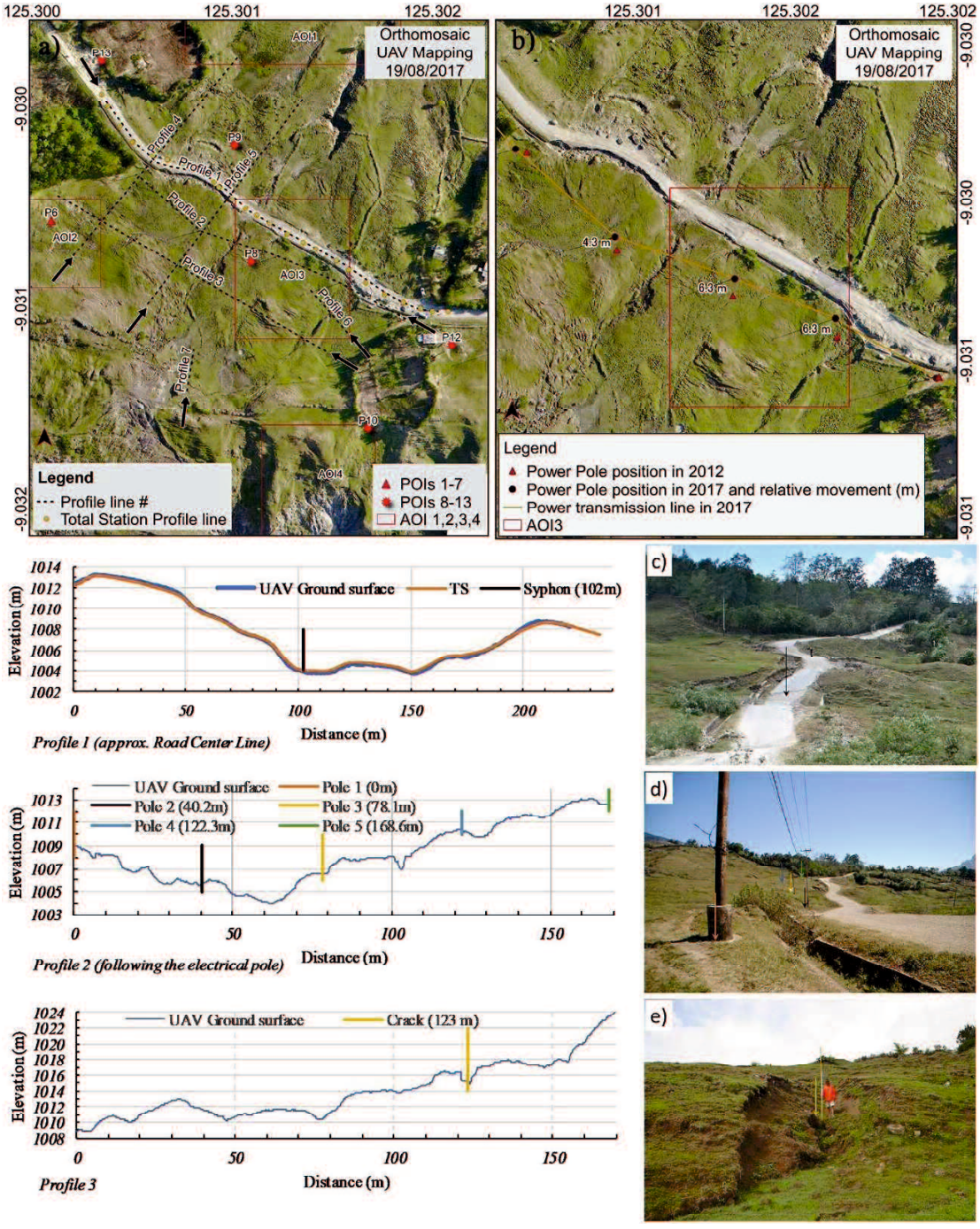


**Figure 5.12.** **a**) Position of terrain profile section, **b**) Relative horizontal movement of electrical pole, **c**) Illustration of Profile 1, **d**) Illustration of Profile 2, and **e**) Illustration of Profile 3

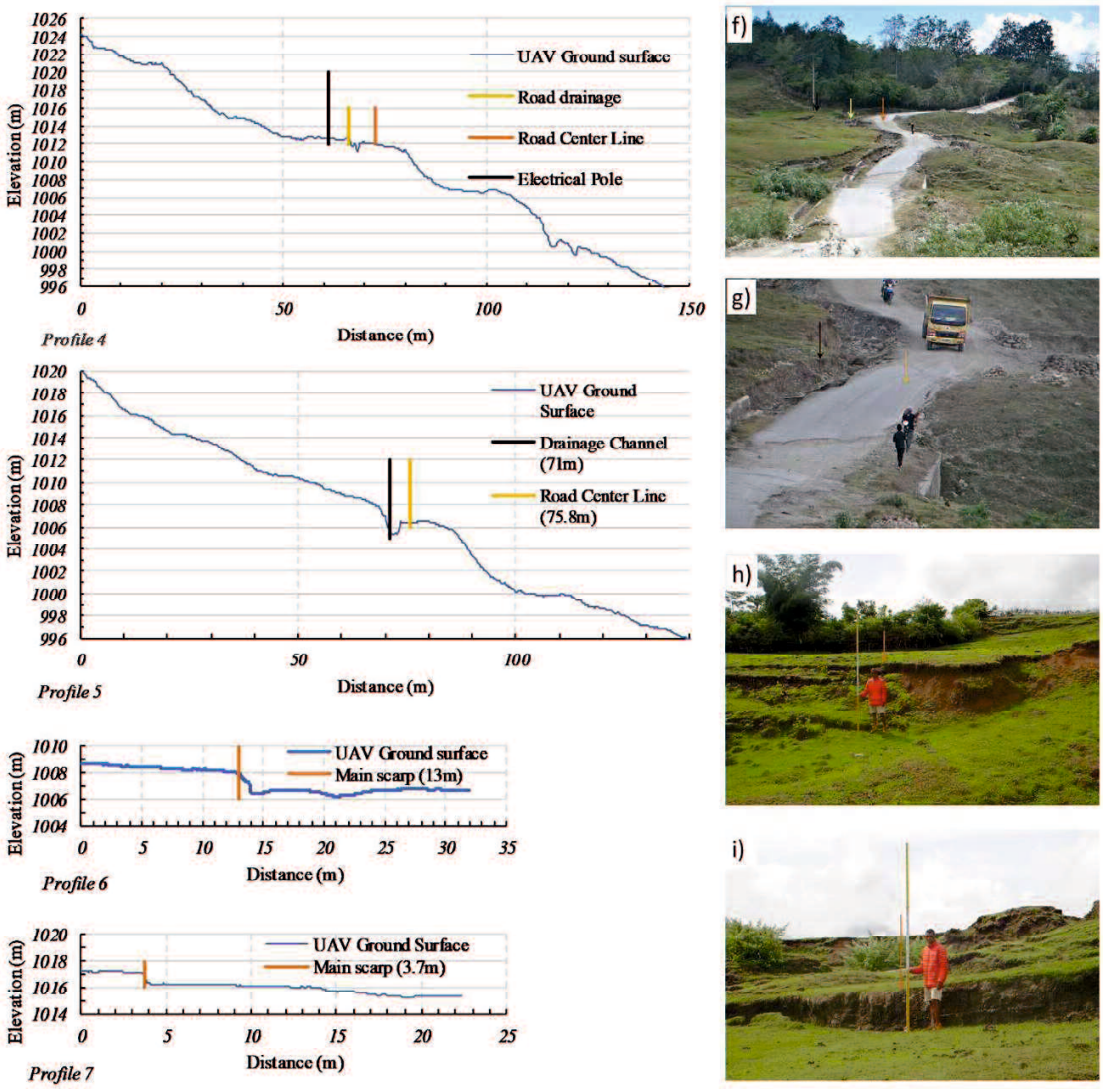


**Figure 5.13. f**) Illustration of Profile 4, **g**) Illustration of Profile 5, **h**) Illustration of Profile 6, and **i**) Illustration of Profile 7

Additionally, the PALSAR1 and PALSAR2 LOS displacement time-series were gathered with the earthquake data from the USGS Earthquake Catalogue and the daily rainfall data from CFSR/NCEP and local ground stations in order to find their relationship in time occurrences, as presented in Figure 5.14. Even with a moderate slope with approximately 12

degrees of inclination, the ground deformation continues and slides in the northeast in the same direction as the watercourses. From the LOS displacement values and the UAV orthomosaic and DEM images interpretation results, some representative POIs, such as P2, P6, P8, and P9, were chosen. At the end of the second period, P8 and P9 reached maximum values of more than 200 mm. These two POIs are located on either side of the deformed road alignment (Figure 5.11). The relevant earthquake attributes, the magnitude scale starting from 4.5 up to the maximum recorded values, and the hypocenter depth were selected. The rainfall data available from CFSR only covered the first period and continued until 31 July 2014. Unfortunately, for the second period the daily rainfall data were not totally collected due to time and technical limitations. The rainfall data collected from the ground station rainfall data logger partially covered the second period, starting from 7 March 2017 and continuing until the end of the period of study. The earthquake events were extracted according to the study period and the epicenter position within a radius of 100 km from the study location. For the first and second periods, 21 and 34 earthquake events were selected, respectively. The earthquakes were generally shallow, with hypocenter depths of less than 50 km for both periods.

Some previous works have confirmed these factors that influence the dynamic process of the geological and tectonic formations of the island. Audley-Charles (1968) considered the tropical rainfall as the factor responsible for the rugged topography of the Bobonaro region characterized by deep gullies, landslides, and knobby hillsides, as shown in Figure 3.2. Due to the location of Timor Island in the arc-collision zone (Audley-Charles, 1968; Barber, 1981; Hamilton, 1979; Norvick, 1979; Kaneko et al, 2007; Nugroho et al, 2009; Ota et al, 2010), Norvick (1979) illustrated the tectonic mechanism and high seismic activity reflected in the mountain characteristics, followed by the fragmented and chaotic structures of the thrust and fold zones shown in Figure 2.1b.

In this study, some interpretations are presented based on Figure 5.14. During the first year, from 1 January 2007 to 1 July 2007 eight earthquake events were recorded, one with a maximum magnitude of 5.1 and practically all occurring during rainy months, however with low amounts of rainfall. The ground deformation presented the maximum value of −38.1

mm. During the fourth year, January 2010 to January 2011, six earthquake events were recorded with an average magnitude of 4.5, and the rainfall amount was higher than that of the previous years. The ground deformation presented the maximum value of −65.7 mm. However, for the third year, January 2009 to January 2010, only two earthquakes were recorded, with magnitudes of 5.1 and 5.0 and a moderate amount of rainfall. The ground deformation presented the maximum value of −46.9 mm. During the sequences of events in the second period, the earthquake reached the maximum magnitude of 6.5 and the hypocenter depth of 20 km on 4 November 2015. In the same month, 16 earthquake events were recorded, with an average magnitude of 5.0. At this stage, no rainfall contribution could be found. However, one landslide occurrence was recorded in January 2017 during heavy rainfall. Based on this evidence, it was assumed that the rainfall in 2017 was high. From November 2015 to March 2017, the ground deformation presented the maximum value of −102. 6 mm. For the next few years, the LOS displacement values showed positive evolution linked with the rainy season and seismic activity until the end of the study period. From January 2018 to April 2019, the ground deformation presented the maximum value of −82.4 mm.

It is well known that the occurrence of an earthquake with a certain magnitude or greater triggers the reactivation of landslides. However, the influence does not always appear immediately after the earthquake. On the other hand, heavy or long rainfall events induce landslides and/or changes in the ground, and their influence can appear a relatively short time after the event under specific ground conditions. This is because the time it takes rainfall water to infiltrate into the ground depends on the degree of development of the catchment areas, the permeability of the ground, and the presence of cracks in the ground (Zhou and Tang, 2014; Fan et al. 2019). Considering the above characteristics, it can be denied that the timing of ground deformation, earthquake events, and periodic rainfall are clearly related to and based on the results of the LOS displacement time-series for either period. As a practical approach, Figure 5.11 presents important information that should be considered as complementary data for this study. In future works, a more precise approach will be needed to reach an acceptable conclusion.

During the first period, the maximum earthquake magnitude was 5.1 and the hypocenter depth was 25 km, it occurred on 8 March 2007. Figure 5.14 shows that the LOS displacement values increased after or during the earthquake. During the fourth year, it is clear that the earthquake and the rainfall acted together to drastically change the LOS displacement values. Throughout the sequences of the events in the second period, the earthquake reached the maximum magnitude of 6.5 and the hypocenter depth of 20 km, recorded on 4 November 2015. In the same month, 16 earthquake events were recorded with an average magnitude of 5.0. After that, the LOS displacement values changed drastically followed by four more earthquake events. At this stage, no rainfall contribution could be found. After that, the ground surface tended to stabilize, even though four earthquake events with an average magnitude of 4.5 and high rainfall were recorded. However, during the next stage, the LOS displacement values drastically changed with one earthquake event that was recorded with a magnitude of 5.1 and high rainfall during the wet season. The LOS displacement time-series for both periods show that the time occurrences of the ground surface deformation, earthquake events sequences and periodic rainfalls are clearly related.

The correlation of P2 and P6 at the end of the first period and at the beginning of the second period apparently showed that from 2011 to 2015 the ground was stable. Indeed, during this period, only nine earthquake events were recorded, and the rainfall is not well distributed compared with the first period. However, on 6 July 2013, the highest rainfall amount of about 164 mm/day was recorded. From 2009 to 2010, the LOS values also showed the same characteristics, after that the LOS values increased. Otherwise, the LOS displacement of P9 showed high displacement right after the second period started. To verify this conclusion, related information and data are required for confirmation and further analysis.

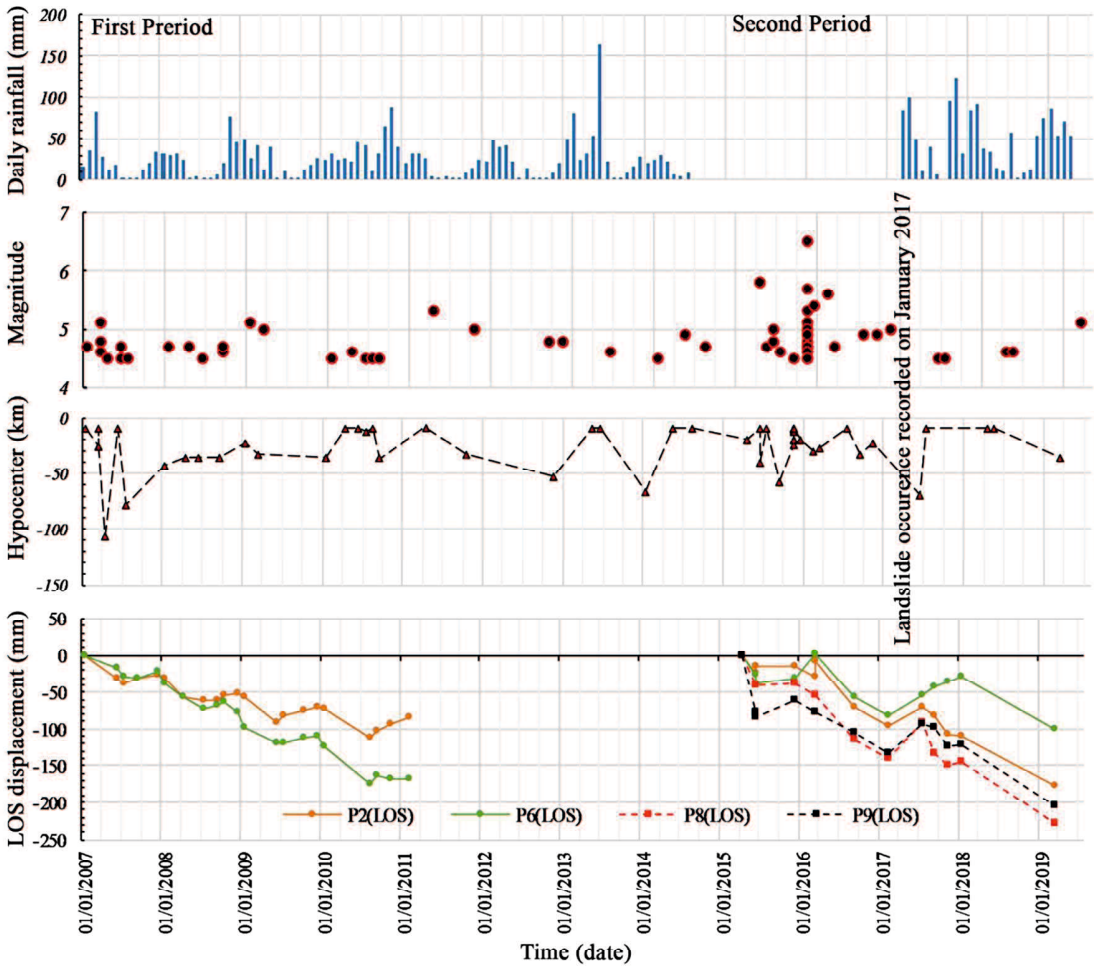


**Figure 5.14.** Relationship in time occurrences of PALSAR1 and PALSAR2 LOS displacement time-series with earthquake events and daily rainfall data.

## 5.7 Conclusion

The natural phenomenon of ground surface deformation in Bobonaro, near the village of Oeleo, has been taking place over the last many years, generating a great deal of material losses for its citizens and considerable financial loss of the state budget spent in vain on road construction and maintenance.

In this study, it was proved that multi-temporal DInSAR is capable of detecting ground surface deformation on a local scale within the extension of an area of less than 1 $km^2$. The

results of the LOS displacement showed the trend in the ground surface deformation during the two periods of study. The main advantage of this technique is that it is useful for ground surface deformation screening, even in small areas of interest and under moderate slope conditions. The latest PALSAR2 LOS displacement corresponds well with the ground surface deformation morphology mapped by the small UAV DJI Mavic Pro. UAV high-resolution data, obtained by orthomosaic means and DEM, were useful for making interpretations and performing highly accurate measurements of the ground surface deformation. The measurements varied from centimeters to meters in both vertical and horizontal directions. Furthermore, on-site field observations were used to clarify the UAV photogrammetry results. The evidence given in this work shows that the DInSAR and UAV photogrammetry techniques, used in combination, present agreeable results.

This combination is one of the solutions for monitoring ground surface deformation in Timor-Leste. A detailed mapping of the ground deformation will serve as a base for developing further specialized fields of study related to this phenomenon, such as geological structures, geomorphology, climate and hydrology, the geotechnical properties of the rock, and excavation engineering. The achievements of these studies will contribute to supporting the infrastructure development specifically for road design and construction and generally to the risk management strategies of the country.

The results of the LOS displacement time-series showed that the time occurrence of the ground deformation, earthquake sequences, and periodic rainfalls are notably related. From the first period, it was found that earthquakes and rainfalls sometimes took place consecutively or simultaneously. It might be possible that the ground deformation was initiated by an earthquake, even that of a moderate magnitude, and that months or years afterwards the rainfall it certainly contributed to the continuing process of ground surface deformation.

**Acknowledgments**

We would like to express our deepest gratitude to JAXA for providing ALOS1 PALSAR1 and ALOS2 PALSAR2 data as well as all individuals and institutions who directly or indirectly provided valuable support and information for this chapter.

**References**

Ardi ND, Iryanti M, Asmoro CP, Nurhayati N, Agustine E (2018) Mapping Landslide Potential Area using Fault Fracture Density Analysis on Unmanned Aerial Vehicle (UAV) Image. In IOP Conference Series: Earth and Environmental Science vol 145. https://doi.org/10.1088/1755-1315/145/1/012010

Burdziakowski P (2018) Low cost real time UAV stereo photogrammetry modelling technique–accuracy considerations. In E3S Web of Conferences vol 63:1-5. https://doi.org/10.1051/e3sconf/20186300020

Carrillo LRG, López AED, Lozano R, Pégard C (2012) Combining stereo vision and inertial navigation system for a quad-rotor UAV. Journal of intelligent & robotic systems 65(1-4):373-387. https://doi.org/10.1007/s10846-011-9571-7

Costantini M (1998) A novel phase unwrapping method based on network programming. IEEE Transactions on geoscience and remote sensing, 36(3):813-821. https://doi.org/10.1109/36.673674

Djimantoro MI, Suhardjanto G (2017) The Advantage by Using Low-Altitude UAV for Sustainable Urban Development Control. In IOP Conference Series: Earth and Environmental Science vol 109. https://doi.org/10.1088/1755-1315/109/1/012014

Fan X, Scaringi G, Korup O, West AJ, van Westen CJ, Tanyas H, Hovius N, Hales TC, Jibson RW, Allstadt KE, Zhang L, Evans SG, Xu C, Li G, Pei X, Xu Q, Huang R (2019) Earthquake-induced chains of geologic hazards: Patterns, mechanisms, and impacts. Reviews of geophysics, 57(2),421-503. [https://doi.org/10.1029/2018RG000626]

Fan X, Scaringi G, Korup O, West AJ, van Westen CJ, Tanyas H, Hovius N, Hales TC, Jibson RW, Allstadt KE, et al. (2019) Earthquake-induced chains of geologic hazards: Patterns, mechanisms, and impacts. Rev. Geophys, 57, 421–503, [https://doi:10.1029/2018RG000626]

Goldstein RM, Werner CL (1998) Radar interferogram filtering for geophysical applications. Geophysical research letters, 25(21):4035-4038. https://doi.org/10.1029/1998GL900033

Hanssen RF (2001) Radar interferometry: data interpretation and error analysis. Remote sensing and digital image processing vol 2:308p, Springer Science & Business Media. ISBN:0306476339 9780306476334

He H, Chen T, Zeng H, Huang S (2019) Ground Control Point-Free Unmanned Aerial Vehicle-Based Photogrammetry for Volume Estimation of Stockpiles Carried on Barges. Sensors 19(16):3534. https://doi.org/10.3390/s19163534

Hu S, Qiu H, Pei Y, Cui Y, Xie W, Wang X, Yang D, Tu X, Zou Q, Cao P, Cao M (2018) Digital terrain analysis of a landslide on the loess tableland using high-resolution topography data. Landslides 16(3):617-632. https://doi.org/10.1007/s10346-018-1103-0

Li CC, Zhang GS, Lei TJ, GONG AD (2011) Quick image-processing method of UAV without control points data in earthquake disaster area. Transactions of Nonferrous Metals Society of China 21:523-528. https://doi.org/10.1016/S1003-6326(12)61635-5

Li XQ, Chen ZA, Zhang LT, Jia D (2016) Construction and accuracy test of a 3D model of non-metric camera images using agisoft photoscan. Procedia Environ. Sci. 2016, 36, 184–190. [https://doi:10.1016/j.proenv.2016.09.031]

Liu JG, Mason PJ (2013) Essential image processing and GIS for remote sensing. John Wiley & Sons. Print ISBN:9780470510322, Online ISBN:9781118687963, https://doi.org/10.1002/9781118687963

Moreira A, Prats-Iraola P, Younis M, Krieger G, Hajnsek I, Papathanassiou KP (2013) A tutorial on synthetic aperture radar. IEEE Geoscience and remote sensing magazine 1(1):6-43. https://doi.org/10.1109/MGRS.2013.2248301

Patrucco G, Rinaudo F, Spreafico A (2019) Multi-Source Approaches For Complex Architecture Documentation: The" Palazzo Ducale" In Gubbio (Perugia, Italy). International Archives of the Photogrammetry, Remote Sensing & Spatial Information Sciences vol 17(2):953-960. https://doi.org/10.5194/isprs-archives-XLII-2-W11-953-2019

Pepe A, Calò F (2017) A review of interferometric synthetic aperture RADAR (InSAR) multi-track approaches for the retrieval of Earth's surface displacements. Applied Sciences 7(12):1264. https://doi.org/10.3390/app7121264

quan Li X, an Chen Z, ting Zhang L, Jia D (2016) Construction and Accuracy Test of a 3D Model of Non-Metric Camera Images Using Agisoft PhotoScan. Procedia Environmental Sciences 36:184-190. https://doi.org/10.1016/j.proenv.2016.09.031

Sandwell DT, Myer D, Mellors R, Shimada M, Brooks B, Foster J (2008) Accuracy and resolution of ALOS interferometry: Vector deformation maps of the Father's Day intrusion at Kilauea. IEEE Transactions on Geoscience and Remote Sensing 46(11):3524-3534. https://doi.org/10.1109/TGRS.2008.2000634

Sanz-Ablanedo E, Chandler J, Rodríguez-Pérez J, Ordóñez C (2018) Accuracy of unmanned aerial vehicle (UAV) and SfM photogrammetry survey as a function of the number and location of ground control points used. Remote Sensing 10(10):1606. https://doi.org/10.3390/rs10101606

Tang W, Liao M, Yuan P (2016) Atmospheric correction in time-series SAR interferometry for land surface deformation mapping–A case study of Taiyuan, China. Advances in Space Research 58(3):310-325. https://doi.org/10.1016/j.asr.2016.05.003

Turner D, Lucieer A, Watson C (2012) An automated technique for generating georectified mosaics from ultra-high resolution unmanned aerial vehicle (UAV) imagery, based on structure from motion (SfM) point clouds. Remote sensing, 4(5), 1392-1410. [https://doi.org/10.3390/rs4051392]

Windle AE, Poulin SK, Johnston DW, Ridge JT (2019) Rapid and Accurate Monitoring of Intertidal Oyster Reef Habitat Using Unoccupied Aircraft Systems and Structure from Motion. Remote Sensing, 11(20):2394. https://doi.org/10.3390/rs11202394

Zhang Y, Yue P, Zhang G, Guan T, Lv M, Zhong D (2019) Augmented Reality Mapping of Rock Mass Discontinuities and Rockfall Susceptibility Based on Unmanned Aerial Vehicle Photogrammetry. Remote Sensing, 11(11):1311. https://doi.org/10.3390/rs11111311

Zhou W, Tang C (2014) Rainfall thresholds for debris flow initiation in the Wenchuan earthquake-stricken area, southwestern China. Landslides, 11, 877–887, [https://doi:10.1007/s10346-013-0421-5]

Zhou W, Tang C(2014) Rainfall thresholds for debris flow initiation in the Wenchuan earthquake-stricken area, southwestern China. Landslides, 11(5),877-887. [https://doi.org/10.1007/s10346-013-0421-5]

# Chapter 6

# CONCLUSION AND RECOMMENDATIONS FOR FUTURE WORK

## 6.1 Conclusion

In this chapter, a conclusion will be presented for this study based on the four objectives mentioned previously in this dissertation, as follows: a) application of DInSAR to detect and evaluate the recent ground surface deformation since 2007 in a Complex Landslide Slope in Bobonaro, b) employment of Unmanned Aerial Vehicle (UAV) Photogrammetry to detect the detailed ground deformation, c) relation of ground deformation to earthquakes and hard rainfall events, and d) finding the people's consciousness and preparedness for geo-disasters.

a) The multi-temporal DInSAR is capable of detecting the ground surface deformation even in local scale within the extension of an area of less than 1 $km^2$ and under a moderate slope condition of about 12 degrees. The results of the LOS displacement time-series clearly revealed the trend in the ground surface deformation during the two periods of study.
b) UAV orthomosaic and DEM data are capable of revealing detailed features and important information on the ground surface morphology. Based on UAV data, it was possible to conduct ground surface measurements with centimeter-order accuracy and to interpret the ground surface deformation morphology and the direction of the ground movement.
c) The LOS displacement time-series revealed that the time occurrence of the ground deformation, earthquake sequences, and periodic rainfalls are notably related.
   It might be possible that the ground deformation was initiated by an earthquake and that, months or years afterwards, the rainfall certainly contributed to the continuing process of ground surface deformation.
d) The majority of people have experienced geo-disasters. Consequently, their consciousness about geo-disasters is thought to be high. However, their preparedness is very low and they tended to ignore the concept of preparing for. To overcome this situation, is very important to introduce soft countermeasure methods through

education. By introducing knowledge about the prevention and reduction of natural and man-made disasters into the school curriculum, geo-disasters preparedness will certain increase to a value of 50%, at least in the short term.

## 6.2 Recommendations for future work

The results given in this work show that the DInSAR and UAV Photogrammetry techniques, used in combination, are capable of screening ground deformation in vast areas and detecting detailed ground surface deformation. Both methods area advantageous in that they do not require any sensors. DInSAR is capable for screening usual and unusual ground behavior, and UAV Photogrammetry is flexible to use and capable of detecting ground displacements with centimeter-order accuracy after DInSAR screening.

Therefore, the combination of DInSAR and UAV Photogrammetry is one of the solutions for monitoring ground deformation in Timor-Leste. The first step is to develop a ground deformation screening campaign by DInSAR that covers the entire national territory. The second step is to develop UAV mapping after identifying the spatial distribution of the ground deformation detected by DInSAR for further detailed analysis and interpretation. A detailed mapping of the ground deformation will serve as a base for developing further specialized fields of study related to this ground instability, such as geological structures, geomorphology, climate and hydrology, geotechnical properties of the rock and excavation engineering.

**Appendix 1 – An example of literature review table on UAV Photogrammetry Landslide Monitoring**

| Auhors | DOI | Main objective | Technique and Materials | | | | Descrption | Geoenvironment factors |
|---|---|---|---|---|---|---|---|---|
| Walstra et al, 200; | 10.1144/SP283.5 | Landslide Monitoring | Phogrammetry | Orthomosaic | DEM | 3DView | Provide detailed information and measurement | |
| Gong et al, 2010 | 10.1007/s10346-010-0201-4 | Geological hazadrs Mapping | Phogrammetry | Orthomosaic | | | Aid the classificatio accuracy assesment | |
| Niethammer et al, | 10.1016/j.enggeo.2011.03.012 | Landslide Monitoring | Phogrammetry | Orthomosaic | DEM | 3DView | Imaging fissures and displacement | |
| Lucieer at al, 2014 | 10.1177/0309133313515293 | Mapping Landslide | Phogrammetry | Orthomosaic | DEM | 3DView | Visual interpretation and Quantify terrain displacement | |
| Turner et al, 2015 | 10.3390/rs70201736 | Landslide Monitoring | Phogrammetry | Orthomosaic | DEM | 3DView | Planimetric and vertical error assesment (Elevation Profile) | AUV and Total Station | Time Series Analysys of Landslide Dynamics | |
| Peppa et al, 2016 | 10.5194/isprsarchives-XLI-B5-895-2016 | Landslide Monitoring | Phogrammetry | Orthomosaic | DEM | 3DView | Planimetric and vertical error assesment (Elevation Profile) | AUV and Total Station | UAV accuracy assesment | |
| Peternel et al, 201 | 10.1007/s10346-016-0759-6 | Landslide Monitoring | Phogrammetry | Orthomosaic | DEM | 3DView | Planimetric and vertical error assesment (Elevation Profile) | AUV and Total Station | Displacement measurement using UAV and TS | |
| Fan et al, 2017 | 10.1007/s10346-017-0907-7 | Landslide Monitoring | Phogrammetry | Orthomosaic | DEM | 3DView | Planimetric and vertical error assesment (Elevation Profile) | | Interpretation of failure mechanism and kinematic using UAV and Ground-based SAR | |
| Hu et al, 2018 | 10.1007/s10346-018-1103-9 | Landslide Monitoring | Phogrammetry | Orthomosaic | DEM | 3DView | Planimetric and vertical error assesment (Elevation Profile) | | Landslide undertanding throuh gromorphologc evolution | Geology and Rainfall |
| Ma et al, 2018 | 10.1007/s10346-018-1104-z | Landslide Monitoring | Phogrammetry | Orthomosaic | DEM | 3DView | Planimetric and vertical error assesment (Elevation Profile) | | Interpratalon of geometric and kinematic landslide based on UAV DEM | |
| O'Driscol, 2018 | 10.1016/j.ascrep.2018.09.010 | Landscape studies | Phogrammetry | Orthomosaic | DEM | 3DView | Planimetric and vertical error assesment (Elevation Profile) | | Landscape modelling and visual intrepretation | |
| Rossi et al, 2018 | 10.1007/s10346-018-0978-0 | Landslide Monitoring | Phogrammetry | Orthomosaic | DEM | 3DView | | | Multitemporal landslide mapping and geomorphological features characterization | Geology and Rainfall |
| Zhu et al, 2019 | 10.1007/s10346-019-01262-z | Landslide Monitoring | Phogrammetry | Orthomosaic | DEM | 3DView | Planimetric and vertical error assesment (Elevation Profile) | | Describe the characteristics and failure mechanism of landslide | Geology and Rainfall |
| Li et al, 2020 | 10.1007/s10346-019-01334-0 | Landslide Monitoring | Phogrammetry | Orthomosaic | DEM | 3DView | | | Investigation of failure mechanism, hazard and risk analysis using UAV and Ground-based SAR | Geology and Rainfall |

# Appendix 2 – Questionnaire and answer charts

*[bhm2018]*

**TIMOR-LESTE - NATURAL HAZARD CONCERN AND PREPAREDNESS QUESTIONNAIRE**

This questionnaire is designed to identify and investigate the community's concerns and preparedness about natural hazards. The questionnaire should be completed by an adult, preferably the homeowner or the head of the household. All individual responses are strictly confidential and for research purposes only.

**GENERAL HOUSEHOLD INFORMATION**

Gender?
□ male □ female
Age? _____
Address? Aldeia_____ Suco _____ Posto Admin. _____ Município _____
Occupational status? _____
Educational level?
□ Did not attend school □ Primary school □ Junior high school □ High school □ College/University □ Vocational training

**QUESTIONNAIRE**

How concerned are you about the following disasters affecting your community? Please give each hazard a priority rating as follows ***(Q1)***

| Type of natural disasters | Extremely concerned | Very concerned | Concerned | Somewhat concerned | Not concerned |
|---|---|---|---|---|---|
| Landslide | | | | | |
| Ground deformation | | | | | |
| Debris flow | | | | | |
| Rain storm | | | | | |
| Wind storm | | | | | |
| Drought | | | | | |
| Wildfire | | | | | |
| Others | | | | | |

How long do you live in this place? ***(Q2)***
□ Less than a year □ 1 to 5 years □ 5 to 10 years □ 10 to 15 years □ 15 to 20 years □ 20 years or more

Have you received information about your location being located in a natural risk zone? ***(Q3)***
□ Yes □ No

If "YES" from whom (person/institution) you have received the information? ***(Q4)***
□ Elders people □ Local authority □ ONGs □ Others _____

In the past ten years have you or someone in your household experienced a natural disaster? ***(Q5)***
□ Yes □ No

If "YES" which of these natural disasters? (Allowed to check more than that apply) ***(Q6)***
□ Landslide □ Ground deformation □ Debris flow □ Rain storm □ Wind storm □ Drought Wildfire
□ Others _____

Have you ever received information about how to make your family home safer from natural disasters? ***(Q7)***
□ Yes □ No

Have you received any logistic and financial support? ***(Q8)***
□ Yes □ No

If "YES" from whom (person/institution) you have received the support? ***(Q9)***
□ Neighbors □ Government □ NGOs □ Others _____

What is the most effective way for you to receive information about how to make your home safer from natural disasters? (Check all that apply) ***(Q10)***

□ Television □ Radio □ Billboard □ Local Authority □ Public Meetings □ Newspaper □ Not follow

In the following list, please check those activities that apply. (□ If not participate no need to answer) ***(Q11)***

| Have you or someone in your household: | Have done | Plan to do | Not done | Unable to do |
|---|---|---|---|---|
| Attended meetings or received written information on natural disasters or emergency preparedness? | | | | |
| Talked with family members about what to do in case of a disaster or emergency? | | | | |
| Developed a "Household/Family Emergency Plan" in order to decide what everyone would do in the event of a disaster? | | | | |
| Prepared a "Disaster Supply Kit" (extra food, water, medications, batteries, first aid items and other emergency supplies)? | | | | |
| In the last year, has anyone in your household been trained in First Aid or Cardio-Pulmonary Resuscitation (CPR)? | | | | |

Natural & human caused disasters can have a significant impact on a community but planning for these events can help lessen the impact. Is important for the future, Authority and Community elaborate a plan to face those hazards? **(Q12)**

□ Very important □ Important □ Neutral □ Not very important □ Not important

Did you consider the possible occurrence of a natural hazard when you bought/moved into your current home? ***(Q13)***

□ Yes □ No

Would you be willing to spend more money on a home that has features that make it more disaster resistant? ***(Q14)***

□ Yes □ No

Did you consider choosing traditional house? (wood, leaf/grass or zinc?) ***(Q15)***

□ Yes □ No

Did you consider by yourself or public agency to choose a safety place to build house? ***(Q16)***

□ Yes □ No

**COMMENT/OTHER INFORMATION**

**Thank you very much for providing this information**

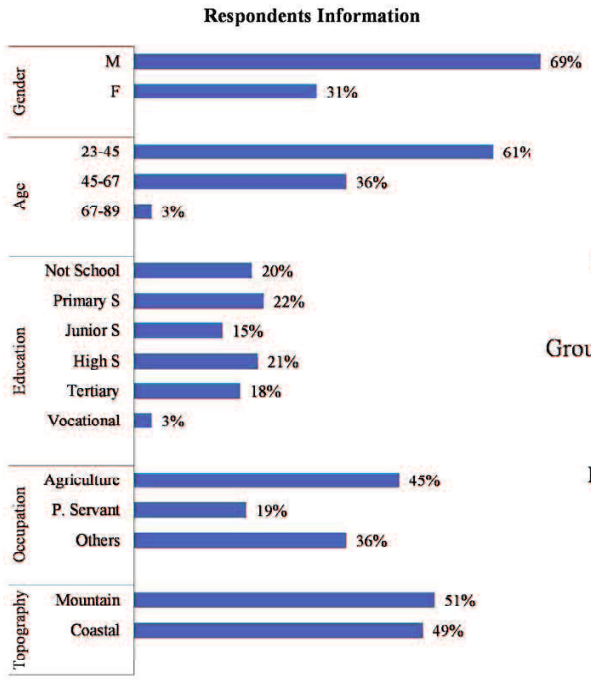
Respondents Information
Gender
M
F
69%
31%
Age
23-45
45-67
67-89
61%
36%
3%
Education
Not School
Primary S
Junior S
High S
Tertiary
Vocational
20%
22%
15%
21%
18%
3%
Occupation
Agriculture
P. Servant
Others
45%
19%
36%
Topography
Mountain
Coastal
51%
49%

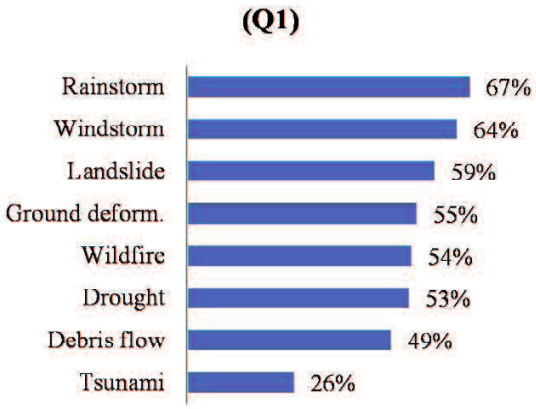
(Q1)
Rainstorm 67%
Windstorm 64%
Landslide 59%
Ground deform. 55%
Wildfire 54%
Drought 53%
Debris flow 49%
Tsunami 26%

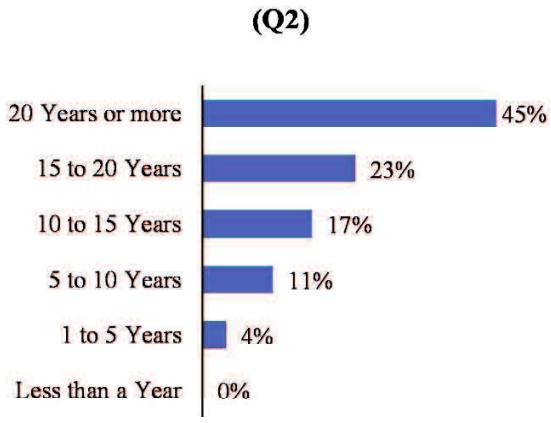
(Q2)
20 Years or more 45%
15 to 20 Years 23%
10 to 15 Years 17%
5 to 10 Years 11%
1 to 5 Years 4%
Less than a Year 0%

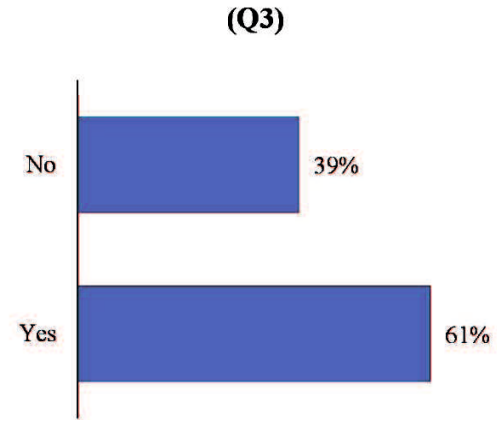
(Q3)
No 39%
Yes 61%

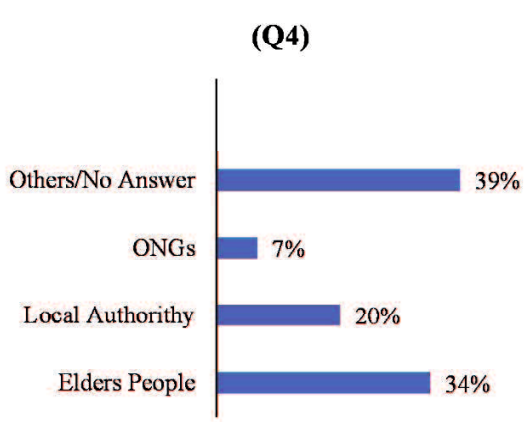
(Q4)
Others/No Answer 39%
ONGs 7%
Local Authorithy 20%
Elders People 34%

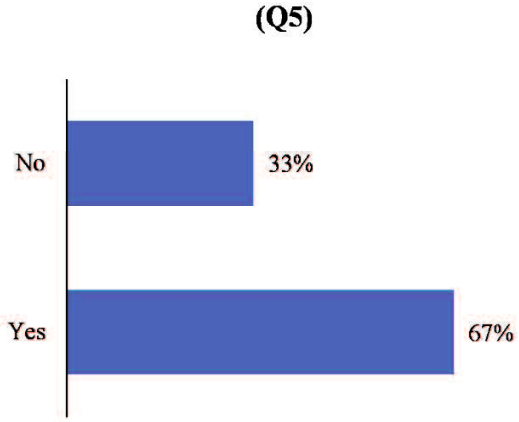
(Q5)
No 33%
Yes 67%

**(Q6)**

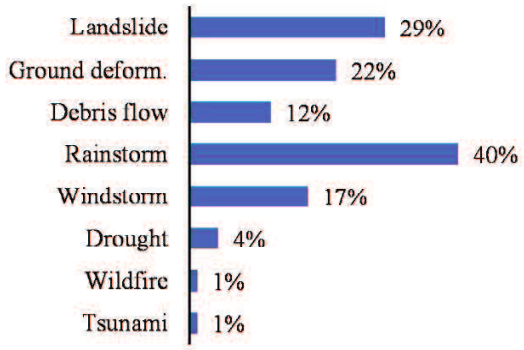


**(Q7)**

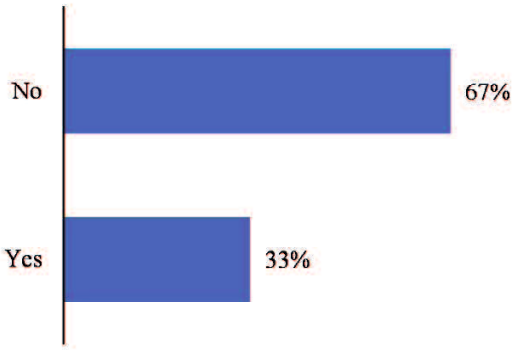


**(Q8)**

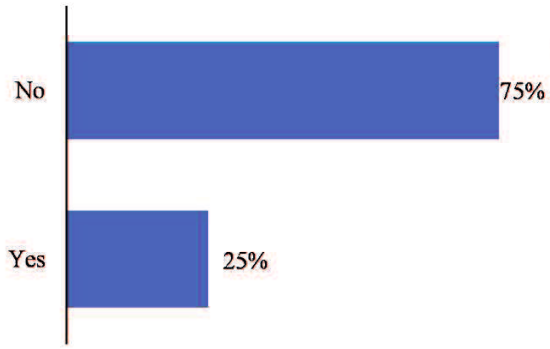


**(Q9)**

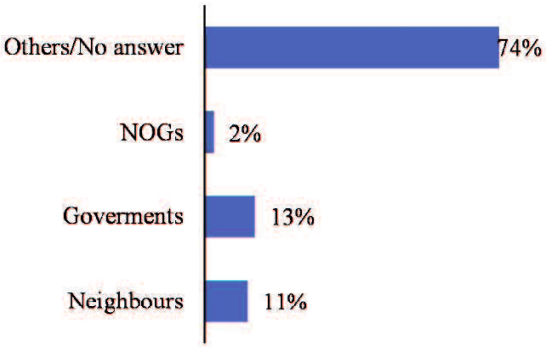


**(Q10)**

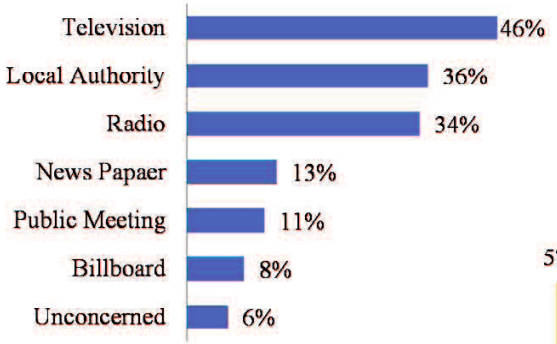


**(Q11)**

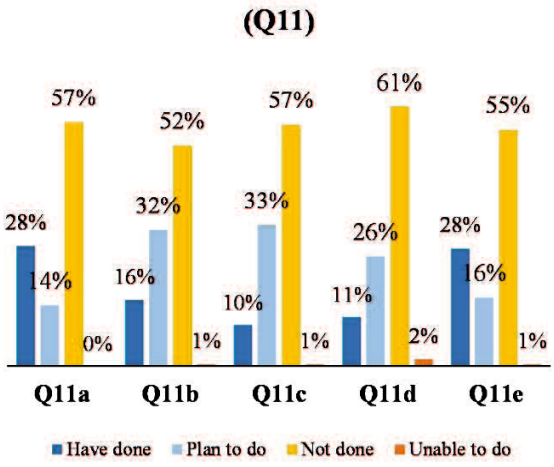

**(Q12)**

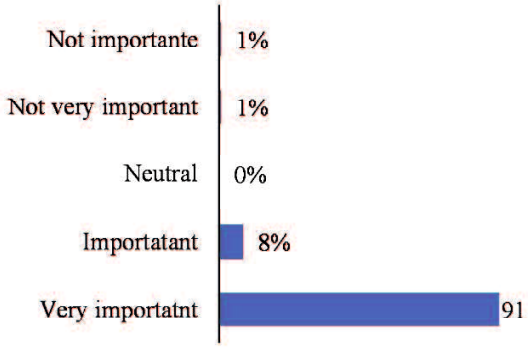


**(Q13)**

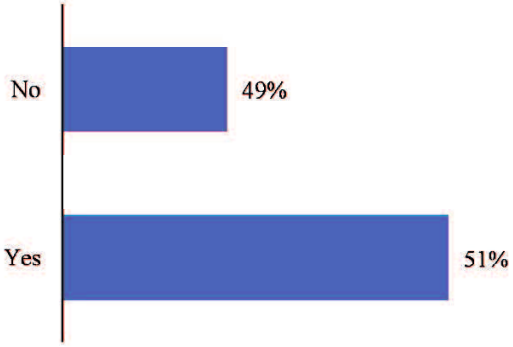


**(Q14)**

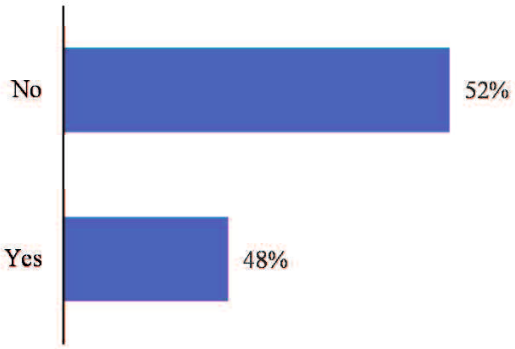


**(Q15)**

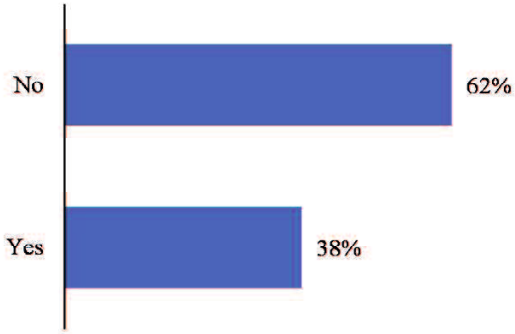


**(Q16)**

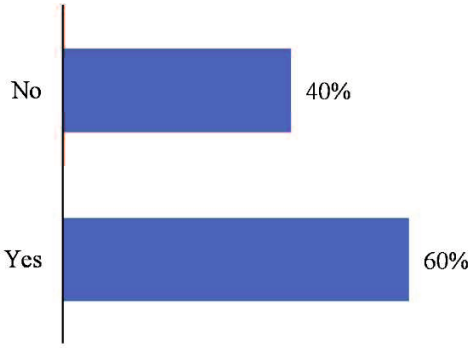

## Appendix 3 – ALOS1 PALSAR1 and ALOS2 PALSAR2 Dataset

| Index | Satellite Name | Sensor Name | Operation Mode | Scene ID | OBS Path Number | Centre Frame Number | Observation Date | Orbit Direction | Off Nadir Angle | Polarization |
|---|---|---|---|---|---|---|---|---|---|---|
| 1 | ALOS | PALSAR | FBS | ALPSRP053027000 | 404 | 7000 | 22/01/2007 | Ascending | 34.3 | HH |
| 2 | ALOS | PALSAR | FBD | ALPSRP073157000 | 404 | 7000 | 09/06/2007 | Ascending | 34.3 | HH+HV |
| 3 | ALOS | PALSAR | FBD | ALPSRP079867000 | 404 | 7000 | 25/07/2007 | Ascending | 34.3 | HH+HV |
| 4 | ALOS | PALSAR | FBD | ALPSRP086577000 | 404 | 7000 | 09/09/2007 | Ascending | 34.3 | HH+HV |
| 5 | ALOS | PALSAR | FBS | ALPSRP099997000 | 404 | 7000 | 10/12/2007 | Ascending | 34.3 | HH |
| 6 | ALOS | PALSAR | FBS | ALPSRP106707000 | 404 | 7000 | 25/01/2008 | Ascending | 34.3 | HH |
| 7 | ALOS | PALSAR | FBD | ALPSRP120127000 | 404 | 7000 | 26/04/2008 | Ascending | 34.3 | HH+HV |
| 8 | ALOS | PALSAR | FBD | ALPSRP133547000 | 404 | 7000 | 27/07/2008 | Ascending | 34.3 | HH+HV |
| 9 | ALOS | PALSAR | FBD | ALPSRP140257000 | 404 | 7000 | 11/09/2008 | Ascending | 34.3 | HH+HV |
| 10 | ALOS | PALSAR | FBS | ALPSRP146967000 | 404 | 7000 | 27/10/2008 | Ascending | 34.3 | HH |
| 11 | ALOS | PALSAR | FBS | ALPSRP153677000 | 404 | 7000 | 12/12/2008 | Ascending | 34.3 | HH |
| 12 | ALOS | PALSAR | FBS | ALPSRP160387000 | 404 | 7000 | 27/01/2009 | Ascending | 34.3 | HH |
| 13 | ALOS | PALSAR | FBD | ALPSRP180517000 | 404 | 7000 | 14/06/2009 | Ascending | 34.3 | HH+HV |
| 14 | ALOS | PALSAR | FBD | ALPSRP187227000 | 404 | 7000 | 30/07/2009 | Ascending | 34.3 | HH+HV |
| 15 | ALOS | PALSAR | FBD | ALPSRP193937000 | 404 | 7000 | 14/09/2009 | Ascending | 34.3 | HH+HV |
| 16 | ALOS | PALSAR | FBS | ALPSRP200647000 | 404 | 7000 | 30/10/2009 | Ascending | 34.3 | HH |
| 17 | ALOS | PALSAR | FBS | ALPSRP207357000 | 404 | 7000 | 15/12/2009 | Ascending | 34.3 | HH |
| 18 | ALOS | PALSAR | FBS | ALPSRP214067000 | 404 | 7000 | 30/01/2010 | Ascending | 34.3 | HH |
| 19 | ALOS | PALSAR | FBD | ALPSRP240907000 | 404 | 7000 | 02/08/2010 | Ascending | 34.3 | HH+HV |
| 20 | ALOS | PALSAR | FBD | ALPSRP247617000 | 404 | 7000 | 17/09/2010 | Ascending | 34.3 | HH+HV |
| 21 | ALOS | PALSAR | FBD | ALPSRP254327000 | 404 | 7000 | 02/11/2010 | Ascending | 34.3 | HH+HV |
| 22 | ALOS | PALSAR | FBS | ALPSRP267747000 | 404 | 7000 | 02/02/2011 | Ascending | 34.3 | HH |

| Index | Satellite Name | Sensor Name | Operation Mode | Scene ID | OBS Path Number | Centre Frame Number | Observation Date | Orbit Direction | Off Nadir Angle | Polarization |
|---|---|---|---|---|---|---|---|---|---|---|
| 23 | ALOS2 | PALSAR-2 | SM3 | ALOS2038817010-150210 | 124 | 7010 | 10/02/2015 | Ascending | 28.2 | HH+HV |
| 24 | ALOS2 | PALSAR-2 | SM3 | ALOS2061587010-150714 | 124 | 7010 | 14/07/2015 | Ascending | 28.2 | HH+HV |
| 25 | ALOS2 | PALSAR-2 | SM3 | ALOS2071937010-150922 | 124 | 7010 | 22/09/2015 | Ascending | 28.2 | HH+HV |
| 26 | ALOS2 | PALSAR-2 | SM3 | ALOS2092637010-160209 | 124 | 7010 | 09/02/2016 | Ascending | 28.2 | HH+HV |
| 27 | ALOS2 | PALSAR-2 | SM3 | ALOS2115407010-160712 | 124 | 7010 | 12/07/2016 | Ascending | 28.2 | HH+HV |
| 28 | ALOS2 | PALSAR-2 | SM3 | ALOS2125757010-160920 | 124 | 7010 | 20/09/2016 | Ascending | 28.2 | HH+HV |
| 29 | ALOS2 | PALSAR-2 | SM3 | ALOS2146457010-170207 | 124 | 7010 | 07/02/2017 | Ascending | 28.2 | HH+HV |
| 30 | ALOS2 | PALSAR-2 | SM3 | ALOS2169227010-170711 | 124 | 7010 | 11/07/2017 | Ascending | 28.2 | HH+HV |
| 31 | ALOS2 | PALSAR-2 | SM3 | ALOS2179577010-170919 | 124 | 7010 | 19/09/2017 | Ascending | 28.2 | HH+HV |
| 32 | ALOS2 | PALSAR-2 | SM3 | ALOS2198207010-180123 | 124 | 7010 | 23/01/2018 | Ascending | 28.2 | HH+HV |
| 33 | ALOS2 | PALSAR-2 | SM3 | ALOS2208557010-180403 | 124 | 7010 | 03/04/2018 | Ascending | 28.2 | HH+HV |
| 34 | ALOS2 | PALSAR-2 | SM3 | ALOS2214767010-180515 | 124 | 7010 | 15/05/2018 | Ascending | 28.2 | HH+HV |
| 35 | ALOS2 | PALSAR-2 | SM3 | ALOS2262377010-190402 | 124 | 7010 | 01/04/2019 | Ascending | 28.2 | HH+HV |

## Appendix 4 – SBAS DInSAR time-series logical workflow

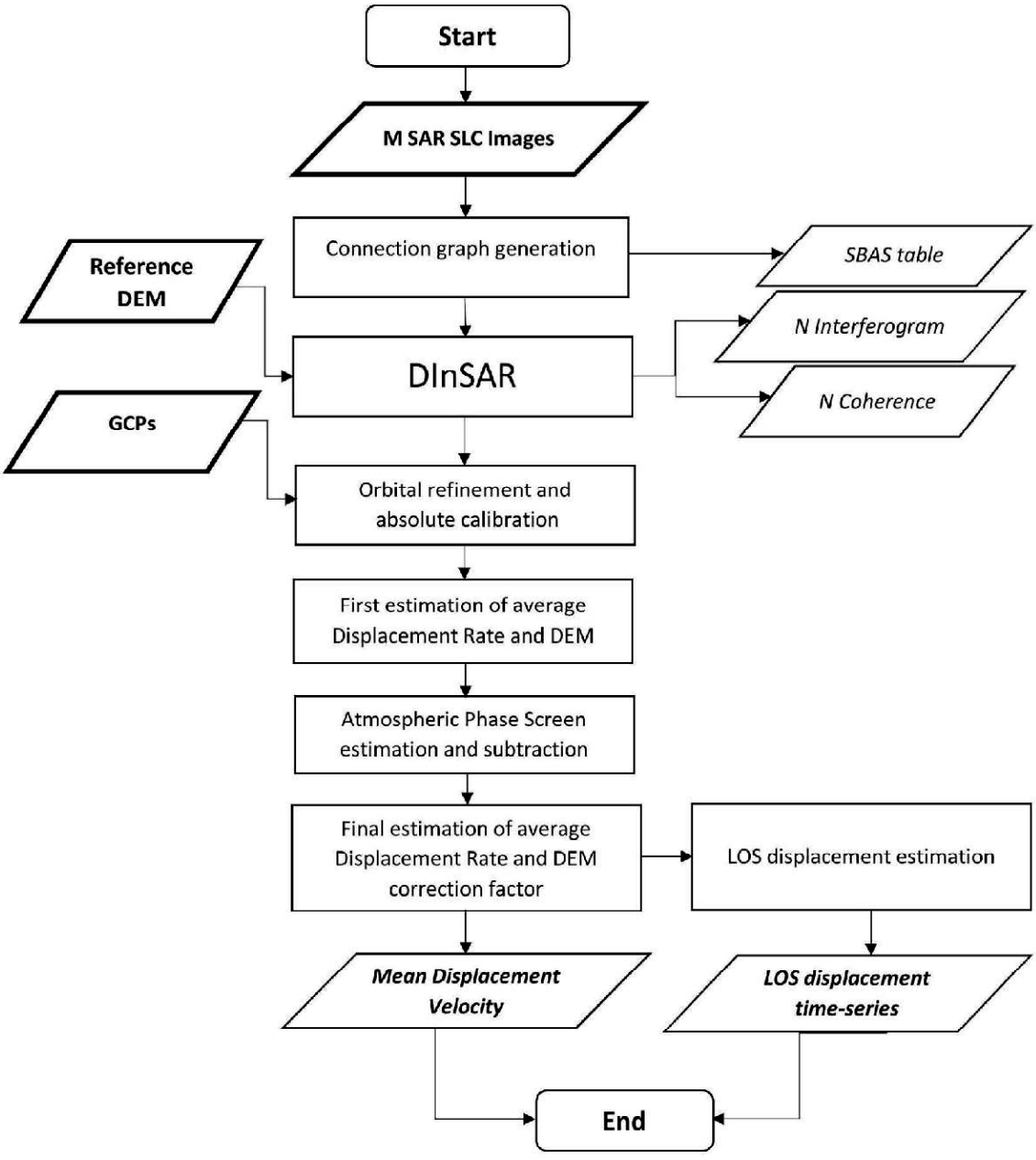


*SBAS DInSAR time-series Logical workflow, modified from sarmap,* ***2013***

## Appendix 5 – ALOS1 PALSAR1 LOS displacement maps

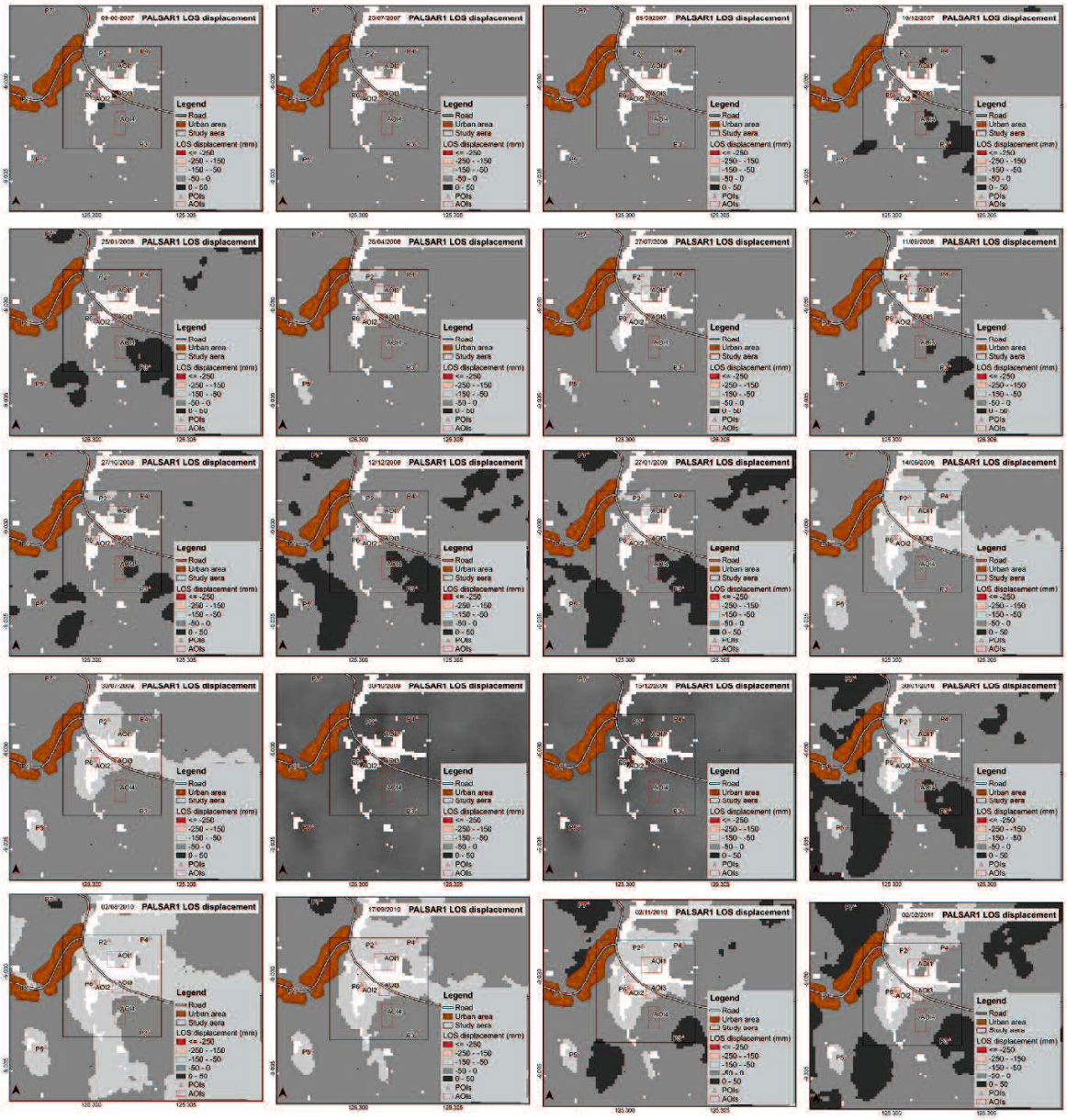

## Appendix 6 – ALOS2 PALSAR2 LOS displacement maps

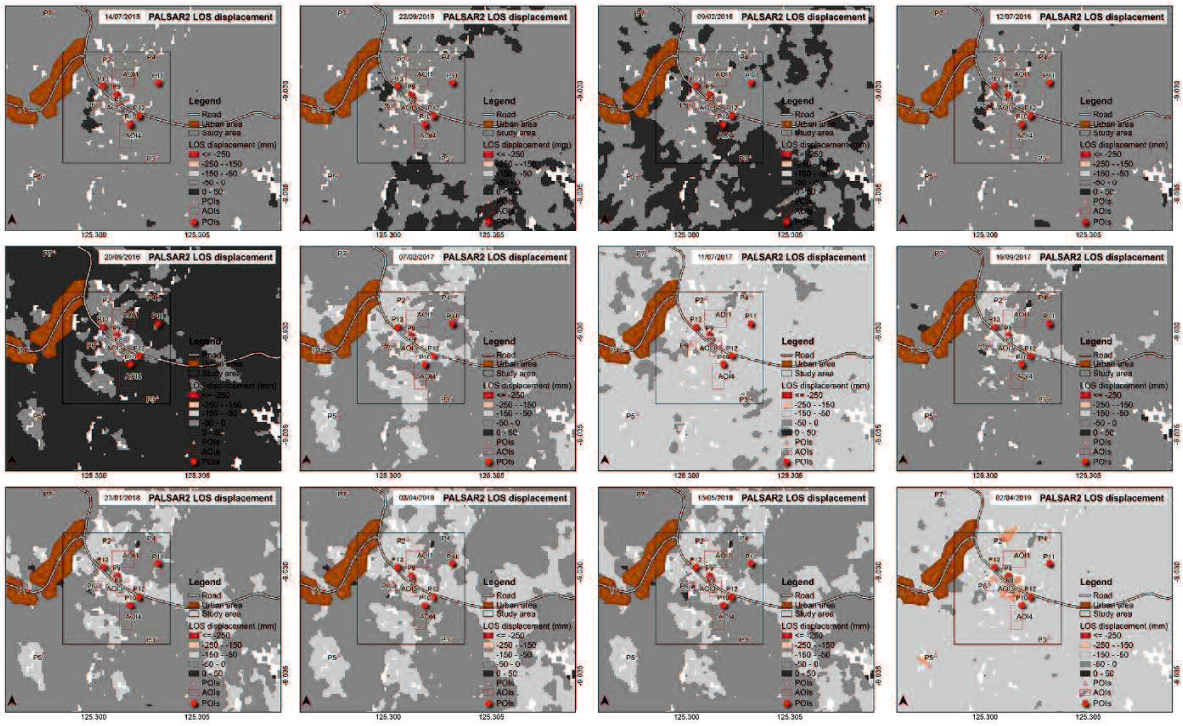

## Appendix 7 – Unmanned Aerial Vehicle (UAV) DJI Mavic Pro specifications

| Aircraft | |
|---|---|
| Dimensions (with propeller folded) | Height 83 x width 83 x depth 198mm |
| Diagonal dimension (without propeller) | 335 mm |
| Weight (including battery and propeller) | 734g (without gimbal cover)<br>743g (with gimbal cover) |
| Maximum climb speed | 5m/s in sports mode |
| Maximum descent speed | 3m/s |
| Maximum speed | 64.8km/h in sport mode (no wind) |
| Operational limit altitude (above sea level) | 5,000m |
| Maximum flight time | About 27 minutes |
| Maximum hovering time | 24 minutes |
| Maximum flight distance | 13km, calm |
| Operating environment temperature | 0-40°C |
| GPS mode | GPS / GLONASS |
| Hovering accuracy | Vertical:<br>+/- 0.1 m (when Vision Positioning is active)<br>or +/-0.5 m<br>Horizontal:<br>+/- 0.3 m (when Vision Positioning is active)<br>or +/-1.5 m |
| Cruising flight time | 21 minutes (for normal flight, 15% battery remaining) |
| Operating frequency | FCC:<br>2.4-2.4835GHz; 5.150-5.250 GHz; 5.725-5.850 GHz<br>CE:<br>2.4-2.4835GHz; 5.725-5.850 GHz<br>SRRC:<br>2.4-2.4835 GHz; 5.725-5.850 GHz |
| Output (EIRP) | 2.4GHz<br>FCC:<=26 dBm; CE: <=20 dBm; SRRC:<=20 dBm; MIC:<=18 dBm<br>5.2 GHz<br>FCC:<=23 dBm<br>5.8 GHz<br>FCC:<=23 dBm; CE <=13 dBm; SRRC: <=23 dBm; MIC:- |

[https://www.dji.com/jp/mavic/info#specs]

| Camera | |
|---|---|
| sensor | 1/2.3" (CMOS),<br>effective pixels: 12.35 million pixels (total pixels: 12.71 million pixels) |
| lens | Viewing angle: 78.8°, 26mm (35mm format equivalent) f/2.2<br>distortion <1.5% focus 0.5m to infinity |
| ISO range | 100-3200 (video), 100-1600 (photo) |
| Electronic shutter | 8 seconds to 1/8000 seconds |
| Maximum still image size | 4000 x 3000 |
| Still image mode | Single shot<br>Burst shot: 3, 5, 7<br>Auto exposure bracket (AEB): 3, 5<br>(0.7EV step)<br>Interval shooting |
| Video mode | DCI4K: 4096×2160 24p<br>UHD4K: 3840×2160 24/25/30p<br>2.7K: 2720x1530 24/25/30p<br>FHD: 1920×1080 24/25/30/48/50/60/96p<br>HD: 1280×720 24/ 25/30/48/50/60/120 |
| Maximum video bit rate | 60Mbps |
| Supported file system | FAT32 (32GB or less), exFAT (32GB) |
| Still image | JPEG, DNG |
| Video | MP4, MOV (MPEG-4 AVC/H.264) |
| Compatible SD card | microSD™<br>Maximum capacity: 128GB Class 10 or UHS-1 standard required |
| Operating environment temperature | 0-40°C |

## Appendix 8 – UAV Aerial photos - 19 August 2017


DJI_0562.JPG
DJI_0563.JPG
DJI_0564.JPG
DJI_0565.JPG
DJI_0566.JPG
DJI_0567.JPG
DJI_0568.JPG
DJI_0569.JPG
DJI_0570.JPG
DJI_0571.JPG
DJI_0572.JPG
DJI_0573.JPG
DJI_0574.JPG
DJI_0575.JPG
DJI_0576.JPG
DJI_0577.JPG
DJI_0578.JPG
DJI_0579.JPG
DJI_0580.JPG
DJI_0581.JPG
DJI_0582.JPG
DJI_0583.JPG
DJI_0584.JPG
DJI_0585.JPG
DJI_0586.JPG
DJI_0587.JPG
DJI_0588.JPG
DJI_0589.JPG
DJI_0590.JPG
DJI_0591.JPG
DJI_0592.JPG
DJI_0593.JPG
DJI_0594.JPG
DJI_0595.JPG
DJI_0596.JPG
DJI_0597.JPG
DJI_0598.JPG
DJI_0599.JPG
DJI_0600.JPG
DJI_0601.JPG
DJI_0602.JPG
DJI_0603.JPG
DJI_0604.JPG
DJI_0605.JPG
DJI_0606.JPG
DJI_0607.JPG
DJI_0608.JPG
DJI_0609.JPG


DJI_0610.JPG
DJI_0611.JPG
DJI_0612.JPG
DJI_0613.JPG
DJI_0614.JPG
DJI_0615.JPG
DJI_0616.JPG
DJI_0617.JPG
DJI_0618.JPG
DJI_0619.JPG
DJI_0620.JPG
DJI_0621.JPG
DJI_0622.JPG
DJI_0623.JPG
DJI_0624.JPG
DJI_0625.JPG
DJI_0626.JPG
DJI_0627.JPG
DJI_0628.JPG
DJI_0629.JPG
DJI_0630.JPG
DJI_0631.JPG
DJI_0632.JPG
DJI_0633.JPG
DJI_0634.JPG
DJI_0635.JPG
DJI_0636.JPG
DJI_0637.JPG
DJI_0638.JPG
DJI_0639.JPG
DJI_0640.JPG
DJI_0641.JPG
DJI_0642.JPG
DJI_0643.JPG
DJI_0644.JPG
DJI_0645.JPG
DJI_0646.JPG
DJI_0647.JPG
DJI_0648.JPG
DJI_0649.JPG
DJI_0650.JPG
DJI_0651.JPG
DJI_0652.JPG
DJI_0653.JPG
DJI_0654.JPG
DJI_0655.JPG
DJI_0656.JPG
DJI_0657.JPG

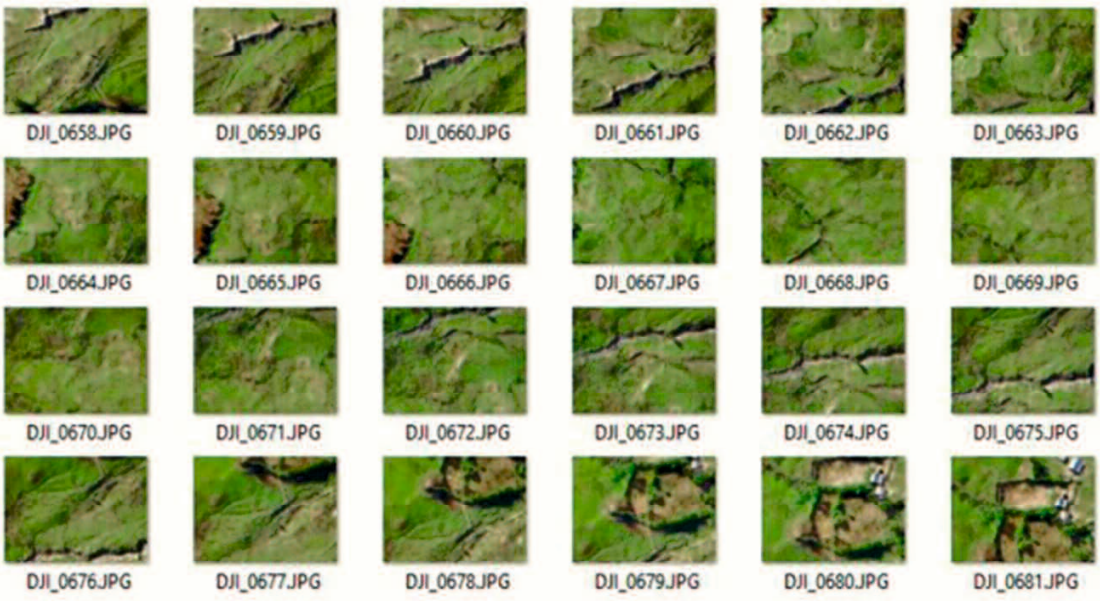
DJI_0658.JPG
DJI_0659.JPG
DJI_0660.JPG
DJI_0661.JPG
DJI_0662.JPG
DJI_0663.JPG
DJI_0664.JPG
DJI_0665.JPG
DJI_0666.JPG
DJI_0667.JPG
DJI_0668.JPG
DJI_0669.JPG
DJI_0670.JPG
DJI_0671.JPG
DJI_0672.JPG
DJI_0673.JPG
DJI_0674.JPG
DJI_0675.JPG
DJI_0676.JPG
DJI_0677.JPG
DJI_0678.JPG
DJI_0679.JPG
DJI_0680.JPG
DJI_0681.JPG

**Appendix 9 – UAV Orthomosaic - 19 August 2017 – AOI1 map**

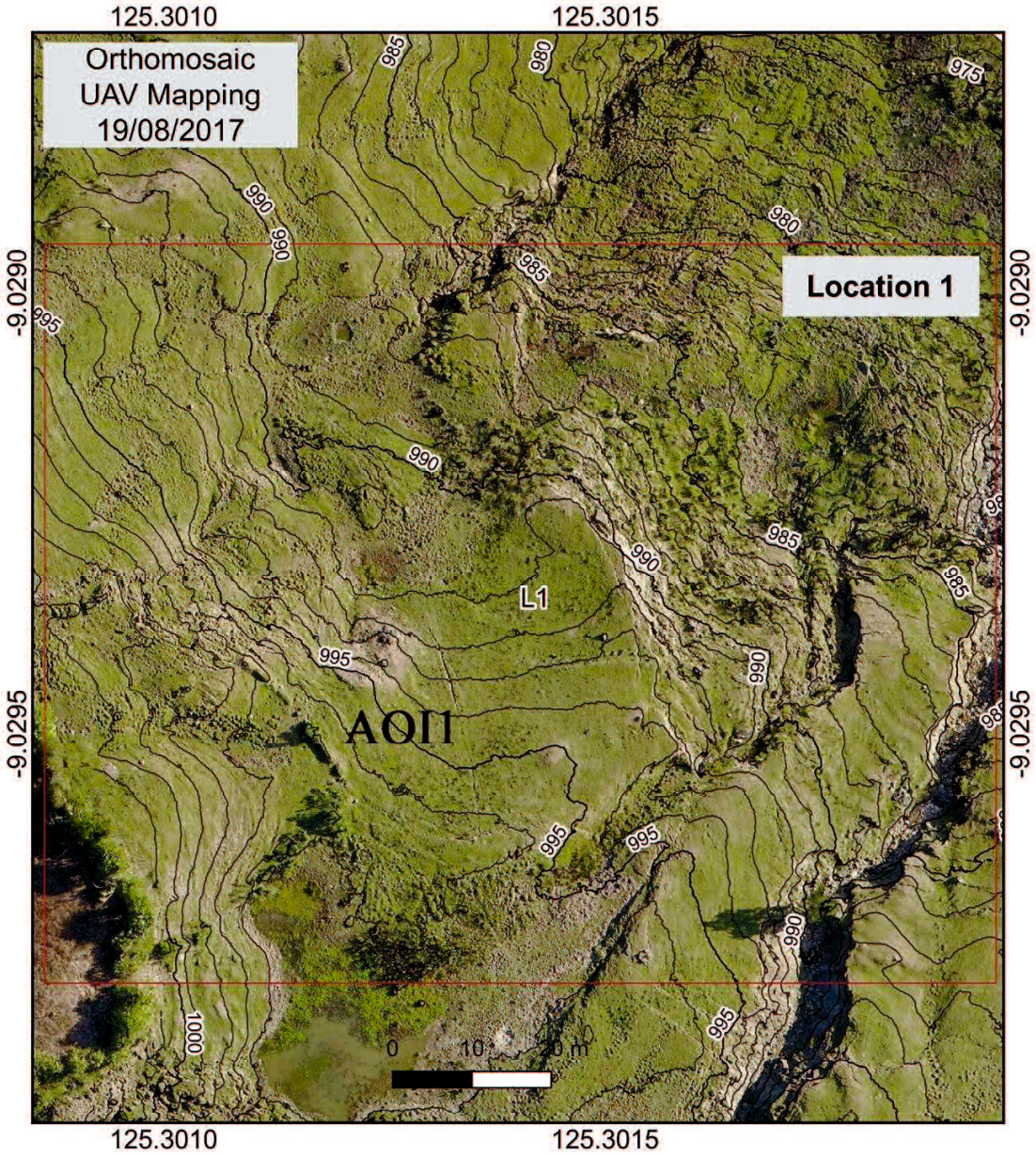

**Appendix 10 – UAV Orthomosaic - 19 August 2017 – AOI2 map**

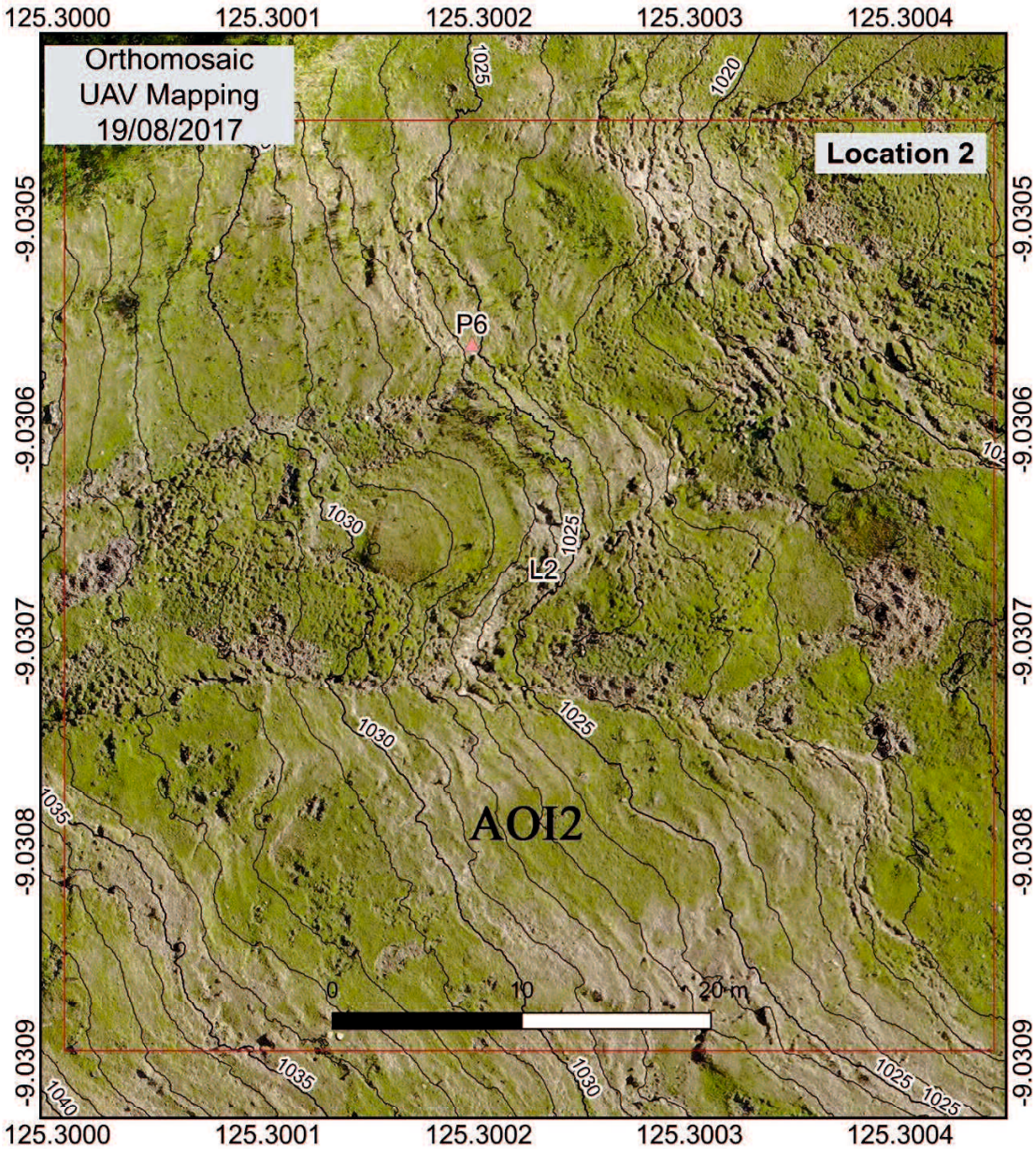

**Appendix 11 – UAV Orthomosaic - 19 August 2017 – AOI3 map**

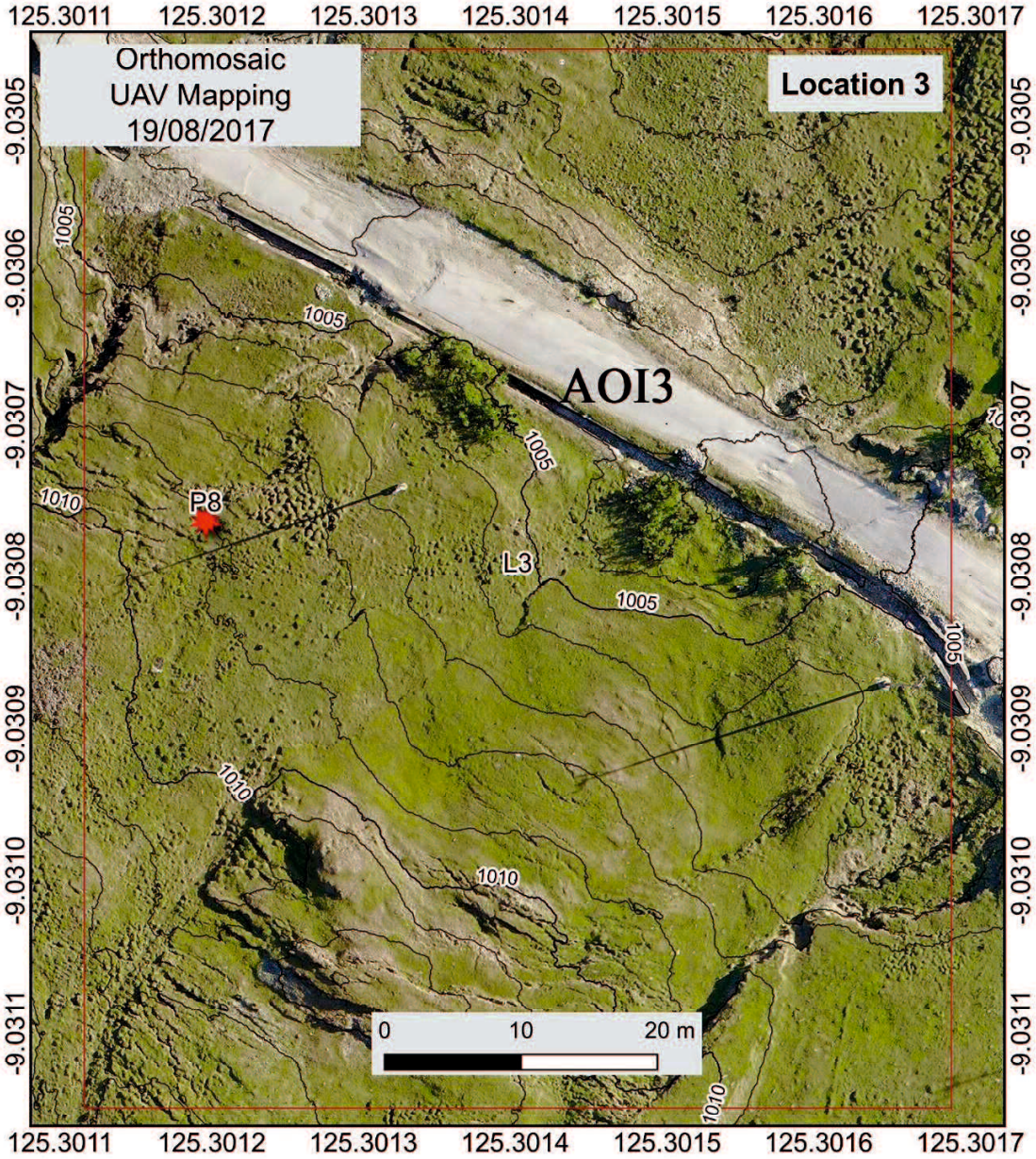

## Appendix 12 – Road Surface elevation and distance measurement comparison between UAV DEM and Total Station

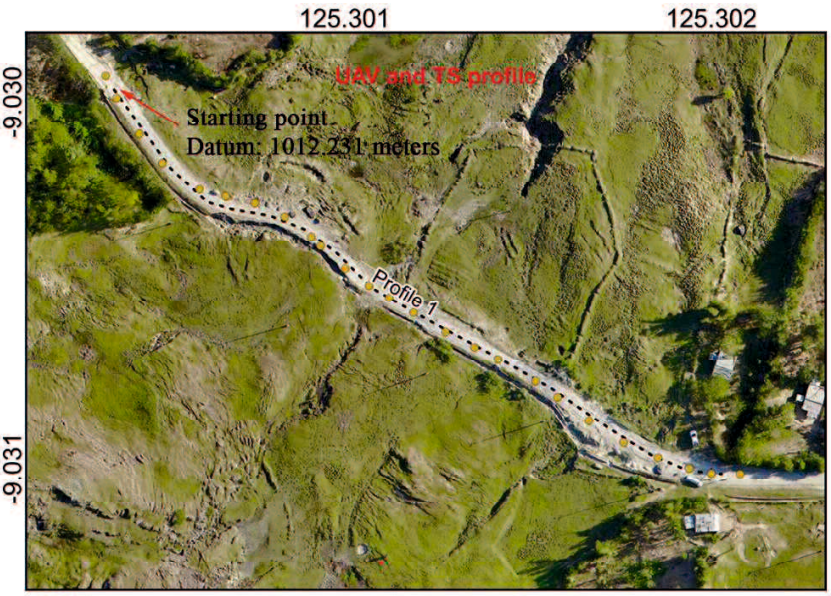


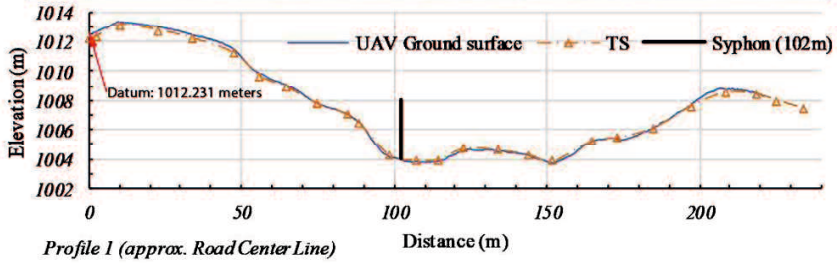


*Profile 1 (approx. Road Center Line)*

UAV and TS measurements comparison (meters)

| Index | Hdistance | Zts | Zuav | Zts-Zuav |
|---|---|---|---|---|
| *Local Datum* | *0* | *1012.231* | *1012.231* | *0.000* |
| 1 | 2.500 | 1012.350 | 1012.613 | *-0.263* |
| 2 | 10.008 | 1013.120 | 1013.263 | *-0.143* |
| 3 | 22.759 | 1012.758 | 1012.936 | *-0.178* |
| 4 | 33.940 | 1012.204 | 1012.362 | *-0.158* |
| 5 | 47.545 | 1011.219 | 1011.406 | *-0.187* |
| 6 | 55.722 | 1009.702 | 1009.828 | *-0.126* |
| 7 | 64.680 | 1008.955 | 1009.021 | *-0.066* |
| 8 | 74.543 | 1007.811 | 1007.809 | *0.002* |
| 9 | 84.571 | 1007.119 | 1007.058 | *0.061* |
| 10 | 88.511 | 1006.518 | 1006.513 | *0.005* |
| 11 | 98.551 | 1004.275 | 1004.131 | *0.144* |
| 12 | 107.316 | 1003.974 | 1003.838 | *0.136* |
| 13 | 114.385 | 1004.022 | 1003.852 | *0.170* |
| 14 | 122.973 | 1004.763 | 1004.579 | *0.184* |
| 15 | 134.217 | 1004.653 | 1004.496 | *0.157* |
| 16 | 144.092 | 1004.334 | 1004.255 | *0.079* |
| 17 | 152.029 | 1003.917 | 1003.740 | *0.177* |
| 18 | 165.084 | 1005.321 | 1005.238 | *0.083* |
| 19 | 173.238 | 1005.512 | 1005.374 | *0.138* |
| 20 | 184.999 | 1006.183 | 1006.166 | *0.017* |
| 21 | 197.326 | 1007.675 | 1007.708 | *-0.033* |
| 22 | 208.642 | 1008.582 | 1008.734 | *-0.152* |
| 23 | 218.552 | 1008.446 | 1008.458 | *-0.012* |
| | | **Zts and Zuav comparison** | | |
| | | | **RMSE** | 0.135 |

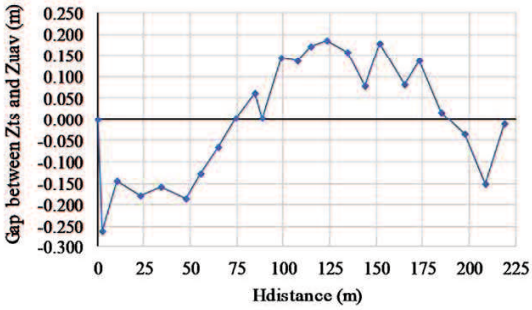

## Appendix 13 – Electrical Pole elevation and distance measurement comparison between UAV DEM and Total Station


**A comparison of Position and Altimetry measurements between UAV and Total Station**

| UAV Surveying (meter) | | | | | | | | | *Precision* | |
|---|---|---|---|---|---|---|---|---|---|---|
| P | Easting | Northing | Elevation | | Name | d(interval) | | d(interval-diff) | Relative Elevation | dH(diff) | dV(diff) |
| UAV-1 | 752915.134 | 9000997.201 | 1012.952 | | EDTL-1 | d1-1 | 0.000 | 0.000 | 3.256 | 2.1339 | -0.3604 |
| UAV-2 | 752949.776 | 9000966.306 | 1010.223 | | EDTL-2 | d1-2 | 46.417 | -0.463 | 0.527 | 1.6144 | -0.5254 |
| UAV-3 | 752991.680 | 9000951.359 | 1006.699 | | EDTL-3 | d2-3 | 44.489 | -0.192 | -2.997 | 1.5709 | -0.5013 |
| UAV-4 | 753026.723 | 9000936.890 | 1005.641 | | EDTL-4 | d3-4 | 37.912 | 0.130 | -4.055 | 1.6512 | -0.5642 |
| UAV-5 | 753061.443 | 9000916.022 | 1009.696 | Datum UAV | EDTL-5 | d4-5 | 40.509 | 0.251 | 0.000 | 1.7497 | 0.0000 |

| Total Station Surveying (meter) | | | | | | | | |
|---|---|---|---|---|---|---|---|---|
| P | Easting | Northing | Elevation | | Name | d(internval) | d(interval-diff) | Relative Elevation |
| TS-1 | 752913.186 | 9000998.071 | 1019.216 | | PEDTL-1 | d1-1 | 0.000 | 0.000 | 3.616 |
| TS-2 | 752948.815 | 9000967.603 | 1016.652 | | PEDTL-2 | d1-2 | 46.880 | -0.463 | 1.052 |
| TS-3 | 752990.957 | 9000952.754 | 1013.104 | | PEDTL-3 | d2-3 | 44.682 | -0.192 | -2.496 |
| TS-4 | 753025.866 | 9000938.302 | 1012.109 | | PEDTL-4 | d3-4 | 37.782 | 0.130 | -3.491 |
| TS-5 | 753060.152 | 9000917.203 | 1015.600 | Datum TS | PEDTL-5 | d4-5 | 40.258 | 0.251 | 0.000 |

Note

| | |
|---|---|
| d(interval) : | *Distance between electrical pole* |
| d(interval-diff) : | *Distance differences between UAV and TS Measurements* |
| Relative Elevation : | *Elevation recalculated using individual Datum (UAV and TS)* |
| dH(diff) : | *Horizontal differences between UAV and TS Measurements* |
| dV(diff) : | *Verical differences between UAV and TS Measurements* |

| *RMSE [UAV-TS](meter)* | |
|---|---|
| d(interval-diff) | 0.288 |
| dH(diff) | 1.756 |
| dV(diff) | 0.494 |

**Appendix 14 – Elevation Measurement comparison between UAV DEM surface and Leveling rod scale reading through the photo.**

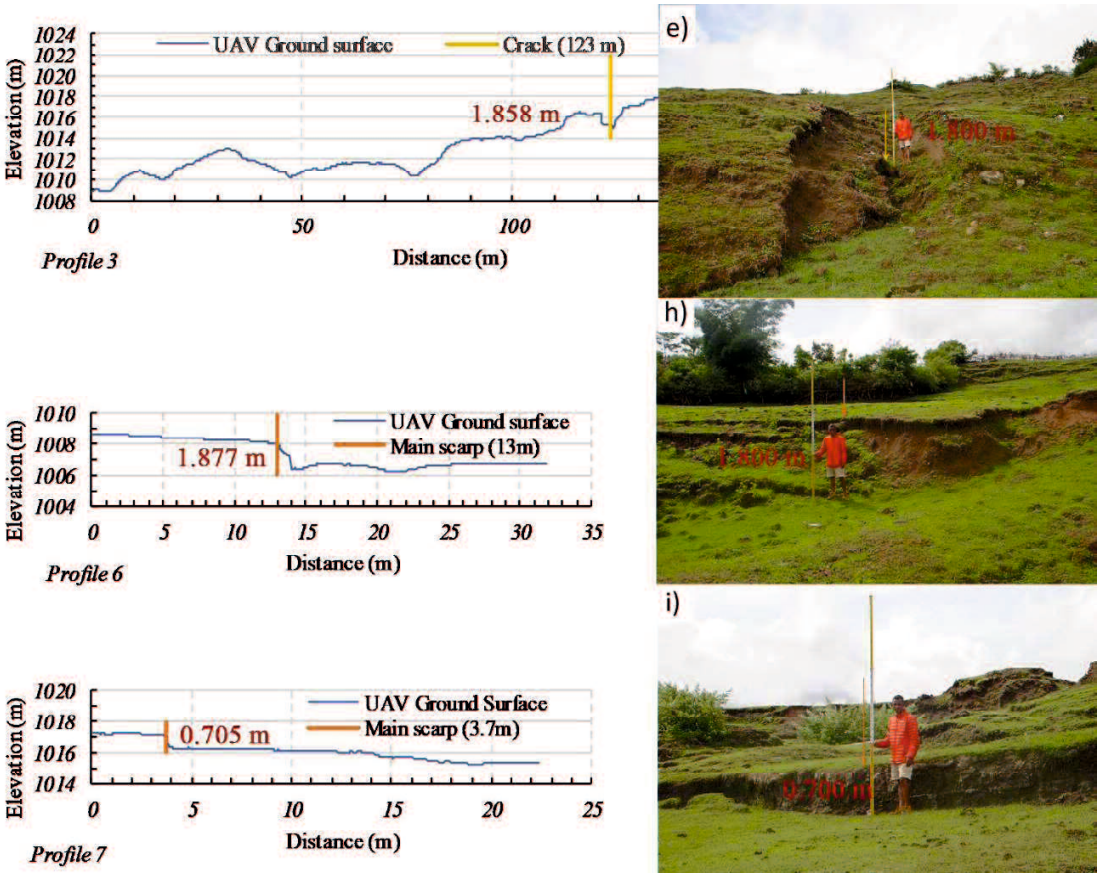


| Profile | UAV ground surface (m) | Levelling scale in photo (m) | Differences (m) |
|---|---|---|---|
| Profile 3 | 1.858 meters | 1.800 meters | 0.058 |
| Profile 6 | 1.877 meters | 1.800 meters | 0.077 |
| Profile 7 | 0.705 meters | 0.700 meters | 0.005 |

## Appendix 15 – Field observation works

Aerial view of the study area

Working with local autohrities and local residents, and collecting information

Rainfall data logger maintenance and data collection

UAV Mapping, Total Station measurement and field observations

**Appendix 16 – An Examples of ground instability and road condition in Timor-Leste**

Old road condition

Excavation processes

New road conditions